DISSERTATION

ANALYSIS OF CREEP BEHAVIOR OF HIGH STRENGTH STEEL COLUMNS AT ELEVATED TEMPERATURE

(高強度鋼柱の高温時におけるクリープ挙動解析)

September 2022

PHAN QUOC TUAN

ANALYSIS OF CREEP BEHAVIOR OF HIGH STRENGTH STEEL COLUMNS AT ELEVATED TEMPERATURE

Phan Quoc Tuan

The Tokyo University of Science, 2022

Supervisor: Professor Mamoru Kohno

This dissertation has reported results of the studies on the behavior of high strength steel columns when subjected to elevated temperatures due to fire. Analytical, computational, and experimental means were incorporated to conduct the research reported in this dissertation. The purpose of this research described in this dissertation is to gain a deeper understanding of the creep behavior of structural steel columns, particularly high strength steel, and to develop creep data and models for better analysis and design of steel structures subjected to fire. The investigation will include both analytical, computational, and experimental examinations of coupon tests and column tests at high temperatures. The study will focus on a number of series of high temperature coupon tests to ascertain the overall material properties, as well as a series of column tests at elevated temperatures. The steel material is not subjected to creep tests in this work, and the creep parameters are determined using general tensile tests at elevated temperatures. The experimental studies will focus on 3 types of high strength steel: YP400, YP500 and H-SA700, for which very little elevated temperature experimental data exists.

Chapter 2 of this dissertation is used to investigate the background of time- and temperature-dependent behavior of structural steel, referred to as thermal creep, and its relevance in forecasting the creep behavior of steel columns exposed to elevated temperatures caused by fire. The chapter began with discussing the definition of structural steel thermal creep. The effect of thermal creep on the stress-strain behavior of structural steel was then quantified using a variety of methods. Following the discussion of various methodologies for calculating the time- and temperature-dependent behavior of structural steel exposed to fire, a literature review was conducted. Important constitutive models for the thermal creep of structural steel at elevated temperatures were further reviewed. After reviewing the previous research and the background information provided on the phenomenon of time- and temperature-dependent stress-strain behavior of structural steel exposed to fire, the importance of creep deformations is proved and this implies that neglecting creep may result in very erroneous structural response estimates for structural steel, particularly for high strength steels. Moreover, there appears to be a lack of data on the creep behavior of high strength steels in general, and specifically YP400, YP500, and H-SA700 steels.

In chapter 3, efforts have been made to describe the phenomenon of time-dependent or creep buckling and its significance in predicting the buckling strength of steel columns subjected to

elevated temperatures due to fire. The chapter was started by introducing the concept of creep buckling and establishing it as a time-dependent inelastic buckling phenomenon. Furthermore, a review of past studies was conducted to acquire a better understanding of the column behavior at elevated temperatures. Nevertheless, several additional potential factors impacting the subject to fire column's behavior are explored. As shown in the literature survey, the experimental data on columns at elevated temperatures are rather limited compared to column tests at normal temperature. Most of the column tests reported in the literature were accompanied by tension coupon tests conducted at room temperature. However, only a few past investigations included material characterization tests conducted at the same temperature as the column test. Nevertheless, the apparent importance of creep together with the limited number of studies related to the influence of creep on column buckling suggest the need for more quality research on elevated-temperature creep phenomenon. Specifically, the understanding of how to quantify creep effects on column buckling is still very limited and adequate experimental data is lacking

Chapter 4 began with an introduction to high strength steel and its mechanical properties. The results of tensile tests conducted at elevated temperatures on high yield point steels YP400 and YP500, as well as high strength steel H-SA700, were given, together with testing methodology and general properties. The process for developing the thermal creep model was also established based on Fields and Fields' creep material model and the actual creep behavior of the critical truss angle steel used in the WTC investigation. To identify the most correct creep parameters for the high strength steel utilized in this work, a trial-and-error approach was conducted to determine the most accurate stress-strain curves for the FE model that fit experimental data at various temperatures. The plastic material properties were then defined using hypothetical curves based on the observed stress-plastic strain relationship during experimental tests at various temperatures. Then, these thermal creep models were validated by comparing the stress-strain curves generated by Abaqus analytical results to those generated by experimental data. The experimental program and results described in this chapter generated essential experimental data on the influence of thermal creep on the elevated-temperature response of high strength steels, thereby filling significant gaps in the database of high strength steel mechanical properties at elevated temperatures. The test results provided in this chapter demonstrate that creep strains can be fairly severe in fire-prone building structures. This shows that disregarding creep may result in very erroneous structural response estimates for some types of structure-fire problems, such as steel columns exposed to fire. Additionally, when compared to experimental data, existing creep models for structural steel subjected to fire may provide inaccurate predictions.

Chapter 5 discussed various experimental results on high-strength steel columns, as well as some other research findings about potential influences on steel column behavior. The results of the computational method for column test based on material creep models provided in Chapter 4 are also analyzed using the Abaqus finite element software and compared to experimental results. Additionally, a thermal expansion coefficient is suggested for each steel grade YP400, YP500, and H-SA700, based on the vertical displacement of the column at

temperatures less than 400 °C and on previously performed experiments. Additionally, two types of imperfection models (local and global buckling modes) are addressed in the study, including a different magnitude of imperfection. The outcomes of analyses with and without creep behavior were also compared. Plastic properties, thermal properties, and initial imperfection have all been investigated as potential influencers of time-dependent behaviors of high strength steels. The proposed method could be used with the same grade of steel without requiring full-scale structural or creep tests. In this study, the simulation analysis was used to determine the peak point of time and temperature versus displacement, deformation shape, and creep properties of the high yield point steel columns. The results were quite accurate when compared to the experimental results. The yield phenomenon may have an adverse effect on the analytical results. The experiment to determine the coefficient of thermal expansion is implied to be critical for simulating the behavior of steel structures, especially at temperatures below 400 °C. Furthermore, when conducting experiments over a wide temperature range, the absence of data should be avoided.

The final chapter ends with some observations and conclusions from this research. As shown in the literature survey, there is a scarcity of experimental data on thermal creep of structural steels, especially for high strength steels. Ignoring creep may lead to highly inaccurate predictions of structural response for some classes of structure-fire problems such as steel columns subjected to fire. The values of thermal expansion coefficient for high strength steel are identified and smaller than those indicated in standards. The approach of representing plastic properties as a logarithmic equation is well suitable for simulating thermal creep behavior using a finite element program. The approach for developing the creep model through general tensile tests was also demonstrated to be practical, owing to the high similarity between analytical and experimental data.

Several issues have been identified as requiring additional study or research as follows. The accuracy of the analytical solutions developed in this study needs to be improved due to discrepancies between analytical and experimental results at a variety of temperatures. It is necessary to evaluate the thermal creep of structural steel in compression. The creep models given in this study should be validated against various types of steel structures to ascertain their validity for high strength steels. Significant work is required to examine the internal forces that can have a dominating effect on column response. The time effects in the form of stress relaxation are of particular relevance because they may have an effect on the forces generated in steel columns due to restricted thermal expansion. The procedure for determining the creep parameters and creating the creep model needs to be simplified and made more precise.

Table of Contents

Table of Figures

Table of Tables

CHAPTER 1   INTRODUCTION

1.1. Overview

Over the last few decades, significant advances in our understanding of steel's fire behaviour have occurred, and it is now reasonable to assert that steel is better studied in fire than any other framing material. Extensive testing on both small and large scales resulted in the development of modelling and analytical approaches that are now routinely used by a large number of researchers to investigate the behaviour of steel exposed to fire. Steel structures have a fundamental disadvantage in that they are highly susceptible to high temperatures, which results in rapid loss of strength and stiffness. Thermal expansion of the material at elevated temperatures also plays a significant role in the element's failure. The ability to forecast thermal and structural responses to fire is essential to the performance-based design of steel building structures for fire safety. The capability of such predictions to analyse the strength, collapse time, and critical temperature of steel columns at elevated temperatures is also critical. Columns are major structural components, and their failure can result in a structure collapsing.

Numerous factors affect the structural behaviour of steel at elevated temperatures, including the material's thermal and mechanical properties, the effects of constrained thermal expansion, residual stress changes, and creep effects. Steel's time-dependent response, or creep, is extremely crucial for predicting the collapse behaviour of steel columns exposed to elevated temperatures during a fire. However, the effect has only been thoroughly examined recently. At elevated temperatures, this creep characteristic can result in load- and time-dependent displacement increases. While this creep phenomenon contributes to the unpredictable behaviour of steel structures, there is currently no specified formula for this behaviour in the standards. Creep has a less noticeable effect on low-strength steel than it does on high-strength steel.

1.2. Research Goal and Objectives

The overall goal of the research described in this dissertation is to gain a deeper understanding of the creep behaviour of structural steel columns, particularly high strength steel, and to develop creep data and models for better analysis and design of steel structures subjected to fire. The investigation will include both analytical, computational, and experimental examinations of coupon tests and column tests at high temperatures.

The study will focus on a number of series of high temperature coupon tests to ascertain the overall material properties, as well as a series of column tests at elevated temperatures. The steel material is not subjected to creep tests in this work, and the creep parameters are determined using general tensile tests at elevated temperatures.

Specific objectives of this research are as follows:

- Develop analytical models for creep response of each type of high strength steel.

- Omit creep tests to estimate the behavior of steel members at elevated temperatures.
- Develop analytical models for creep behaviours of high strength steel column in Abaqus and compared to experimental ones to demonstrate the method's validity.
- Develop and discuss the procedure for determining steel creep parameters and applying them to predict the creep behavior of other steel structures.

The experimental studies will focus on 3 types of high strength steel: YP400, YP500 and H-SA700, for which very little elevated temperature experimental data exists.

1.3. Outline of Dissertation

To accomplish the objectives outlined above, a complete review of the previous studies was done, followed by a combined analytical, computational, and experimental investigation.

The background for Chapter 2 of this dissertation is the time-dependent or creep behavior of structural steel at elevated temperatures. The chapter began with defining structural steel thermal creep. After quantifying the effect of thermal creep on the stress-strain behavior of structural steel using a variety of methods. Additionally, a review of early studies is addressed on describing the time-dependent stress-strain behavior of structural steel at elevated temperatures. Additionally, the constitutive equations established for the structural steel thermal creep model are discussed.

Chapter 3 discusses the concept of time-dependent or creep behavior of steel columns when exposed to elevated temperatures. Additionally, a review of recent work on steel columns at elevated temperatures is included. Following that, various methodologies for quantifying the effect of steel thermal creep on column strength forecasts were reviewed.

Chapter 4 introduces definition of high strength steel and its mechanical properties. The results of tensile tests conducted at elevated temperatures on high yield point steels YP400 and YP500, as well as high strength steel H-SA700, were given, together with testing methodology and general properties. The process for developing the thermal creep model was also established. A trial-and-error approach was conducted to identify the most correct creep parameters for the high strength steel. The plastic material properties were then defined and the thermal creep models were validated by comparing the stress-strain curves generated by Abaqus analytical results to those generated by experimental data.

Chapter 5 provided various experimental results on high-strength steel columns, as well as some other research findings about potential influences on steel column behavior. The results of the computational method for column test based on material creep models provided in Chapter 4 are also analyzed using the Abaqus finite element software and compared to experimental results. Additionally, a thermal expansion coefficient is suggested for each steel grade YP400, YP500, and H-SA700, based on the vertical displacement of the column at temperatures less than 400 °C and on previously performed experiments. Additionally, two types of imperfection models (local and global buckling modes) are addressed in the study, including a different magnitude of imperfection. The outcomes of analyses with and without creep behavior were compared.

The final chapter, Chapter 6, summarizes the research program's findings. Key observations and discussions from the literature review, and analytical, computational and experimental studies are compiled. Finally, recommendations for more research studies are made.

CHAPTER 2 BACKGROUND ON CREEP BEHAVIOR OF STRUCTURAL STEEL AT ELEVATED TEMPERATURES

2.1. Overview

The structural behavior of steel at elevated temperatures is influenced by a multitude of elements, including the thermal and mechanical properties of steel materials, the effects of constrained thermal expansion, changes in residual stress, and creep effects. The effect of thermal creep of structural steel is one of the elements that can affect the behavior of steel columns at elevated temperatures. To accurately anticipate the creep behavior of steel column members, a thorough understanding of the mechanical properties of structural steel at elevated temperatures is required. Mechanical properties like yield stress, ultimate strength, proportional limit, modulus of elasticity and tangent modulus are all established using the fundamental stress-strain behavior of structural steel at elevated temperatures. One of the most frequently used methods used to determine the stress and strain relationship of structural steel exposed to elevated temperatures is creep and relaxation tests in tension and compression. Another effective method is conducted tension or compression tests of steel coupons at various strain rates and temperatures. These experiments are designed to determine the effect of time on the stress-strain behavior, and thus on the mechanical behavior of structural steel at elevated temperatures.

Numerous prior investigations on the behavior of structural steel at elevated temperatures have employed a variety of different testing methods, which will be discussed in detail in this chapter. However, the chapter's primary focus is on the time-dependent or creep behavior of structural steel, particularly high strength steel. As mentioned in the introduction chapter, one of the critical elements affecting column strength at elevated temperatures is the effect of structural steel thermal creep, which has received the least attention in the literature. While the creep properties of structural steel at elevated temperatures are not well understood or documented, the time-dependent behavior of structural steel at elevated temperatures may be a new issue for certain structural engineers. Throughout this chapter, efforts have been made to introduce some fundamental concepts related to creep and relaxation. The focus of this chapter, as well as the entire dissertation, is on mechanics-based modelling of structural steel thermal creep.

This chapter's primary objective is to familiarize readers with the theory of time-dependent behavior, or thermal creep, of structural steel when exposed to elevated temperatures. Thus, the time- and temperature-dependent stress-strain behavior of structural steel is firstly introduced. Following that, a review of previous research on the stress-strain behavior of structural steel at elevated temperatures is presented. While the main focus is on previous research on the time-dependent or creep effects on mechanical behavior at high temperatures, the literature on creep models is also reviewed in order to present some of the most significant constitutive equations developed for thermal creep of structural steel for structural-fire design applications. Several of these constitutive equations will be utilized later

in this dissertation to analyse the creep behavior of high strength steel columns. Finally, the chapter concludes with some general remarks on the phenomenon of structural steel thermal creep and its application to the prediction of the strength of steel columns exposed to fire, as well as a critical evaluation of prior research.

2.2. Creep phenomenon of structural steel

2.2.1. Definition of Creep phenomenon

When steel constructions are exposed to elevated temperatures, they undergo progressive permanent deformations over time, even if the applied stress is less than the yield stress; this time-dependent deformation is referred to as creep. Thus, creep can be described as an increase in strain over time in a solid material subjected to steady stress.

Creep tests are frequently undertaken on materials by subjecting them to steady stress and temperature and then measuring strain as a function of time. As illustrated in Figure 2-1, typical creep curves are separated into three sections. The primary stage of the creep curve is nonlinear and begins with a high creep strain rate and gradually lowers. This stage is developed mostly as a result of the materials' sub-grain structure becoming more dislocated. A consistent creep strain rate characterizes the secondary stage, referred to as the steady-state phase and the creep strain rate is the minimal compared with those of the primary and tertiary stages. In the tertiary stage, this creep strain rate increases rapidly until a fracture occurs due to the necking of the cross section. It is critical to keep in consideration that not all materials will reach the tertiary phase within the time frames, stress levels, and temperature ranges required for structural fire safety design. Additionally, the primary region of this curve is extremely small in structural steels and is frequently overlooked during modeling.
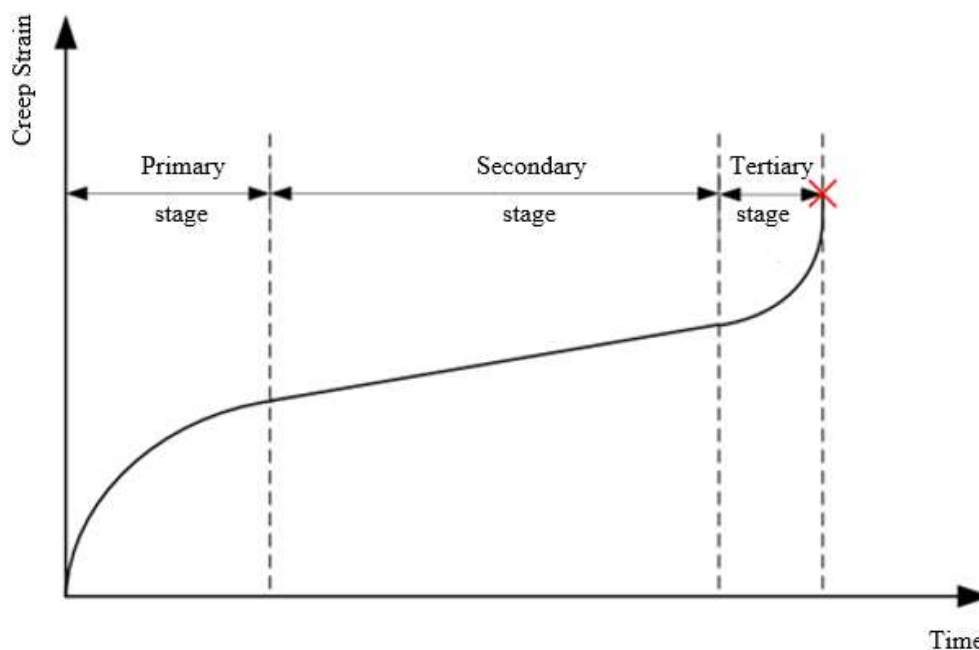
Figure 2-1 Typical creep strain versus time curve under constant stress and temperature

2.2.2. True stresses and true strains for Structural Steel at Elevated Temperatures

The stress-strain behavior of structural steel is determined by conducting tests on small specimens under uniaxial tension or compression, either at room temperature or at elevated temperatures. Coupons or coupon specimens are typically small specimens that are rectangular or cylindrical in shape. The stresses and strains measured in these tests are frequently stated in engineering or nominal values. More precisely, the stresses recorded in these tests are determined by dividing the recorded loads by the coupon's decreased cross-sectional area. Additionally, the stresses measured in these tests are calculated using the provided initial gauge length. However, constitutive models that accurately capture the real behavior of structural steel are required for stress analysis of structural components that are subjected to significant deformations. As a result, the stress and strain values obtained during characterisation should be stated in true values.

The relationship between true strain and nominal strain is established by expressing the nominal strain as follows:

$$\varepsilon_{true} = \ln\left(1 + \varepsilon_{nominal}\right) \qquad (2.1)$$

The expression of true stress can be given by this equation:

$$\sigma_{true} = \sigma_{nominal}(1 + \varepsilon_{nominal}) \qquad (2.2)$$

In equations (2.1) and (2.2), $\sigma_{nominal}$ and $\varepsilon_{nominal}$ denote nominal stress and strain or can be called engineering stress and strain.

These formulations are valid up until the development of necking, at which point the assumption of uniform strain distribution over a coupon's gauge length is roughly valid. True stresses and strains become significant in the context of analytical processes. As will be demonstrated later in this dissertation, it is necessary to conduct creep analysis on steel specimens at constant high temperatures in order to get data useful to structural-fire design applications. Consequently, in order to use such data in nonlinear structural computations, it becomes critical to present creep behavior of structural steel in terms of true stresses and strains.

2.3. Methods of characterizing thermal creep behavior of structural steel

As discussed previously, several methodologies are utilized to describe structural steel's time-dependent or creep behavior under elevated temperatures caused by fire. The four primary sorts of methods that the majority of researchers employ will be outlined in this section as steady-state temperature tests, transient-state temperature tests, steady-state temperature creep tests, and steady-state temperature relaxation tests. The following methods will give a brief summary of how to determine creep behavior for steel structures at high temperatures. It should be noted those tests are not considered in the studies on the timed-dependent behavior of structural steel in this dissertation. However, alternative approach based on general tensile testing without creep testing has been presented, which will be discussed in Chapter 4.
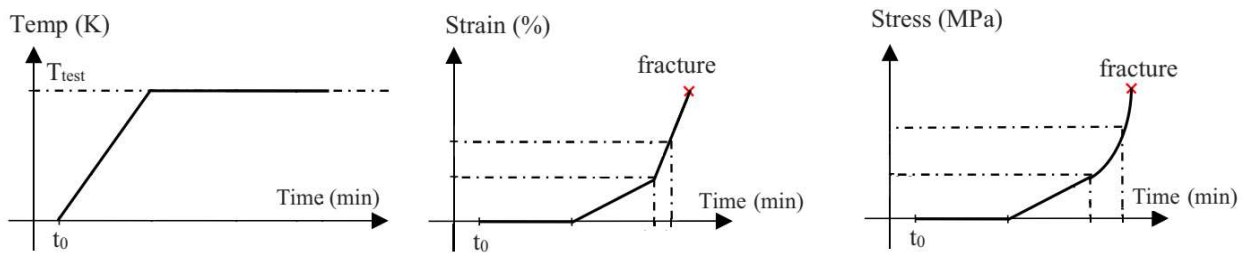
Figure 2-2 Test procedure for Steady-State temperature tests
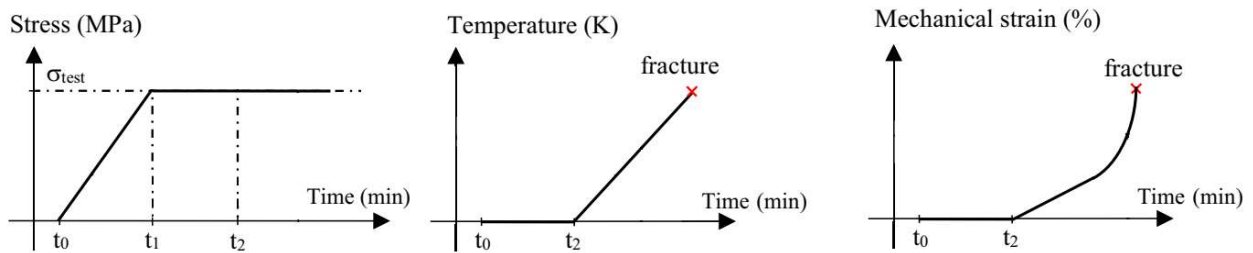
Figure 2-3 Test procedure for Transient-State temperature tests

2.3.1. Steady-State temperature tests

In steady-state temperature experiments, the temperature is maintained at a constant value. Steel specimen will be subjected to varying strain rates during the stressing process. As a result, during a steady-state temperature test, the steel specimen is constantly stressed to failure while maintaining a constant temperature as shown in Figure 2-2. As a result, the magnitude of the unchanging temperature and the rate of strain application are the two critical parameters impacting the steel's behavior during steady-state temperature testing. Similarly, for any particular temperature, the strain rate is used to illustrate the effect of thermal creep on the stress-strain behavior of structural steel.

2.3.2. Transient-State temperature tests

Transient-state temperature tests, as the name indicates, are conducted at varying temperatures. As a result, the steel specimen is heated to failure in a transient-state temperature test while the tension remains constant as shown in Figure 2-3. It is reasonable to presume that the amount of the steady tensile or compressive stress and the rate of temperature increase are two critical factors determining the steel's behavior in transient-state temperature material testing. Additionally, the heating rate is used to indicate the influence of thermal creep on the stress-strain behavior of structural steel under constant stress.

2.3.3. Steady-State Temperature Creep Tests

As previously stated, both steady-state and transient-state temperature tests can only depict the influence of thermal creep on the stress-strain behavior of structural steel at elevated high temperatures implicitly. More precisely, steady-state temperature tests simulate the impact of thermal creep by anticipating various stress-strain curves for various strain rates. Similarly, transient-state temperature tests simulate thermal creep by projecting distinct stress-strain curves for various heating rates. As a result of the inherent nature of these two material characterisation tests, the influence of thermal creep on the stress-strain behavior of
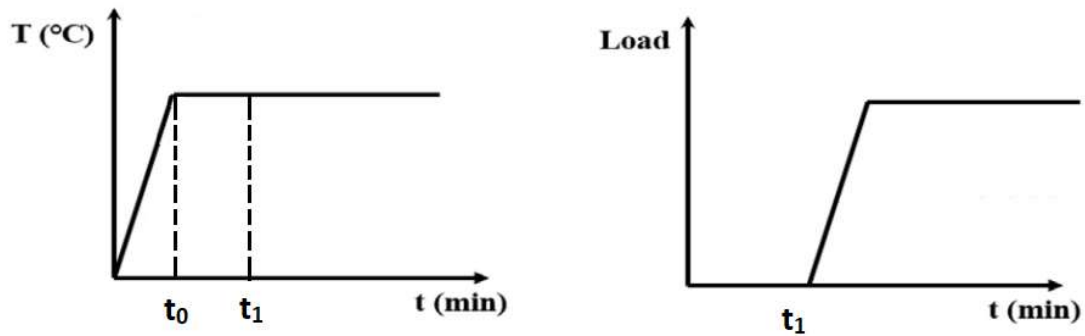
Figure 2-4 Creep test procedure

structural steel at high temperatures cannot be clearly anticipated. In other words, neither of these two approaches is capable of predicting the influence of time on structural steel's stress-strain behavior.

Steady-state temperature creep experiments are used to explicitly consider the influence of thermal creep on the stress-strain behavior of structural steel. A steady-state temperature creep test begins by heating the steel specimen to the specified temperature without applying any stress. The steel specimen is subsequently subjected to tensile or compressive stress. Notably, the stress should be given quickly enough that time-dependent effects may be neglected. Both the applied stress and temperature are thus maintained constant as illustrated in Figure 2-4, and the coupon specimen elongates or compresses exclusively according to the thermal creep of steel, as described in 2.2.1. Typically, the creep test is used to establish the minimum creep rate in the secondary stage. Thus, in steady-state temperature creep tests, the magnitudes of the constant tensile or compressive stress and the constant temperature are the two critical factors controlling the deformation behavior.

2.3.4. Steady-State Temperature Stress Relaxation Tests

To collect the result data, the typical approach requires testing several specimens at various stress and temperature levels over an extended period of time, which is costly and inefficient and is always a significant obstacle to understanding the new material's behavior. The stress relaxation test in which the steel coupons are subjected to constant strain and temperature, and stress is measured as a function of time, is a practical approach to generate high-temperature design curves without long-time creep tests. Short time stress relaxation test generates plots of stress versus either stress rate or inelastic strain rate. On the basis of these plots, the high-temperature performance then can be represented in several ways. Thus, in steady-state temperature relaxation testing, the magnitudes of the constant tensile or compressive strain and the constant temperature are the two critical factors controlling the stress relaxation behavior.

2.4. Survey of previous works

In this section, previous studies on the behavior of structural steel at elevated temperatures are reviewed. It is important to note that time-dependent or creep effects are present in stress-

strain curves for structural steel observed in material tests at elevated temperatures independent of the methods used to perform such tests.

As will be seen, the focus of most of the studies described in the following literature review is on characterizing the effect of thermal creep on the stress-strain behavior of structural steel exposed to fire temperatures through either strain rates or heating rates. In contrast, the literature on the explicit effect of thermal creep on the behavior of steel exposed to fire is quite merger. In fact, to the knowledge of the author of this dissertation, experimental research at Tokyo Institute of technology (Fujimoto, 1980), more recently material studies done at the National Institute of Technology, NIST (NIST, 2005) and done by Wang et al. for high strength steel Q460 (Wang W., 2017) are among the few experimental studies on the explicit effects of thermal creep on the mechanical behavior of structural steel at high temperatures for structural-fire design application purposes.

2.4.1. Research at Tokyo Institute of Technology (Fujimoto, 1980)

The primary objective of the Tokyo Institute of Technology's creep material investigations was to characterize the creep behavior and relationship between creep strain and elastic-plastic strain in structural steel SS 41. This work is limited to the investigation of steel creep behavior under constant load and temperature conditions.

Some of the main traits of the tests, as well as some of the experimental results acquired at Tokyo Institute of Technology's creep material investigations, are discussed, and reviewed below. The following sections provide and discuss only the results of creep material tests on SS 41 structural steel (Fujimoto, 1980).

2.4.1.1. Test specimens

Steel specimens were cut out in the same direction as hot rolling from 25mm thick steel plates. Figure 2-5 illustrates the specimen's size. Tables 1 and 2 contain information on the mechanical properties and chemical composition of SS 41 steel. The gauge length is 50.8mm.
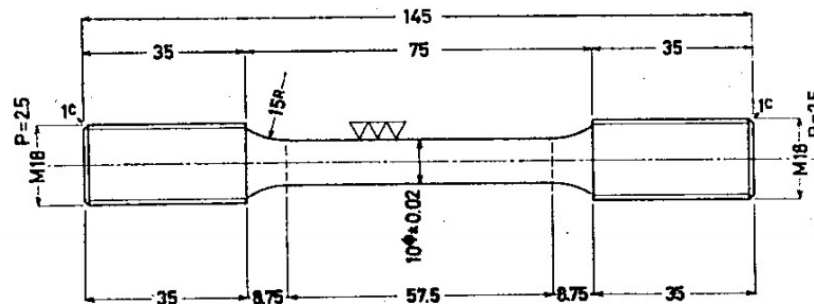
Figure 2-5 Shape and size of a specimen of SS 41 steel (unit:mm) (Fujimoto, 1980)

Table 2-1 Chemical compositions of SS 41 steel (%) (Fujimoto, 1980)

JIS grade	C	Si	Mn	P	S
SS 41	0.18	0.24	0.73	0.016	0.017

Table 2-2 Mechanical properties of SS 41 steel (Fujimoto, 1980)

JIS grade	Yield point (kg/mm^2)	Tensile strength (kg/mm^2)	Elongation (%)
SS 41	24.89	44.0	38.0
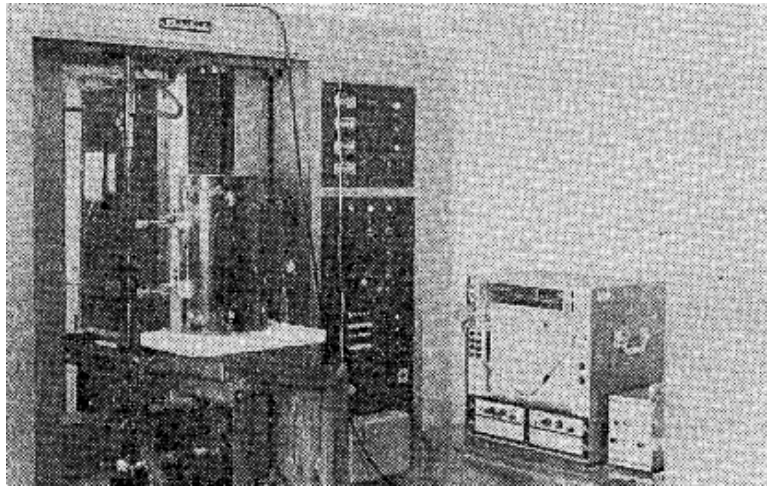
Figure 2-6 General view of the testing machine with furnace and loading assembly (Fujimoto, 1980)

2.4.1.2. Testing procedure

On a universal screw-power testing machine equipped with an electric furnace, creep tests were conducted as shown in Figure 2-6. A time-proportioning, integrating, and differentiating controller was used to regulate the temperature of the furnace.

Special tensile tools made of heat-resistant steel were designed and manufactured for the purpose of transferring load from the crosshead of the testing machine to the specimen within the furnace. The differential transformer for the deformation recording system was installed on small aluminium holders beneath the furnace. These were screwed to four extension arms, which were screwed to the specimen via springs. Figure 2-6 and Figure 2-7 illustrate a specimen with the loading assembly and a high temperature extensometer.

At Tokyo Institute of Technology, all material testing were conducted using steady-state temperature tensile tests, in which the temperature was elevated to the target temperature first and then stresses were applied while the temperature remained constant. The first series of testing included steady-state temperature tension tests, in which strains were applied and increased continually until the steel specimens fractured at constant test temperatures. The second round of tests included steady-state temperature creep experiments in which stresses were introduced and maintained constant at constant temperature. It should be noted that the rate at which stresses are applied to heated coupons can have a substantial effect on their creep and tensile behaviors, particularly at elevated temperatures and stresses. Regrettably, the researchers from Tokyo Institute of Technology did not specify the rate at which stresses were applied to the steel coupons during tension testing or at the start of creep material tests.

At Tokyo Institute of Technology, creep material testing was conducted over a temperature range of 350 °C to 600 °C in 25 °C increments. Additionally, steel coupons were evaluated at three to five different stress levels in 2.5 kg/mm2 (4 ksi) increments at each temperature. Six hours of creep material testing were conducted. Additionally, one steel coupon was evaluated at each combination of stress and temperature.

2.4.1.3. Test results

The results of steady-state temperature tension tests conducted at Tokyo Institute of Technology on specimens of SS 41 structural steel are shown in Figure 2-8. The curves in this figure clearly demonstrate the effect of increased temperatures on the fundamental shape of SS 41 structural steel stress-strain curves. More precisely, at elevated temperatures, the stress-strain curves for SS 41 structural steel become very nonlinear, with the yield plateau disappearing at roughly 400 °C. Additionally, Figure 2-8 illustrates the effect of increased temperatures on the strength and stiffness of SS 41 structural steel. Moreover, the SS 41 structural steel exhibits significant losses in both strength and stiffness at temperatures near and above roughly 500 °C.
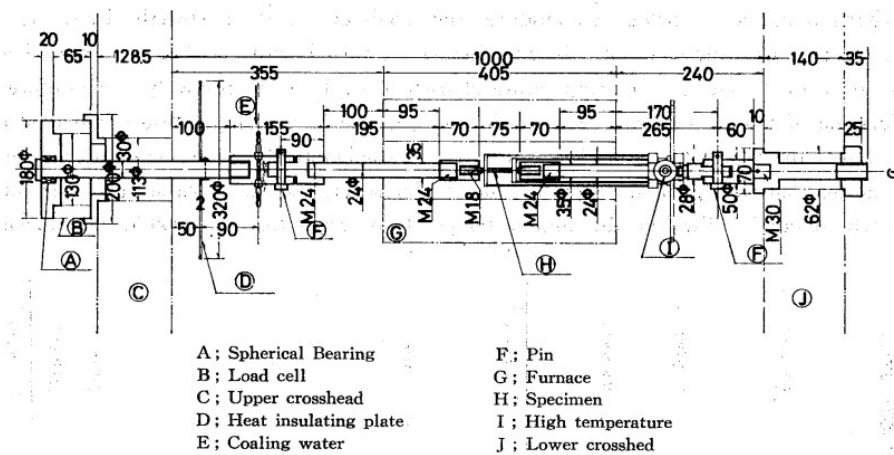
Figure 2-7 The details of the loading assembly and extensometer (Fujimoto, 1980)
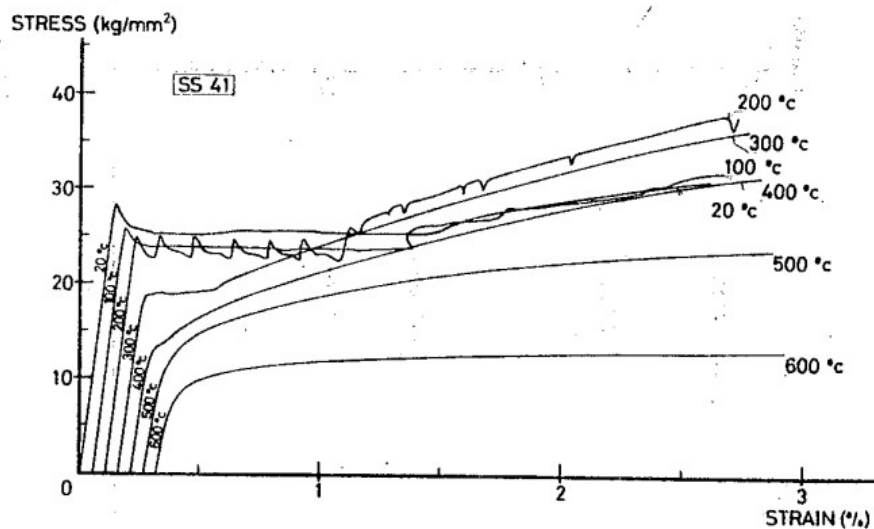
Figure 2-8 Stress-strain curves of SS 41 steel at high temperature (Fujimoto, 1980)

The mechanical properties of SS 41 steel were summarized in Table 2-3 through the steady-state temperature tension tests.

The results of steady-state temperature creep tests conducted at Tokyo Institute of Technology on specimens of SS 41 structural steel are shown in Figure 2-9 and Figure 2-10. These figures illustrate the results of creep testing in the form of total strain as a function of time for various temperature and load combinations. It should be noted that the little arrows depicted in the graphs in Figure 2-9 and Figure 2-10 represent the strains created by the applied stresses at the start of the creep testing.

The strain-time curves depicted in Figure 2-9 and Figure 2-10 demonstrate the critical role of thermal creep in determining the deformation behavior of SS 41 structural steel at high temperatures, particularly above around 450 °C. Additionally, as illustrated in Figure 2-9 and Figure 2-10, creep strains are strongly influenced by the combined effects of temperature, stress, and time. To be more precise, the strain versus time curves presented in these figures demonstrate that at elevated temperatures and stresses, particularly stresses greater than the yield stress at the corresponding temperature, thermal creep of the SS 41 structural steel becomes highly nonlinear, and deformations grow extremely rapidly into the tertiary part.

Perhaps the most significant information supplied by the strain-time graphs in Figure 2-9 and Figure 2-10 is the rapid increase in deformations with time within 30 minutes after the creep material testing on SS 41 structural steel specimens began. This significant increase in deformations during the early phases of thermal creep, in the opinion of the dissertation's author, is another evidence of the potential usefulness of primary creep in anticipating the behavior of steel structural elements and structures exposed to fire.

Table 2-3 Mechanical properties of SS 41 steel at elevated temperatures (Fujimoto, 1980)

Temperature (°C)	Yield strength (kg/mm^2)	Modulus of Elasticity (kg/mm^2)
R.T	24.89	21500
100	23.69	20300
200	22.32	20700
300	18.69	18600
400	16.52	18700
500	15.47	16000
600	10.47	14800
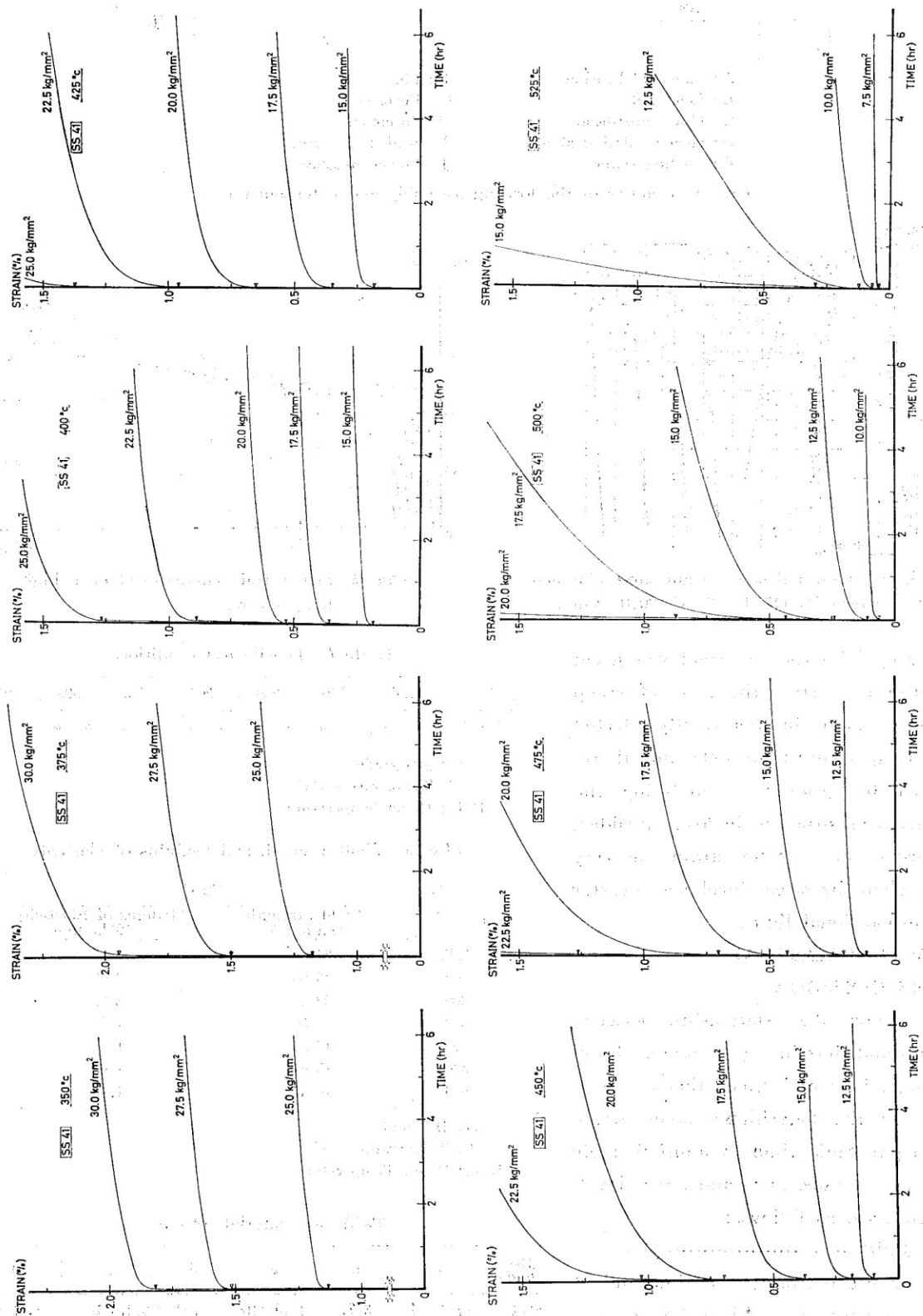
Figure 2-9 Total strain versus time at indicated temperature and stress levels of SS 41 steel
(Fujimoto, 1980)
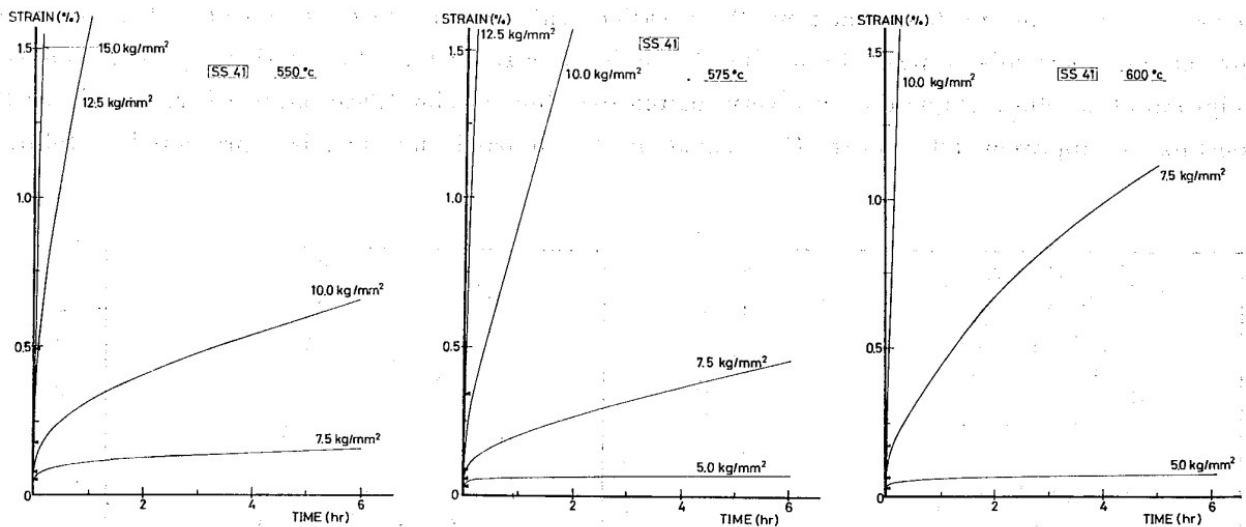
Figure 2-10 Total strain versus time at indicated temperature and stress levels of SS 41 steel (Fujimoto, 1980)

2.4.1.4. Critical observations on Creep material studies

Following Fujimoto's investigation (Fujimoto, 1980), the following observations can be reached:

Axial strains depicted as a function of time represent total strains that take into account the effect of applied loads. Additionally, it is apparent that the temperature, stress level, and time all have a major effect on the creep deformation behavior of structural steel exposed to fire. Moreover, the critical role of primary creep in the deformation behavior of structural steel during a fire is evident in Figure 2-9 and Figure 2-10, where strains develop rapidly during the early stages of creep tests.

2.4.2. Research on World Trade Center structures to the fire (NIST, 2005)

The NIST World Trade Center Disaster Investigation was a report that the National Institute of Standards and Technology (NIST) conducted to establish the likely technical causes of the three building failures that occurred at the World Trade Center following the September 11, 2001 terrorist attacks. This section reviewed and discussed the NIST tensile and creep tests in order to establish the most accurate and simple approach for determining creep behavior.

2.4.2.1. Tensile tests (NIST, 2005)

2.4.2.1.1   Test procedures

Two distinct machines were used to conduct high-temperature tensile tests. The floor truss steels were tested using an electromechanical testing machine (Instron 8562) equipped with a contact extensometer with a gauge length of 12.5 mm. The furnace is a split design with $MoSi_2$ elements. The specimens are classified ASTM International (ASTM) E 21 type Flat C2. The uniform cross section is 32 mm in length and 3 mm in width. They were fitted with superalloy wedge grips that were pin aligned. A K-type thermocouple positioned within 1 mm of the specimen surface was used to measure the specimen temperature. The specimens

were loaded as soon as the furnace temperature reached the test temperature, which was typically within 20 minutes. The specimen temperature was always within 5 °C of the intended temperature during the temperature stabilization procedure. The crosshead speed was 0.0325 mm/s in these experiments, resulting in a strain rate after yielding of roughly 0.001 s^{-1} as recorded by the extensometer. Prior to yield, the displacement rate of the crosshead resulted in a specimen stressing rate of 4±2 MPa/s. These rates comply with ASTM E 8 and E 21.

The majority of the remaining tests were conducted using a second electromechanical machine equipped with a high-temperature extensometer with a gauge length of 1.0 in. The furnace is a split design in which the specimen is heated by quartz lamps. The specimens, type Flat C1, have a 1.1 in. uniformly long and 0.25 in. wide cross section. Typically, the specimen thickness was the same as the plate's initial thickness. These tests were conducted in accordance with ASTM E 21's loading protocol. The initial displacement rate of the crosshead was 0.00167 mm/s. After a few percent strain was applied, the crosshead rate was increased to 0.0167 mm/s, as specified by E 21, which results in a perceptible step in the flow stress during elevated temperature tests.

2.4.2.1.2   Tensile test results

The curves in Figure 2-11, which depict data from specimen N8-C1B1A-FL, are representative of high-temperature stress-strain curves for all specimens tested. Because the researcher frequently removed the extensometer before to failure, the end points of the curves are not always indicative of failure. Due to the fact that part of these tests followed the ASTM E 21 loading technique, there is a significant increase in flow stress at approximately = 0.02 that corresponds to the obligatory extension rate change. The jump is minor at low temperatures, where the strain rate sensitivity is low, but it can be as great as 5 ksi at elevated temperatures.
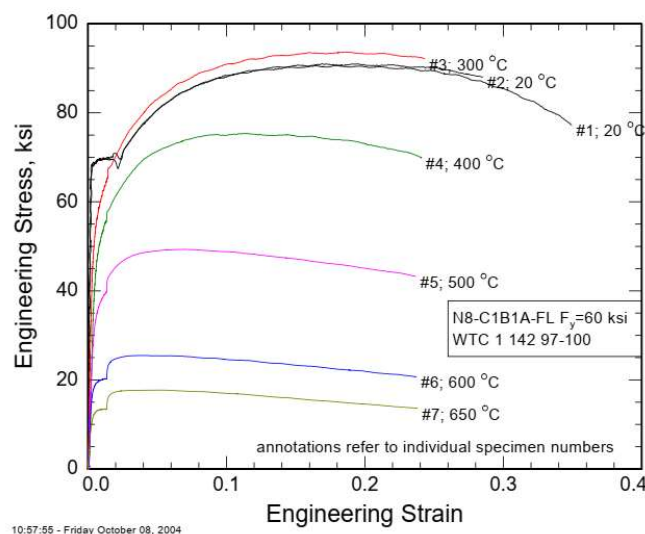
Figure 2-11 Elevated temperature stress-strain curves for specimen N8-C1B1A-FL (F-$_y$=60ksi) from a perimeter column flange plate from WTC 1 column 142 between floors 97–100 (NIST, 2005)

At elevated temperatures, the stress-strain curves become extremely nonlinear, with the yield plateau disappearing at approximately 300 °C. Additionally, Figure 2-11 depicts the influence of elevated temperatures on the strength and stiffness of steel obtained from specimen N8-C1B1A-FL. Moreover, the steel with Fy=60ksi demonstrates considerable strength and stiffness losses at temperatures around and above approximately 600 °C.

2.4.2.2. Creep tests (NIST, 2005)

2.4.2.2.1   Test procedures

Two distinct types of machinery were used in creep testing. Several researchers used the same electromechanical test machine equipped with a $MoSi_2$ furnace as in the previous high-temperature tensile testing. The majority of testing were conducted using two identical classic dead-load lever-arm creep frames (Applied Test Systems) equipped with split, wire-wound, three-zone NiCr furnaces. These furnaces employ averaging, clamp-on extensometers with a nominal gauge length of 25.4 mm. Loading the specimens was accomplished manually by adding masses to the weight pan. In most cases, it took less than three minutes to achieve maximum capacity. Throughout the test, the operator decreased mass from the weight pan in approximately 3% strain increments to maintain consistent stress. The strain-time curves exhibit kinks as a result of these modifications. The specimens used in the tests were of type Flat C2. Temperatures of 400 °C, 500 °C, 600 °C, and 650 °C were used to conduct creep experiments. Each specimen was subjected to one stress-temperature condition. Individual specimen stresses ranged from 100 to 445.8 MPa. Generally, tests were terminated after two hours if the specimen did not fail, while some tests were allowed to run longer.

2.4.2.2.2   Creep test results

Truss steel from a 2 in. × 1.5 in. × 0.25 in. truss top chord angle from specimen C-132 was characterized for creep. This steel was specified to conform to A 242 with Fy = 50 ksi. The creep test matrix comprised of twenty creep tests conducted until failure or until several hours had passed. The creep curves for examples from the truss upper chord are shown in Figure 2-12 to Figure 2-15.

2.4.2.3. Critical observations on Creep material studies

Following NIST's investigation (NIST, 2005), the following observations can be reached:

One important observation on Figure 2-12 to Figure 2-15 is that the creep deformation behavior of structural steel subjected to fire is significantly affected by the temperature, stress level and time. Specifically, the strain versus time curves in these figures demonstrate that at elevated temperatures and stresses, particularly stresses greater than the yield stress at the corresponding temperature, thermal creep of A242 steel becomes highly nonlinear, and deformations grow extremely rapidly.
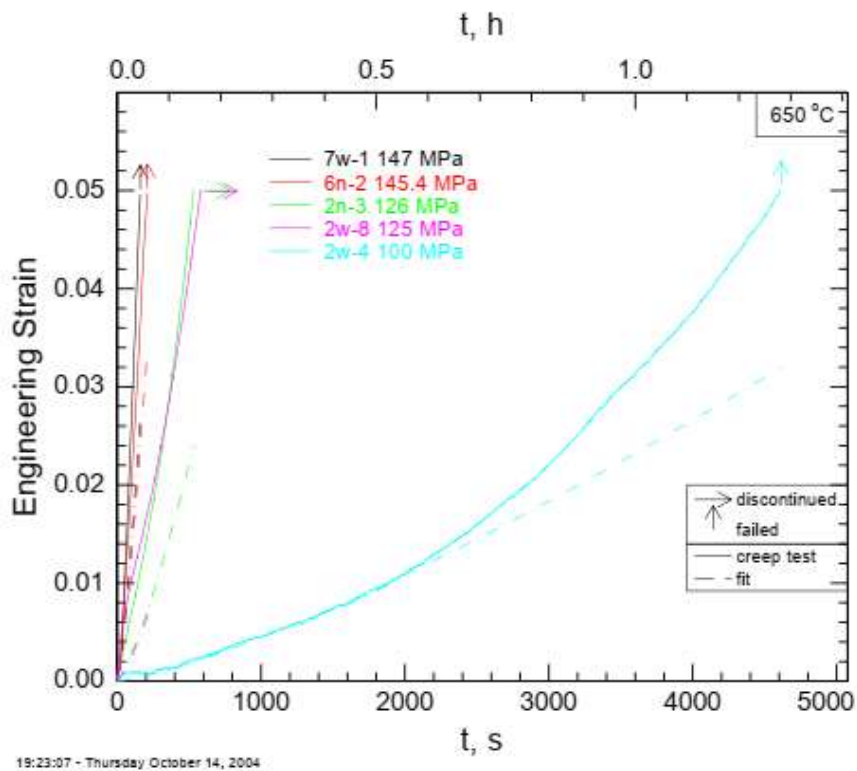
Figure 2-12 Creep curves of A 242 truss steel from specimen C-132 at 650 °C (NIST, 2005)
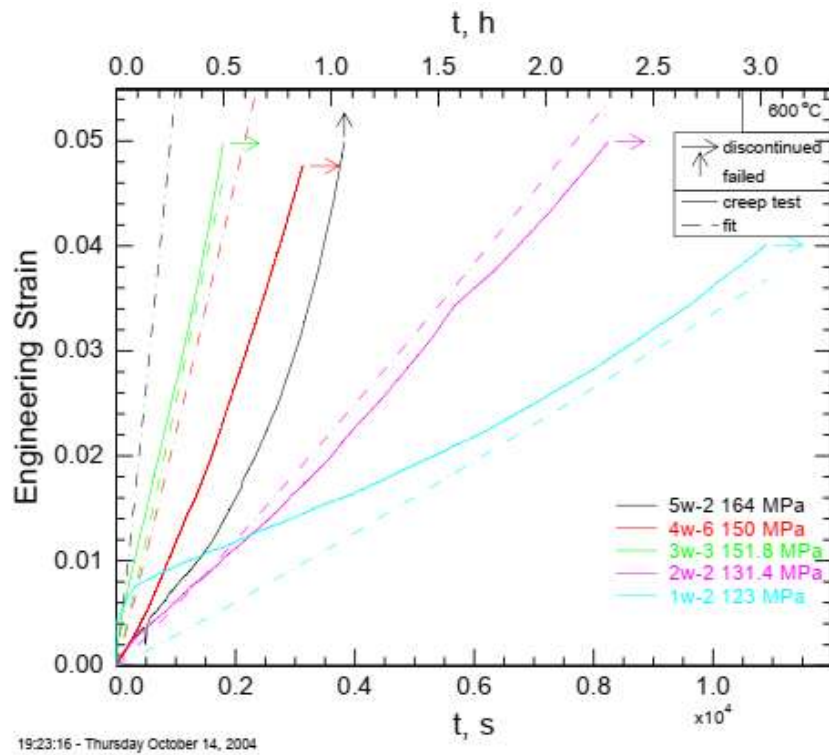
Figure 2-13 Creep curves of A 242 truss steel from specimen C-132 at 600 °C (NIST, 2005)
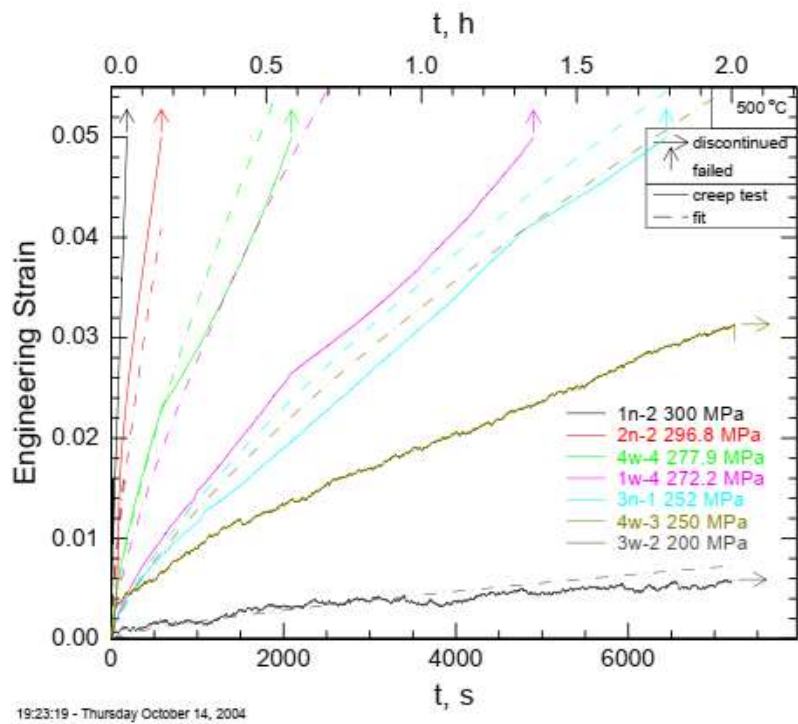
Figure 2-14 Creep curves of A 242 truss steel from specimen C-132 at 500 °C (NIST, 2005)
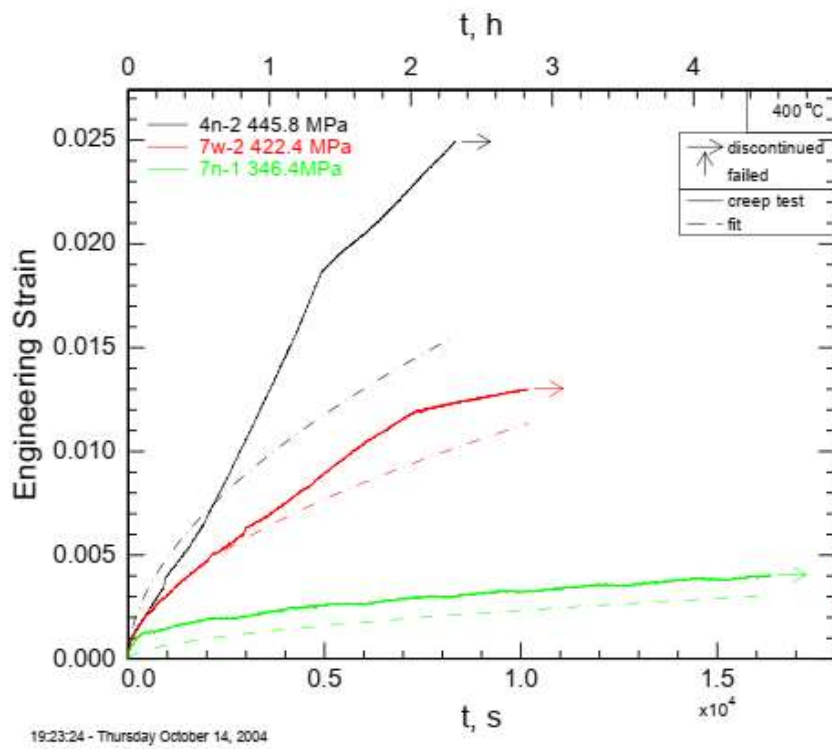
Figure 2-15 Creep curves of A 242 truss steel from specimen C-132 at 400 °C (NIST, 2005)

2.4.3. Research on Q460 steel (Wang W., 2017)

One such widely used high strength steel in building applications in China and Far East region is Q460 steel. To gain a better understanding of the mechanical behavior of high strength steel at elevated temperatures, this section reviewed and discussed the tensile and creep tests done by Wang and his colleagues.

2.4.3.1. Tensile strength tests

Prior to conducting creep tests, tensile strength tests were conducted to determine the Q460 steel's stress–strain response under ambient conditions (Wang W., 2017). Tensile strength coupons were designed and manufactured in accordance with GB/T 228.1-2010 (GB/T 228.1-2010, 2010). These experiments were conducted on an MTS-CWT5305 load cell capable of 300 kN. At room temperature, the stress–strain response of Q460 steel is determined using tensile test results.

A total of ten coupon tests (MS-1 to MS10) were conducted, with the specimen consisting of a 20-mm-thick steel sheet. The displacements measured during the tension test were utilized to construct the stress–strain response curves for Q460 steel, which are displayed in Figure 2-16.

As shown in Figure 2-16, the typical trend of stress–strain curves at room temperature is linear-elastic up to yield in steel, which is 492 MPa, followed by a strain hardening response. Steel suffers necking and rupture when the utmost stress is attained, which is 621 MPa. According to the strain–stress curves, the averaged elastic modulus and ultimate strain are 202 GPa and 23.5 percent, respectively.

2.4.3.2. Creep tests at high temperatures

To conduct creep testing on Q460 steel, a complete test program was developed (Wang W., 2017). Creep experiments were conducted at nine different temperatures between 300 and 900 °C, namely 300, 400, 450, 500, 550, 600, 700, 800, and 900 °C, and at varied stress levels ranging from 13 to 509 MPa.
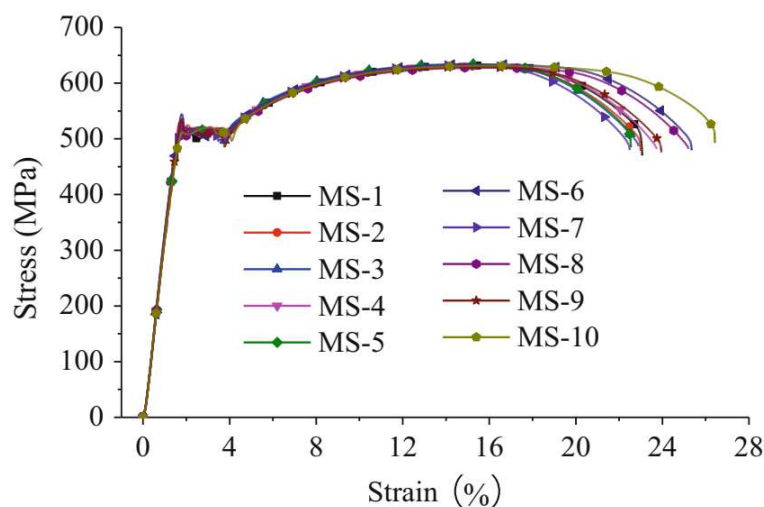
Figure 2-16 Stress-strain curves of Q460 steel at room temperature (Wang W., 2017)

2.4.3.2.1   Test set-up

To conduct high temperature creep tests, specialized high temperature creep test equipment was devised and manufactured (Wang W., 2017). As seen in Figure 2-17, a test setup for high temperature creep includes tensile testing equipment, an electric furnace, a strain measurement device, and a data collecting system. MTS loading system with a load capacity of 50 kN is used for tensile testing. The axial deformation of the test coupon at elevated temperatures can be detected in this equipment using two displacement transducers (10 mm LVDTs) with a sensitivity of 0.001 mm that are mounted outside the furnace via two connecting rods inserted inside in Figure 2-18. The cylindrical chamber of the electric furnace has a maximum heating length of 150 mm. The specimen is clamped between two-cylinder grips with threads on the interior during creep tests. The programmable furnace generates target temperatures of up to 1100 °C at a predetermined rate of temperature rise and maintains the target temperature inside the furnace constant throughout the creep test. Three thermocouples are put inside the furnace to monitor temperatures in the upper, middle, and lower zones, and the average of these three thermocouple readings is used to determine the furnace temperature as shown in Figure 2-19. The furnace and LVDTs are coupled to a data acquisition system and a computer, which allows for the recording of temperature, tension load, and displacements during the creep test.

Figure 2-17 Creep test set-up for Q460 steel (Wang W., 2017)

Figure 2-18 LVDTs systems (instrumentations on test Q460 specimen) (Wang W., 2017)

Figure 2-19 Thermocouples set-up (instrumentations on test Q460 specimen) (Wang W., 2017)
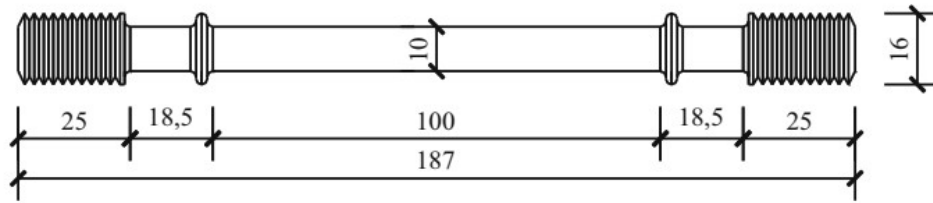
Figure 2-20 Dimensions of Q460 steel coupon for high temperature creep test (unit: mm) (Wang W., 2017)

Table 2-4 Selected temperature and stress level for creep tests of Q460 steel (Wang W., 2017)

Temperature (°C)	Yield strength (MPa)	Stress levels (MPa)	Load levels
300	575	457, 483, 495, 509	0.79–0.89
400	518	406, 432, 457, 476	0.78–0.92
450	532	369, 382, 394, 400, 406	0.69–0.76
500	430	242, 254, 267, 280	0.56–0.65
550	374	165, 178, 204, 210	0.44–0.56
600	367	89,102, 114, 127, 178	0.24–0.49
700	182	25.5, 38,51, 64	0.14–0.35
800	89	13, 19, 25.5, 32, 38	0.15–0.43
900	–	13, 19, 25.5, 32	–

2.4.3.2.2   Test specimens

Numerous round steel coupons were cut from a 20 mm thick Q460 steel sheet for high temperature creep tests (Wang W., 2017). 45 creep test specimens were manufactured in all. The overall length of the test coupons is 187 mm, and the gauge length for creep measurement is 100 mm. The tapered section has a cross section diameter of 10 mm. Figure 2-20 illustrates the structure of a typical creep test coupon. The stress levels (load ratio) and target temperatures used in these experiments are listed in Table 2-4, together with the yield strength (1.0 percent strain) of Q460 at elevated temperatures. The load ratio is defined as the ratio of the applied stress to the yield strength of the specimen at a specified temperature. When the stress level in steel is too high, the coupon will rupture within a short period of time. On the other hand, a coupon demonstrates a subtle creep response when exposed to mild levels of stress. During creep experiments, the stress levels were altered to investigate the creep effect on mechanical behavior at various temperatures.

2.4.3.2.3   Test procedure

Creep experiments were conducted utilizing the test setup mentioned above at various temperatures and load levels. To conduct these creep experiments, steel coupons were placed in the MTS machine's grips and three thermocouples were affixed at the top, bottom, and mid-length of the specimen's gauge length, as shown in Figure 2-19. These thermocouples are used to measure the furnace's real temperature during the creep test. The specimen was then surrounded by an electric furnace, with extra care taken to ensure that the coupon was placed

in the furnace's core. Following that, the furnace is turned on and heated to the specified target temperature at a rate of 10 °C/min. Once the target temperature was reached, the steel coupon was held at that temperature for 30 minutes to establish a steady-state condition, and then held at that temperature for the length of the test. Then, at a rate of 10 kN/min, a predefined load was applied. Because the maximum force applied during the creep testing is 40 kN, the loading phase should not exceed 5 minutes. After the applied load meets the intended load, creep displacements were determined using two highly sensitive LVDTs. The overall length of the coupon exposed to high temperature during a creep test is 150 mm, however only the central 100 mm is used as the gauge length for calculating the corresponding creep strain ($\Delta L/L$).

Creep experiments were conducted using this approach at various stress levels and temperatures. When the creep deformation approaches the maximum allowable displacement of the LVDTs, namely 10 mm, the LVDTs were promptly corrected by hand and the data were collected constantly. This allowed for the measurement of creep deformation over a large displacement range, up to the maximum movement of the hydraulic jack.

2.4.3.2.4   *Creep test results: Creep-time curves at various stress levels*

The creep strains recorded by Wang et al. at various stress levels and temperatures ranging from 300 to 900 degrees Celsius are depicted from Figure 2-21 to Figure 2-23. It is important to note that the creep strain versus time curves shown here do not include the instantaneous strain but simply the resulting creep strain. On the X axis, zero time corresponds to the moment when the coupon received its complete loading. Generally, the creep strain at a higher stress level is greater than the creep strain at a lower stress level at a given temperature. Increased creep strain at increased stress levels can be linked to dislocation movement caused by atomic diffusion at elevated temperatures and stresses.

The creep behavior at lower temperatures (300–400 °C), as illustrated in Figure 2-21, can be classified into two stages, primary and secondary stages. During secondary stage, the increase in secondary creep strain with time is temperature and stress dependent. At low stress levels, secondary creep at 300 and 400 °C is minimal. Tertiary creep, on the other hand, occurs at temperatures of 400 °C and a stress level of 476 MPa.

Secondary creep and tertiary creep increased rapidly, and the majority of specimens ruptured throughout the moderate temperature range of 450–550 °C (Figure 2-22). When stress levels are quite high, the maximum creep strain is relatively low before to rupture. At lower stress levels, however, the maximum creep strain before rupture increases significantly. The increase in maximum creep strain with decreasing stress levels can be attributed to better plasticity development in steel over a longer time period, and creep in steel has a longer duration at lower stress levels. At 500 °C, for example, the maximum creep strain at 267 MPa is significantly greater than that at 280 MPa, despite the fact that both specimens ruptured. At temperatures of 450 and 550 °C, the similar pattern is observed.
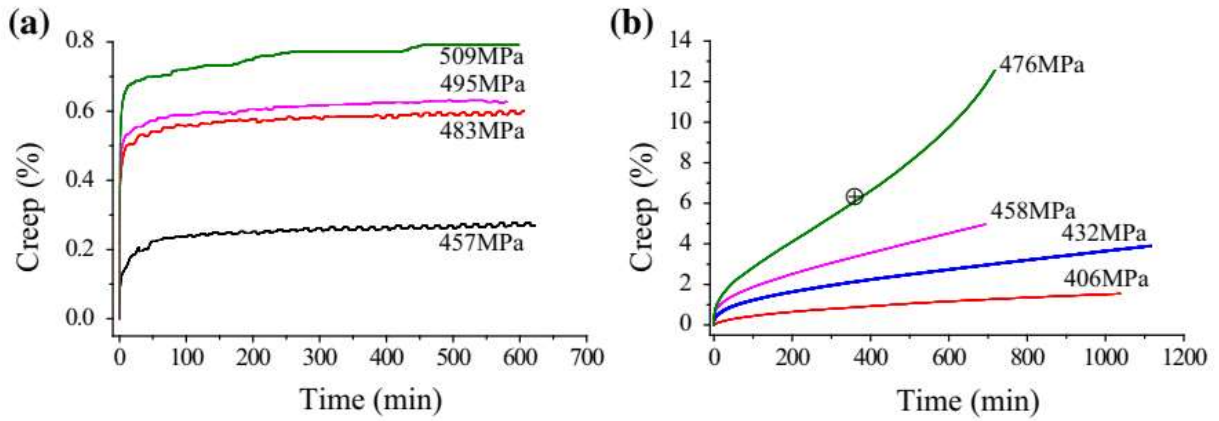
Figure 2-21 Creep strain response in Q460 steel at 300 °C (a) and 400 °C (b) at various stress levels (Wang W., 2017)
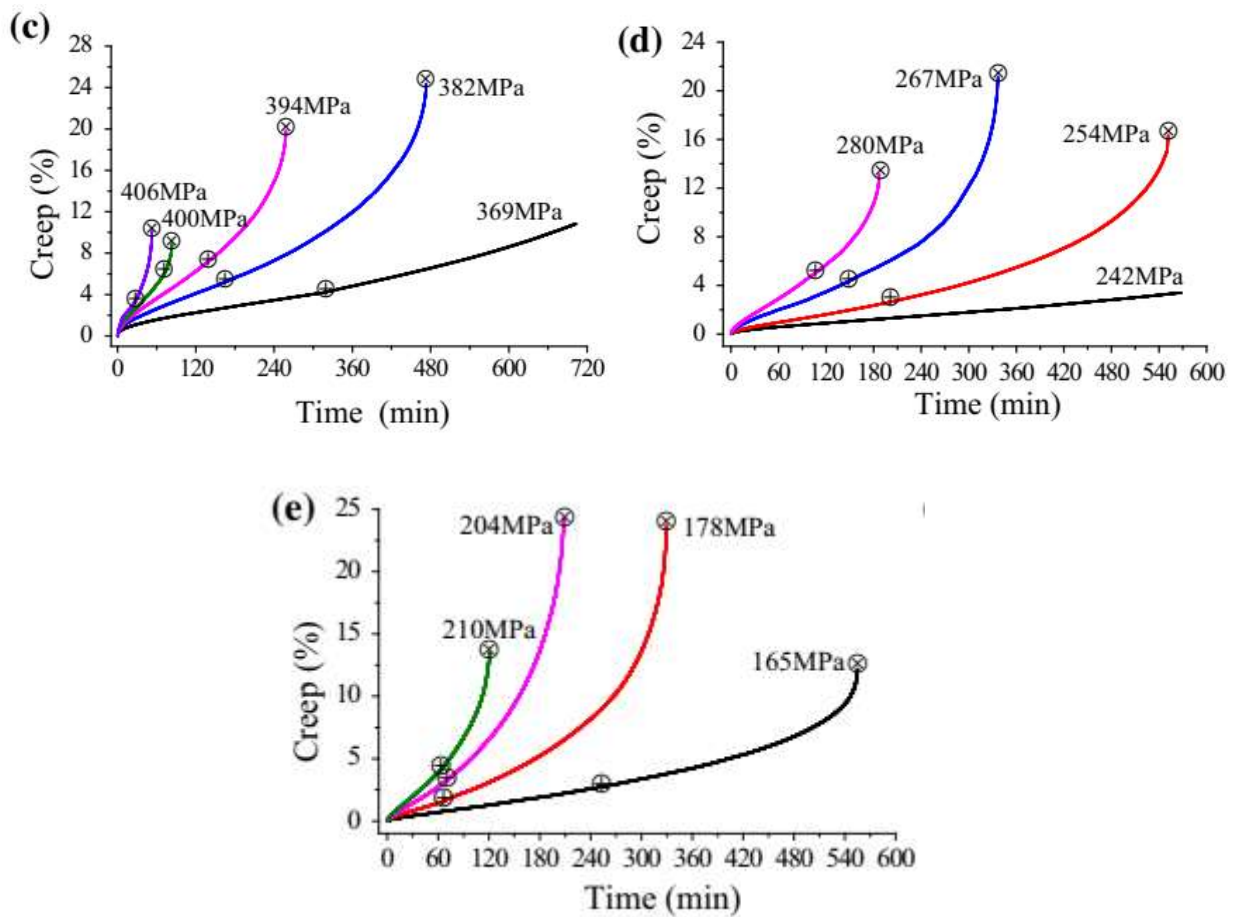
Figure 2-22 Creep strain response in Q460 steel at 450 °C (c), 500 °C (d) and 550 °C (e) at various stress levels (Wang W., 2017)
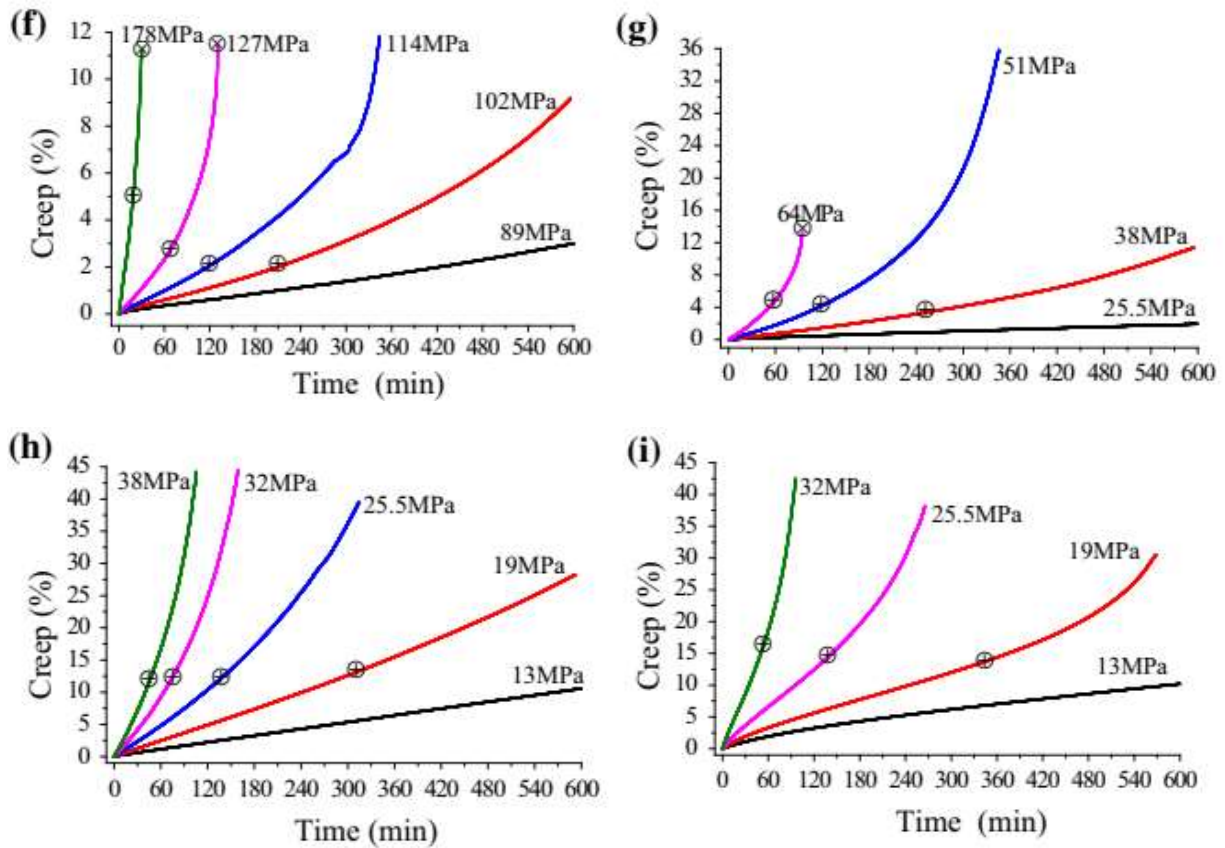
Figure 2-23 Creep strain response in Q460 steel at 600 °C (f), 700 °C (g), 800 °C (h) and 900 °C (i) at various stress levels (Wang W., 2017)

When temperatures are extremely high (600–900 °C), the creep response can also be classified into two stages (Figure 2-23), secondary and tertiary stages. Primary creep becomes extremely rapid, and the deformation is fully formed in a short amount of time. Thermal softening accounts for the rapid increase in creep strain with time in secondary stage. Secondary creep is critical under fire exposure conditions because it dominates the creep reaction, occurs at a steady rate, and occurs rapidly. In tertiary stage, secondary creep accelerates due to the specimen's smaller cross section caused by the necking phenomena, which results in increased stresses for the same applied load. Steel's ductility increases as the temperature rises, and the maximum creep values increase proportionately. Due to the hydraulic jack's restriction on movement, it was not possible to obtain rupture of some specimens between 600 and 900 °C. However, the restricted data has little effect on steel's creep reaction because tertiary creep is not as significant in structural analysis as secondary creep.

2.4.3.2.5   Creep test results: Creep-time curves at various temperature levels

Figure 2-24 illustrates the effect of temperature on the creep response of Q460 steel. As illustrated in Figure 2-24 (a)-(c), creep at a given stress level increased dramatically with temperature in the range 300–700 °C, even when the temperature was only raised 50 °C. For example, at a stress level of 406 MPa, creep at 450 °C is significantly greater than creep at 400 °C. As a result, creep deformation increases with temperature at a given stress level.

26

However, as illustrated in Figure 2-24 (d), the general trend observed above does not hold true at temperatures between 800 and 900 °C. The creep strain at 900 °C is comparable to that at 800 °C under the same stress level, regardless of the stress level. The patterns in the figure illustrate that creep deformation increases significantly as temperature increases up to 800 °C and then remains constant as temperature increases.

2.4.3.3. Critical observations on Creep material studies

Following Wang et al.'s investigation (Wang W., 2017), the following observations can be reached about high strength steels:

Creep strain increases with rising stress level at a given temperature and also with increasing temperature at a given stress level. Even at extremely high stress levels, high temperature creep strain is negligible until 300 °C. Creep strain, on the other hand, becomes dominant at temperatures greater than 400 °C for moderate to high stress levels.

Primary and secondary creep dominate the creep response of steels up to 400 °C, but tertiary creep becomes prominent if the temperature of the steel exceeds 400 °C. At moderate temperatures of 450–550 °C, secondary creep and tertiary creep grew rapidly. As stress levels are extremely high, the maximum creep strain is relatively low prior to fracture; nevertheless, when stress levels are reduced, the maximum creep strain becomes significantly greater prior to fracture. Creep strain increases with temperature up to 800 °C and becomes highly dominating above 500 °C, even at relatively moderate stress levels.
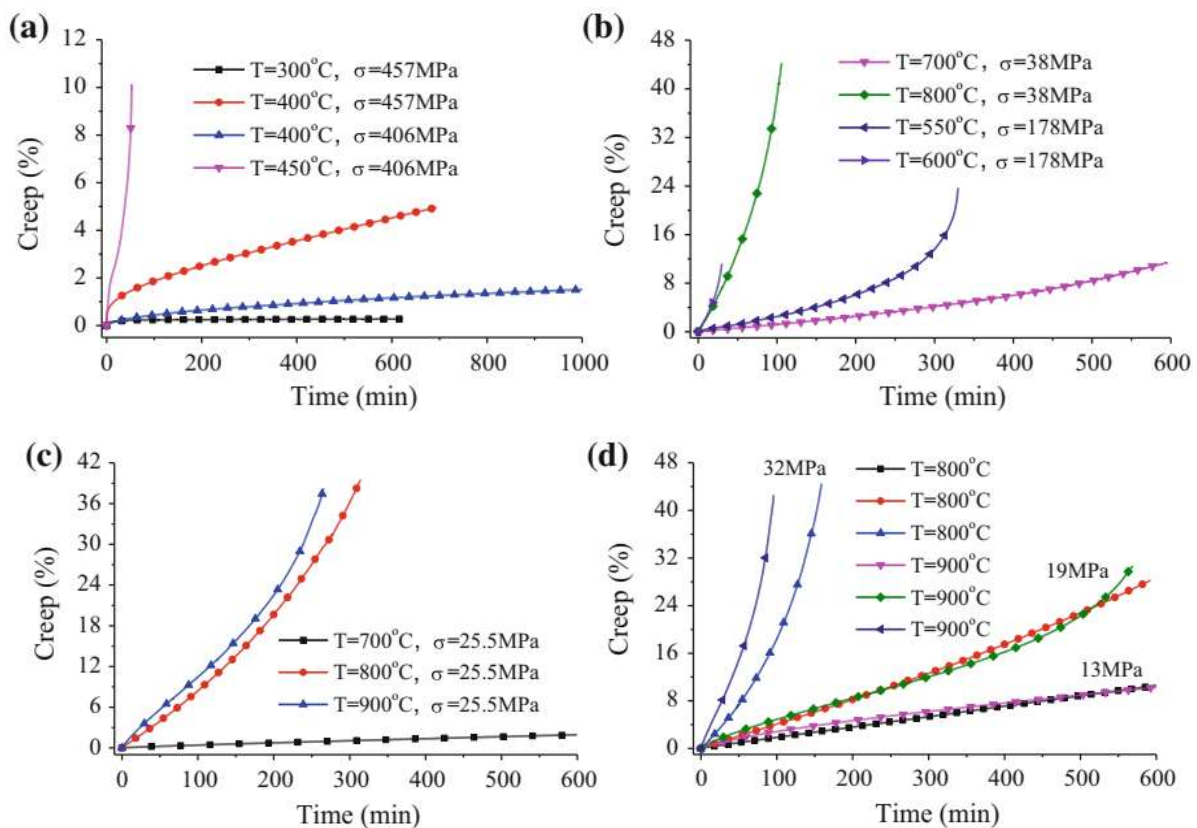
Figure 2-24 Creep strain response in Q460 steel at various temperature levels and at various stress levels (Wang W., 2017)

2.5. Constitutive Models for thermal creep of structural steel

A comprehensive review of the literature on structural steel thermal creep reveals that various researchers have proposed both experimental and empirical constitutive models to characterize structural steel thermal creep for structural-fire design applications (Harmathy (Harmathy, 1967), Fujimoto et al. (Fujimoto, 1980), Williams-Leir (Williams-Leir, 1983), Fields and Fields (Fields, 1989), NIST (NIST, 2005) and Wang (Wang W., 2017). This section reviews and introduces three creep models, one established by Fields and Fields (Fields, 1989), the other by the National Institute of Standards and Technology, NIST (NIST, 2005) and a constitutive creep model for high strength steel Q460 by Wang et al. (Wang W., 2017). Chapter 4 and Chapter 5 will discuss the use of these two creep models Fields and Fields, and NIST to calculating the buckling strength of steel columns exposed to fire temperatures.

It is critical to mention that Fields and Fields (Fields, 1989) material creep models were utilized to investigate the creep behavior of high strength steel columns in this research since they are frequently used and cited in structural-fire engineering applications and also because they have simple forms.

2.5.1. Creep Model proposed by Fields and Fields

Norton's (Norton, 1929) -Bailey's (Bailey, 1930) creep power law is one of the simplest and most commonly used creep models for metals. While the Norton-Bailey law was established principally to represent primary creep, it can also be used to characterize the steady-state or secondary stage of creep. Despite its simplicity, the power-law material creep model (Norton, 1929) (Bailey, 1930) is an extremely useful tool for investigating the phenomenon of time-dependent behavior of structural steel columns exposed to elevated temperatures due to fires.

Another of widely used creep models in structural-fire engineering applications proposed by Fields and Fields (Fields, 1989) also incorporates a power law and represents creep strain, ε_c, in the form of a Norton-Bailey equation using a function that separates the time and stress dependent as follows:

$$\varepsilon_{\mathrm{c}} = At^B\sigma^C \tag{2.3}$$

In this equation, t is time, σ is stress, and parameters A, B and C are temperature dependent material constants. These material constants are calculated by the formulas in equations (2.4)-(2.6).

$$B(T) = B_0 + B_1 T \tag{2.4}$$

where $B_0 = 1.1$ and $B_1 = 0.0035$

$$C(T) = C_0 + C_1 T \tag{2.5}$$

where $C_0 = 2.1$ and $C_1 = 0.0064$

$$A(T) = 10^{-(A_0 + A_1 T)} \tag{2.6}$$

where for $T < 500°C$, $A_0 = 6.10$, $A_1 = 0.573$

and for $T > 500°C$, $A_0 = 13.25$, $A_1 = -0.00851$.

In equation (2.3)-(2.6), T is in °C, t is in minutes, σ is in ksi, and ε_c is in percent (unitless).

It should be noted that Fields and Fields (Fields, 1989) did not conduct any creep experiments themselves; instead, they studied Knight's creep data for AS A149 steel (Knight, 1971) and built a creep model in the form of the Norton-Bailey creep power law. Additionally, they used their model to forecast the strain-time behavior of SS41 steel (Fujimoto, 1980). As a result, Fields and Fields (Fields, 1989) did not build their creep model using ASTM A36 steel creep test results. Indeed, Fields and Fields (Fields, 1989) claimed that, based on similarities in chemical composition and yield strengths, the creep data for AS A149 and SS 41 steels could be utilized to predict the thermal creep of ASTM A36 steel. Additionally, it is critical to note that the model established by Fields and Fields (Fields, 1989) is capable of forecasting creep at temperatures ranging from 350 to 650 ° C. and creep strains up to 6%. Later in this dissertation, the use of this creep model in combination with findings will be described in greater detail.

2.5.2. Creep Model proposed by NIST

During the WTC investigation (NIST, 2005), NIST also discovered that creep behavior is a critical input to finite element models of the WTC structures' response to fires. They characterized the actual creep behavior of the important truss angle steel that made up the chords of the floor trusses in their studies. Furthermore, they developed a methodology for estimating the creep behavior of the other steels in the trusses, truss seat, perimeter columns, and core columns based on literature data. Their analysis retains the formalism of Fields and Fields (Fields, 1989), but they evaluated the temperature dependent parameters A, B, and C using different equations than Fields and Fields.

The constant C is evaluated as the stress exponent for creep rate $\frac{d\varepsilon}{dt}$ using extra strain rate data from the high-temperature tensile tests, and non-linear least squares fit to the $(\frac{d\varepsilon}{dt}, \sigma, T)$ data shown in equation (2.7)

$$C(T) = C_0 + C_1 T \tag{2.7}$$

where $C_0 = 3.233$ and $C_1 = 0.0117$

To ensure accurate representation of the creep behavior near and outside the boundaries of the experimental conditions, the parameter B was evaluated by the non-linear, least-squares fitting method in equation (2.8)

$$B(T) = B_0 + B_1 T^{B_2} \tag{2.8}$$

where $B_0 = 0.3982$, $B_1 = 3.5531 \times 10^{-1}$ and $B_2 = 3.6975$

Using the linear regression method, the parameter A could be represented by an exponential of a quadratic polynomial of temperature as shown in equation (2.9)

$$A(T) = \exp\left(A_0 + A_1 T + A_2 T^2\right) \tag{2.9}$$

where $A_0 = -55.4504$, $A_1 = 9.47600 \times 10^{-3}$ and $A_2 = -3.52064 \times 10^{-5}$; T is in $°C$, t is in seconds, σ is in MPa, and ε_c is in natural units (unitless).

2.5.3. Creep Model proposed by Wang

In China, structural steel with a high strength of Q460 (Wang W., 2017) is commonly utilized in construction. A complete investigation of high temperature creep in Q460 steel having high strength was conducted. A series of creep experiments on Q460 steel coupons was conducted as part of this investigation at various stress levels ranging from 300–900 C. A creep model based on the creep power law as illustrated in (2.3) is developed for Q460 steel using this high temperature creep data.

To simulate the high temperature creep response of Q460 steel using the Fields and Fields creep model, a nonlinear regression fitting tool was used to determine the values of the coefficients a, b, and c at various temperatures using creep test data in Q460 steel. For example, while fitting test data at 300 C, four creep–time curves are chosen, and a predefined Fields and Fields creep model is used. Then the ranges of values for a, b, and c are defined. After finishing fitting, if the corrected R-square is greater than 0.95, the fitting values are accepted. Otherwise, more ranges are defined until the corrected R-square equals 0.95. As with the formulas in equations (2.4)-(2.6), a nonlinear regression fitting tool was used to model the values of the coefficients a, b, and c as a function of temperature using creep test data for Q460 steel (Wang W., 2017). Equations (2.10)-(2.12) provide the values of a, b, and c for Q460 steel.

$$\text{Log}\,a = \begin{cases} -56.797 + 0.2265T - 3.562 \times 10^{-4}T^2 & 300°C \leq T \leq 450°C \\ 2286.225 - 13.65927T + 2.65644 \times 10^{-2}T^2 - 1.6964 \times 10^{-5}T^3 & 450°C \leq T \leq 600°C \\ -69.01 + 0.155T - 1.040 \times 10^{-4}T^2 + 1.420 \times 10^{-8}T^3 & 600°C \leq T \leq 900°C \end{cases} \tag{2.10}$$

$$b = \begin{cases} -2.71 + 0.0128T - 1.20 \times 10^{-5}T^2 & 300°C \leq T \leq 450°C \\ -14.96 + 0.08T - 1.36 \times 10^{-4}T^2 + 7.81 \times 10^{-8}T^3 & 450°C \leq T \leq 600°C \\ 1.18 - 7.07 \times 10^{-3}T + 1.9 \times 10^{-5}T^2 - 1.31 \times 10^{-8}T^3 & 600°C \leq T \leq 900°C \end{cases} \tag{2.11}$$

$$c = \begin{cases} 39.25 - 0.18T + 2.75 \times 10^{-4}T^2 & 300°C \leq T \leq 450°C \\ -1557.61 + 9.21T - 1.78 \times 10^{-2}T^2 + 1.132 \times 10^{-5}T^3 & 450°C \leq T \leq 600°C \\ 22.52 - 2.07 \times 10^{-2}T - 3.34 \times 10^{-5}T^2 + 3.45 \times 10^{-8}T^3 & 600°C \leq T \leq 900°C \end{cases} \tag{2.12}$$

2.6. Summary

The purpose of this chapter is to describe the time- and temperature-dependent behavior of structural steel, referred to as thermal creep, and its relevance in forecasting the creep behavior of steel columns exposed to elevated temperatures caused by fire. The chapter began with discussing the definition of structural steel thermal creep. The effect of thermal creep on the stress-strain behavior of structural steel was then quantified using a variety of methods. Following the discussion of various methodologies for calculating the time- and temperature-dependent behavior of structural steel exposed to fire, a literature review of previous studies was conducted. Important constitutive models for the thermal creep of structural steel at elevated temperatures were further reviewed.

Several major findings are made in the following section based on the background information provided on the phenomenon of time- and temperature-dependent stress-strain behavior of structural steel exposed to fire and on a review of previous research. These observations serve to establish the foundation for the dissertation's research.

> ➢ As demonstrated in this chapter's literature review, creep deformations can be quite significant at temperatures, stress levels, and time durations representative of building structures subjected to fire. This implies that neglecting creep may result in very erroneous structural response estimates for structural steel, particularly for high strength steels.
>
> ➢ A fundamental finding of this chapter's literature assessment is that there is a scarcity of experimental data on thermal creep of structural steels used in building construction at the temperatures, stress regimes, and time durations relevant for structural-fire engineering applications. Additionally, there appears to be a lack of data on the creep behavior of high strength steels in general, and specifically YP400, YP500, and H-SA700 steels.
>
> ➢ Overall, the apparent importance of thermal creep in structural steel, combined with the scarcity of studies on the effect of thermal creep on structural steel's mechanical behavior, indicates the need for additional high-quality research on characterizing time-dependent deformation of high strength steel structure at elevated temperatures. Specifically, our understanding of how to estimate creep effects on structural steel's stress-strain behavior is currently somewhat limited, and adequate experimental data are absent.

CHAPTER 3   BACKGROUND ON CREEP BEHAVIOR OF STEEL COLUMNS AT ELEVATED TEMPERATURES

3.1. Overview

As mentioned in the introductory chapter, at elevated temperatures, the strength of steel columns is indeed a complicated phenomenon and is not as well understood or quantified as the strength at ambient temperature is. Factors that affect column strength at high temperatures include reductions in stiffness and strength of steel, changes to residual stress patterns, effects of restrained thermal expansion, column bowing due to thermal gradients, and the effects of material creep.

A number of past studies on the behavior of steel columns subjected to fire have considered several of these factors, as will be described in this chapter. As noted in the introduction chapter, of the many important factors that may affect column strength at elevated temperatures, the factor that has seen the least attention in experimental, analytical and computational studies is the effect of thermal creep of structural steel.

The aim of this chapter is to provide a background on the concept of time-dependent or creep behavior of steel columns at elevated temperatures. In doing so, the phenomenon of creep buckling is first introduced. A survey of previous work on steel columns at elevated temperatures is then presented. While the emphasis is on the previous research on the time-dependent or creep effects on column behavior at high temperatures, literature on loading- and heating-rate effects on steel columns at high temperatures is also reviewed. Finally, the chapter ends with some general observations on the phenomenon of creep buckling as it relates to steel columns subjected to fire and with critical review of previous studies

3.2. Phenomenon of time-dependent or creep buckling

3.2.1. Effect of Material Creep on Stability of Columns

When an axial load is applied to an imperfect column, it experiences an immediate elastic or plastic increase in curvature. As a result of the column bending, the magnitudes of the stresses on the compression and tension sides of the column differ. If the column is formed of a creeping material, the compression and tension sides will creep at different rates. In other words, the strains will alter at varying rates throughout time, resulting in subsequent column deflections. As a result, the column continues to deflect at an increasing rate under constant load. Growing lateral deflections combined with the column material's nonlinear stress-strain behavior under high stresses will eventually result in the column collapsing.

3.2.2. Theory of elastic stability

As is generally known, the theory of elastic stability evolved from Euler's work on the column buckling problem (Van den Broek, 1947). Euler demonstrated that the elastic buckling load was proportional to the column's length, the moment of inertia of the column's cross section, the restraint conditions at the column's ends, and the elastic modulus or

Young's modulus of the column's material (Van den Broek, 1947). Euler also demonstrated that this buckling load was independent of the column's cross-sectional shape (Van den Broek, 1947). However, the fact that the shape of the cross section has no effect on the buckling load is only applicable when the buckling stress is less than the column material's elastic limit stress. When the average compressive stress associated with the buckling load exceeds the elastic limit (i.e. inelastic buckling), the cross section shape becomes critical in determining the buckling load, particularly for columns with initial imperfection. As described in Chapter 2, creep is defined as a material's time-dependent inelastic characteristic. As a result, creep buckling should be regarded as an inelastic buckling phenomenon in which the cross-sectional shape has an effect on the column's buckling strength.

3.2.3. *Fundamental Time- and Temperature-Dependent Behavior of Steel Columns*

Before discussing creep buckling at elevated temperatures, it is important to review the fundamental behavior of columns at elevated temperatures and to introduce certain terms. The fundamental temperature-dependent behavior of columns can be modelled using the conventional approach to inelastic buckling at elevated temperatures, i.e. using the load-deflection curve concept. Temperature has an effect on the curvature of the load-deflection curve. More precisely, temperature has an effect on all significant characteristics of the load-deflection curve, including the initial slope and peak.

All studies and discussions in this dissertation are based on the assumption that temperature has no effect on the load-deflection behavior of columns. In other words, the time required to reach the peak of a load-deflection curve is sufficiently short to allow for the disregard of time effects. As a result, the load deflection curves are referred to as short-duration or short-time load deflection curves to indicate their time-independent nature.

Obviously, the peak is the most critical aspect of a load-deflection curve since it indicates the buckling load or column strength. Due to the assumption of a short duration load-deflection curve, the time-independent peak is a rational consequence. The term "short-time buckling load" or "time-independent inelastic buckling load" refers to this time-independent peak. Additionally, to emphasize the significance of this peak in terms of the creep buckling phenomenon, the peak of a load-deflection curve is referred to as the zero-time buckling load. It is critical to stress here that the creep buckling phenomena is regarded as the time for columns to buckle. Thus, the zero-time buckling load is essentially a load that causes the column to buckle very instantly upon application.

The words creep buckling, and time-dependent buckling relate to a phenomenon in which a column's critical buckling load is based not only on its slenderness and temperature, but also on the duration of the applied force.

As the temperature rises, the initial buckling load (at time t = 0) reduces due to the material's strength, modulus, and proportional limit decreasing, as discussed in Chapter 2. As a result, as previously stated, the buckling capacity during initial application of load is primarily dependent on temperature (zero-time buckling load is only temperature dependent).

However, as the temperature rises and material creep becomes noticeable, the buckling load is dependent not only on the temperature, but also on the time of the load application. In other words, due to steel's thermal creep, loads less than the zero-time buckling load may cause the column to buckle at a particular temperature. As a result, the column's buckling load capacity decreases with time, becoming more evident at higher temperatures due to the rise in creep effects. Thus, in the case of fire, a column at elevated temperatures may initially be capable of securely carrying its load. However, with time, even if the weight and temperature remain constant, the column may buckle. The creep buckling curves are the load versus time (time-to-buckle) curves.

3.3. Survey of previous work

Creep buckling can occur when steel columns are exposed to high temperatures. In creep buckling, not only does the buckling load for a column depend on its slenderness and temperature, but also on the duration of the temperature and applied load ratio. When designing steel structures for fire safety purposes, the investigation of creep bucking is critical since it can lead to the buckling of steel columns even when the load ratio is small. Analytical creep buckling research used the Rabotnov and Shesterikov (Rabotnov, 1957) creep buckling model as well as the widely known Harmathy (Harmathy, 1967) and Fields and Fields (Fields, 1989) creep material models. Researchers like Furumura (Furumura F., 1984) (Furumura, March 1986) attempted to establish a numerical study of creep buckling based on an expanded model of material behavior. Using an experimental analysis of creep buckling of H-shaped steel at high temperatures with varied slenderness ratios and eccentricities, the deformation and collapse load of a column was assessed. Using a nonlinear numerical simulation, Okabe and Kohno (Okabe, 2007.1) predicted steel column thermal deformation at high temperatures. Numerical analysis can accurately forecast the deformation properties of columns at high temperatures when an appropriate mechanical model and creep strain data of steel materials are employed, as found in this study. Additionally, Morovat (Morovat M. L., 2011) proposed a preliminary model for estimating creep buckling in steel columns subjected to fire. Analytical solutions for creep buckling are devised and compared to computational predictions. This study's findings demonstrated that failing to account for creep effects might lead to incorrect and potentially dangerous estimations of the fire resistance of steel columns. The experimental buckling test was used by Morovat (Morovat M. E., April 2016) to evaluate the time-dependent behavior of ASTM A992 steel columns at extreme temperatures. Results from Eurocode 3 and AISC Specification were used to compare these findings to code-based forecasts. Li (Li, 2012) examined the influence of creep on buckling of axially constrained steel columns to predict buckling temperature and axial deformations in real fires. These researchers used numerical analysis and finite element modelling to study time-dependent behavior for a wide range of steel grades compared to experimental tests; nevertheless, they were unable to analyze the creep behavior of high strength steel. An established finite element model was used to estimate the creep deformation and creep buckling time of high-strength Q460 steel (Wang, 2019), which was validated by the results of the experimental tests. The creep behavior and creep buckling time

are considered by modifying the slenderness ratio, the load ratio, or the starting crookedness. A dearth of experimental studies on the effect of creep on high strength column behavior in a fire environment and the validation of results that may be achieved using alternative methods such as numerical modelling and analytical derivation is also a problem.

In fact, to the knowledge of the author of this dissertation, experimental research at Tokyo Institute of technology (Furumura, March 1986) is reviewed in this dissertation for creep buckling behavior of steel column at high temperatures for structural-fire design application purposes.

3.3.1. Research at Tokyo Institute of Technology (Furumura, March 1986)

Recognizing the potential significance of time-dependent or creep effects on the buckling strength of metal columns at elevated temperatures, researchers at the Tokyo Institute of Technology conducted an experiment to characterize the time-dependent behavior of structural steel columns exposed to fire. In comparison to previous literature, this section elaborates and reviews significant experimental features, as well as certain experimental results and their interpretations from creep buckling research conducted at the Tokyo Institute of Technology.

3.3.1.1. Column test apparatus (Furumura F., 1984)

The creep buckling test is performed on a universal testing machine equipped with an electric furnace weighing 150 tons as shown in Figure 3-1. The furnace has a diameter of 30 cm and a height of 90 cm. The interior space is separated from the heating elements by a stainless-steel plate with a thickness of 4.5 mm, and the heating elements are situated in the top, middle, and bottom of the furnace. A time-proportioning, integrating, and differentiating controller is used to regulate the temperature of the furnace.
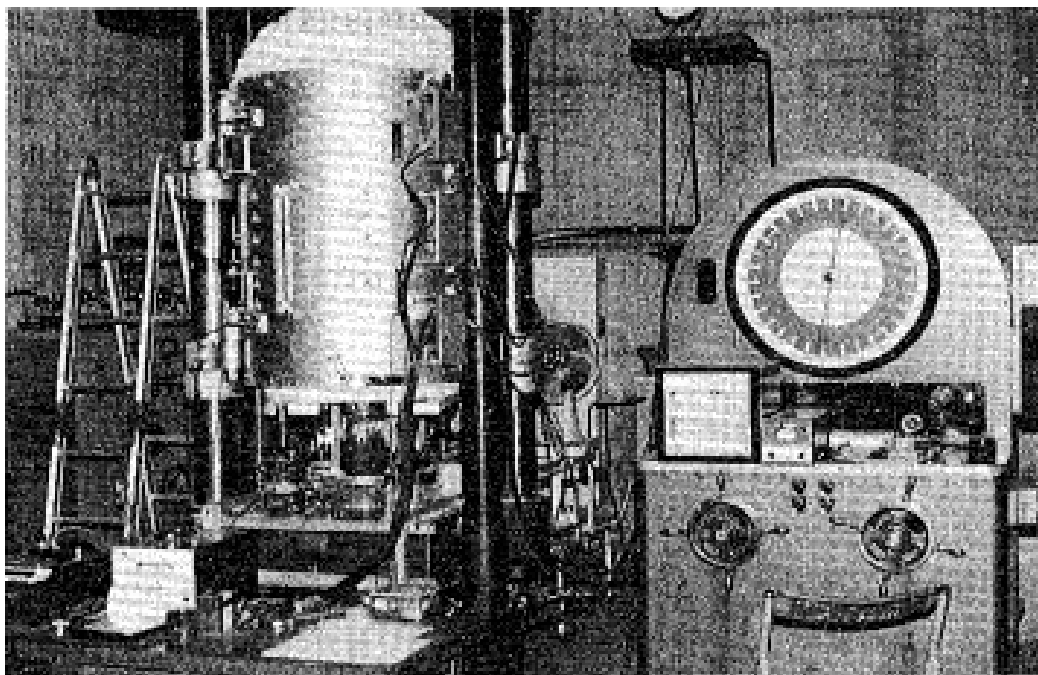
Figure 3-1 General view of testing machine with furnace (Furumura F., 1984)

To conduct creep buckling tests, a unique arrangement was created and built to transfer loads from the testing machine to column specimens inside the furnace while maintaining tight control over alignment and boundary conditions. Figure 3-2 depicts the configuration schematically. Figure 3.85 also contains an enlargement of the testing setup.

Two hinges with small diameter cylindrical pins, one spherical bearing with a significantly larger curved surface, a pair of level adjustor plates, and upper and lower compression tools constitute this assembly. All components in the setup are made of ultra-heat resistant steel to ensure proper operation at testing temperatures and minimal damage during repeated use.

The use of thin mica films to reduce friction in hinges in order to create boundary conditions more nearly like those found in perfect pins at elevated temperatures is one of the test's distinctive setups. Mica is a perfect cleavage mineral, which means it can be easily separated into thin, flexible sheets with extremely smooth surfaces. Furthermore, mica has a very high compressive strength and is resistant to high temperatures. Indeed, when mica films are used, low friction coefficients in the range of 0.05 to 0.1 have been found at room temperature. However, it is unclear how such values might change from the former values at elevated temperatures. This makes quantifying the influence of mica sheets on friction reduction in hinges during buckling tests at elevated temperatures challenging.

Figure 3-3 to Figure 3-6 illustrate assemblies used to determine the lateral and axial displacements of steel columns during creep buckling tests at elevated temperatures. Figure 3-3, and Figure 3-5 illustrate a measuring system for the lateral displacement of columns during creep buckling tests. As can be observed, lateral deflections were determined at three sites along the column specimens' height: one in the center and two 142 mm above and below the mid-height. Dial gauges were used to detect lateral displacements. One side was joined to the quartz glass rods extended into the furnace, and the other side was connected to a digital strainmeter. Additionally, as seen in Figure 3-4, axial deformations were measured using a system comprised of vertical stainless-steel rods extended from the furnace, horizontal rods welded to the flanges of column specimens, and dial gauges coupled to a digital strainmeter. Columns were loaded using the testing frame and custom-made configuration described previously and illustrated in Figure 3-3 and Figure 3-4. It was able to submit columns to eccentric loads with regulated eccentricities using the setup seen in Figure 3-6. The actual unsupported length was 485 mm with the arrangement depicted in Figure 3-6, which was used to calculate slenderness ratios and to evaluate column buckling capacities in analytical studies.
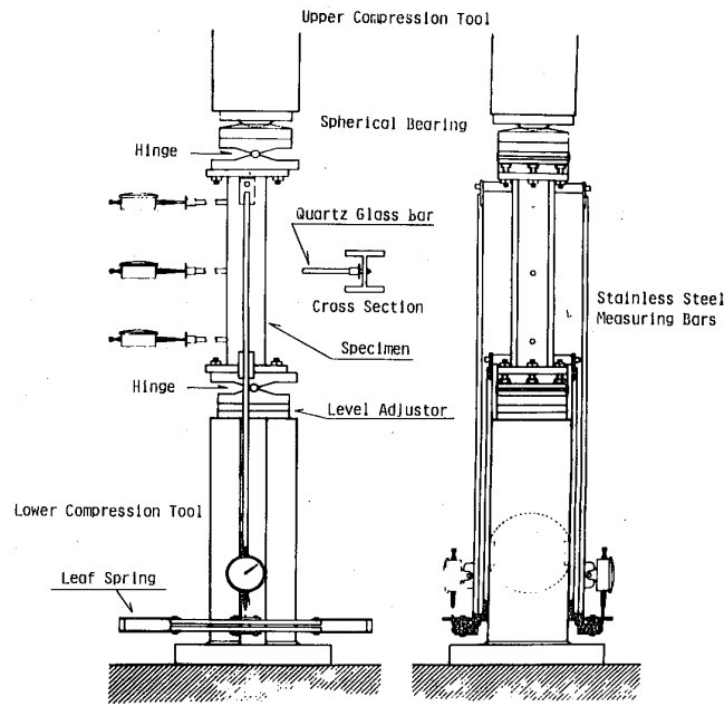
Figure 3-2 Schematic diagram of loading and measuring assembly in creep buckling tests
(Furumura F., 1984)
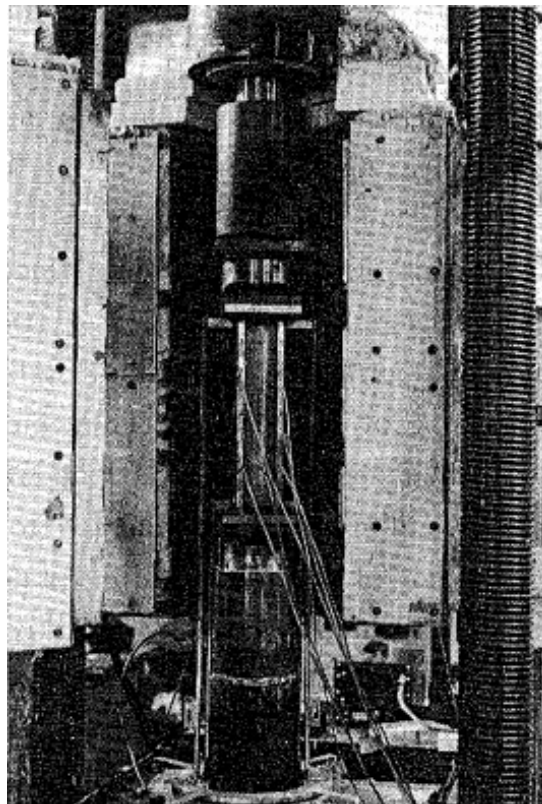
Figure 3-3 Close view of the furnace with loading and measuring assembly and specimen
installed in position in creep buckling tests (Furumura F., 1984)
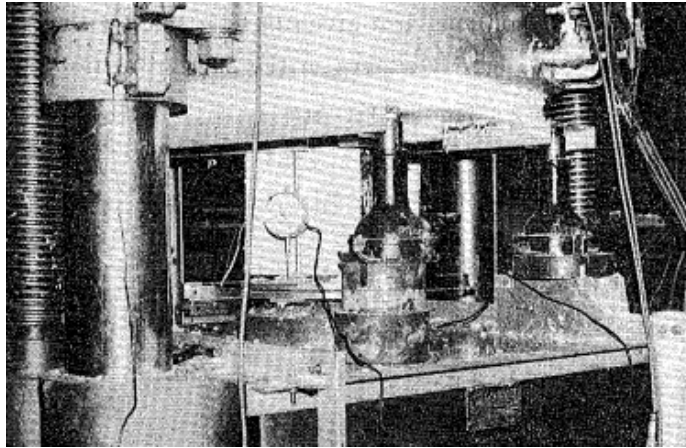
Figure 3-4 Assembly for measuring axial displacement (contraction) in creep buckling tests (Furumura F., 1984)
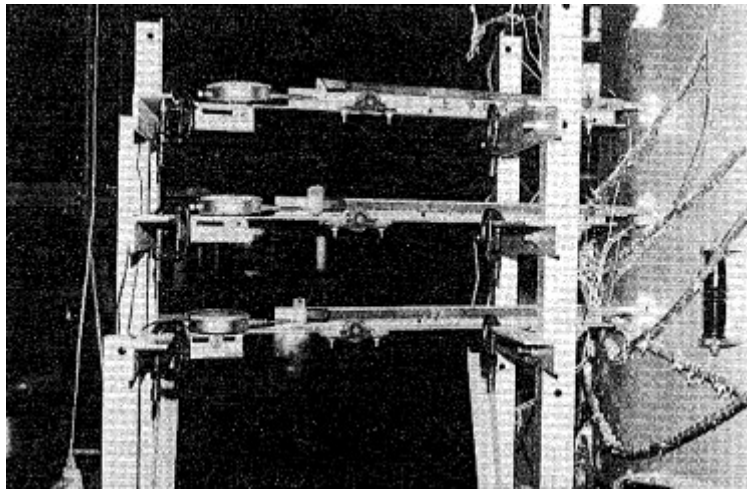
Figure 3-5 Assembly for measuring lateral deflection in creep buckling tests (Furumura F., 1984)
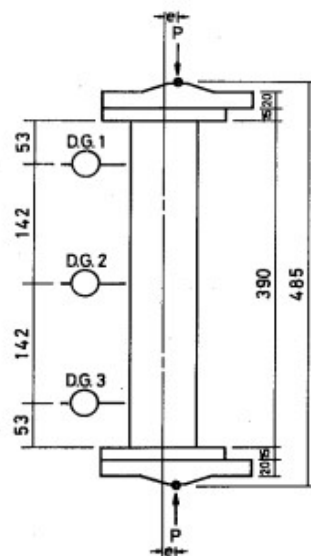
Figure 3-6 Dial gauge and hinge locations for specimen in creep buckling tests (Furumura F., 1984)

3.3.1.2. Column specimens (Furumura F., 1984)

Creep buckling specimens were cut from SM 50A structural steel plates ($F_{u, nom}$ = 50 kg/mm^2). The specimens were cut parallel to the rolling direction and with parallel flanges to the plate surfaces. As a result, column sections designated H-44×40×4×6 and H-85×75×8×12 were cut from plates with a thickness of 50 mm and 100 mm, respectively. Additionally, a constant length of 390 mm was chosen for the column specimens to accommodate the steel columns and the entire setup inside the furnace. Axial displacements were measured over the gauge-length of 360 mm along the height of the column, as given in Figure 3-7 and Figure 3-8.

The geometric characteristics and dimensions of the column specimens with H-44×40×4×6 and H-85×75×8×12 cross sections are shown in Figure 3-7 and Figure 3-8, respectively. The slenderness ratio of test specimens with end plates and attached hinges with varying cross sections, cut from 50 mm thick steel plate (H-44×40×4×6), is around 46.9. This figure was derived by considering the possibility of steel columns in genuine high-rise buildings collapsing in the event of a fire. In this fire scenario, investigators contended that columns could be termed pin-ended due to the absence of connecting parts that provide flexural rigidity. Additionally, the slenderness ratio of test specimens cut from 100 mm thick steel plate (H-85×75×8×12) is around 25.1. This number was established by considering the possibility that steel columns in genuine high-rise structures would buckle under the condition of having fixed ends in a fire, as the flexural rigidities of heated fireroom columns were less than those of the upper and lower floors. The researchers hypothesized that steel columns would behave more like fixed-fixed columns in this fire scenario due to the restraint given by connecting cooler parts. The mechanical properties and chemical constituents of this steel are listed in Table 3-1 to Table 3-4.
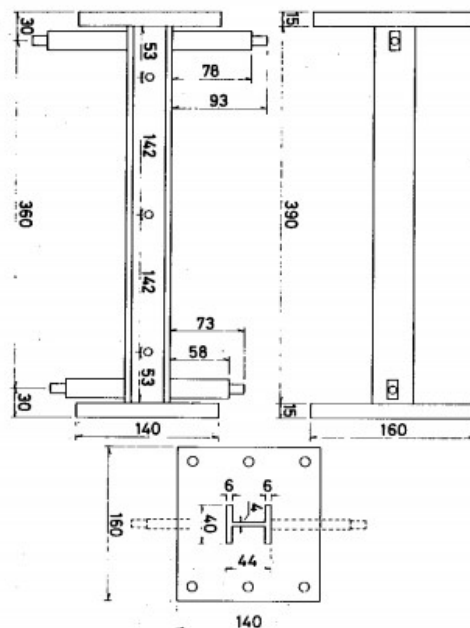
Figure 3-7 Steel column specimen H-44×40×4×6 (slenderness ratio: 46.9) (Furumura F., 1984)
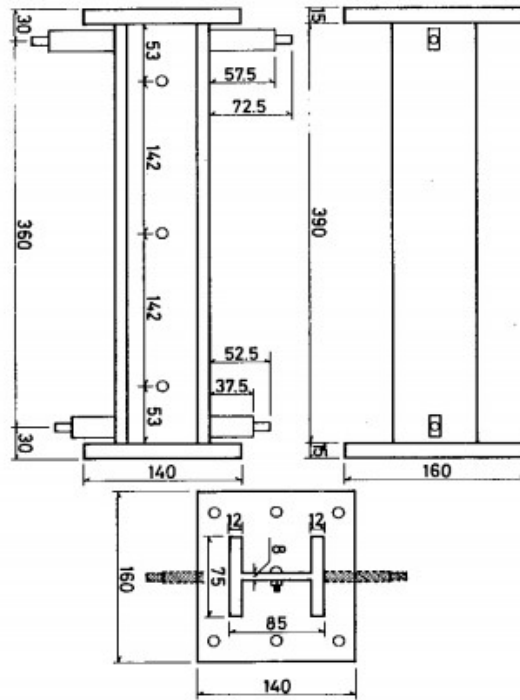
Figure 3-8 Steel column specimen H-85×75×8×12 (slenderness ratio: 25.1) (Furumura F., 1984)

Table 3-1 Mechanical properties of 50mm steel plates (Furumura F., 1984)

JIS grade	Yield strength (Kg/mm^2)	Tensile strength (Kg/mm^2)	Elongation (%)
SM 50A	35.78	54.0	33.0

Table 3-2 Chemical composition (%) of 50mm steel plates (Furumura F., 1984)

JIS grade	C	Si	Mn	P	S	Cu
SM 50A	0.15	0.38	0.15	0.023	0.006	0.01

Table 3-3 Mechanical properties of 100mm steel plates (Furumura F., 1984)

JIS grade	Yield strength (Kg/mm^2)	Tensile strength (Kg/mm^2)	Elongation (%)
SM 50A	32.78	53.0	34.0

Table 3-4 Chemical composition (%) of 100mm steel plates (Furumura F., 1984)

JIS grade	C	Si	Mn	P	S	Cu	Ni
SM 50A	0.19	0.42	1.39	0.019	0.005	0.17	0.08

3.3.1.3. Methods and procedures of column tests (Furumura F., 1984)

At Tokyo Institute of Technology, creep buckling experiments were performed over a temperature range of 475 °C to 550 °C in 25 °C increments. More precisely, the temperature range evaluated for H-44×40×4×6 columns was 500 °C to 550 °C, while the temperature range investigated for H-85×75×8×12 columns was 475 °C to 550 °C. Three thermocouples were used to monitor the temperatures of the steel columns throughout the creep buckling tests. These thermocouples were affixed to the surface of steel columns at the points where lateral displacements were measured. Each test was stated to have good control overachieving the target temperatures, as no temperature variation greater than 2 °C was detected at the middle thermocouple point (mid height of the column specimens). Additionally, no temperature changes greater than 15 °C was recorded at the upper and lower thermocouple locations relative to the measured temperatures at the centre point. (Furumura F., 1984)

Buckling loads were used in creep column testing to simulate the loads seen in typical columns in Japanese high-rise constructions. Through the load ratio β, the applied loads were defined in relation to the squash loads of the respective columns at ambient temperature. β was defined as P/AF, where P denoted the column load in buckling tests, A denoted the cross-sectional area of tested columns, and F (=3.0 ton/cm^2) denoted equal to the yield strength prescribed by the Architectural Institute of Japan's steel structural design code. (Furumura, March 1986)

The values of β vary from 0.275 to 0.4 (H-85×75×8×12) and from 0.225 to 0.35 (H-44×40×4×6), which correspond to the real-world high-rise buildings in Japan. These β values were chosen to produce column stresses equivalent to those used in high-rise columns in Japan, which are roughly 1.0 ton/cm^2 for H-columns and 1.2 ton/cm^2 for box-columns. (Furumura F., 1984)

Researchers conducted buckling tests under both concentric and eccentric axial stresses. Load eccentricities ranging from 0.0 mm to 15.0 mm, in 2.5 mm increments, were examined in creep buckling tests conducted at high temperatures. Specifically, H-44×40×4×6 columns with load eccentricities ranging from 7.5 to 12.5 mm were examined. Meanwhile, load eccentricities ranging from 0.0 to 15.0 mm were investigated in experiments on H-85×75×8×12 columns. While the choice of load eccentricity values was primarily motivated by testing capabilities, additional factors such as expected lateral displacements at column ends owing to beam expansion during a fire, as well as various imperfections and accidental load eccentricities, were also considered. (Furumura F., 1984)

The tests were scheduled to be conducted as follows. A column specimen was installed in the furnace and the strain distribution of the specimen was investigated using twelve wire strain gauges and loadings within the range of elastic deformation. Then the furnace was heated after the specimen was accurately installed. The specimen was loaded with approximately 50–250 kg of weight to prevent it from falling during the entire heating time. After the specimen's temperature was raised to the desired level and a uniform temperature distribution

was achieved, the specimen was put into the target load. The constant loading was continued until the column buckled due to creep or until about two hours had passed since the beginning of loading.

3.3.1.4. Column test results

Figure 3-9 and Figure 3-10 illustrate the general deflected forms of typical column specimens following creep buckling tests on H-44×40×4×6 and H-85×75×8×12 cross sections, respectively. Regrettably, the researchers at the Tokyo Institute of Technology did not specify the temperatures used in these testing. However, these results suggest that columns were buckled around their weaker axis, as expected during the tests.

Several results of the variation of column lateral deflection and contraction versus time under various temperatures, loads and eccentricity are shown in Figure 3-11 to Figure 3-14.
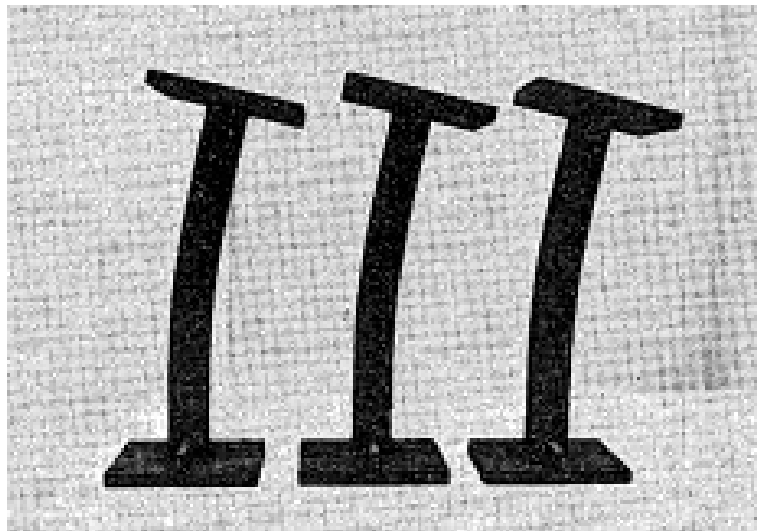
Figure 3-9 Deformation shapes of H-44×40×4×6 specimens after creep buckling tests
(Furumura, March 1986)
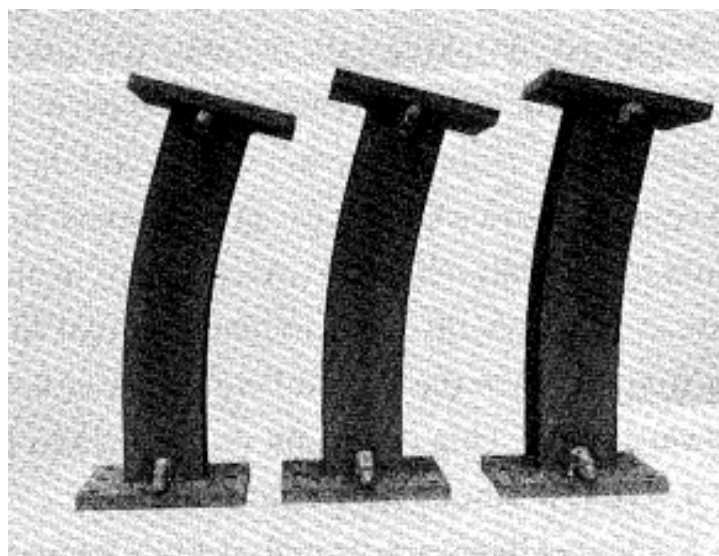
Figure 3-10 Deformation shapes of H-85×75×8×12 specimens after creep buckling tests
(Furumura F., 1984)
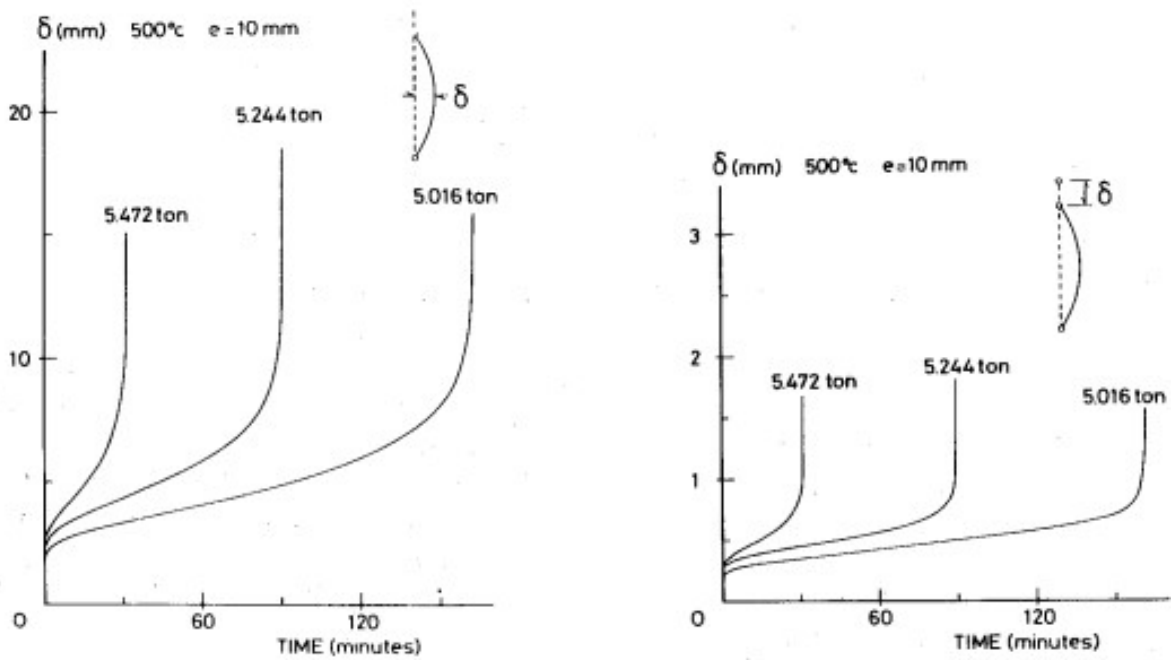
Figure 3-11 Lateral deflection and axial displacement versus time at 500 °C under various constant load (load eccentricity e=10mm) for H-44×40×4×6 columns in creep buckling tests (Furumura F., 1984)
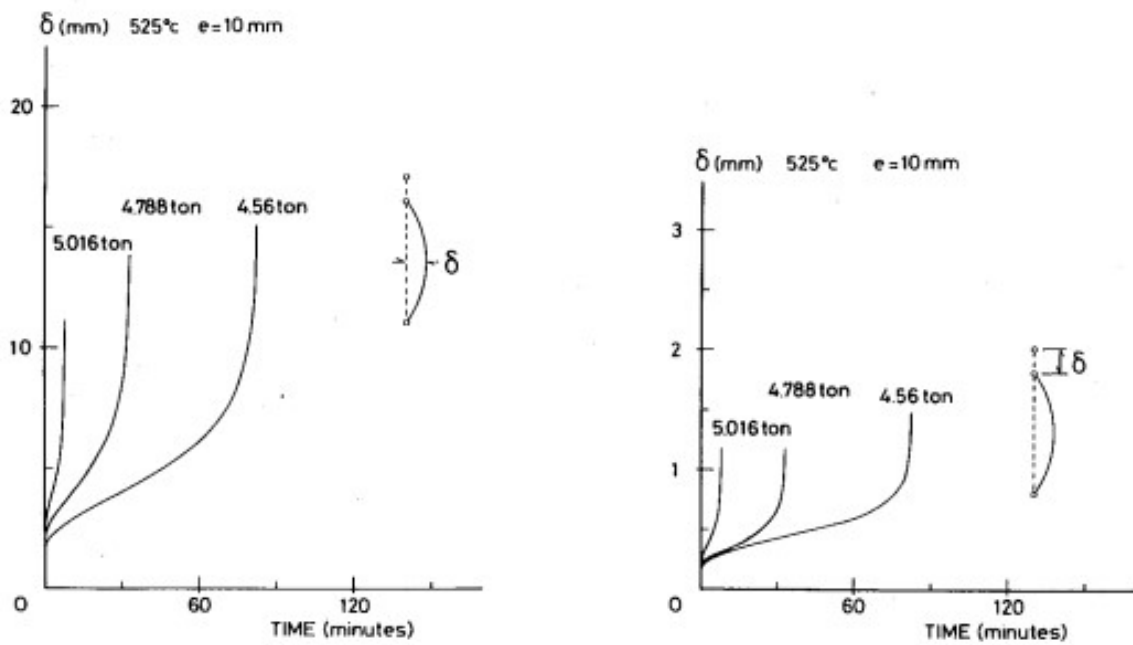
Figure 3-12 Lateral deflection and axial displacement versus time at 525 °C under various constant load (load eccentricity e=10mm) for H-44×40×4×6 columns in creep buckling tests (Furumura F., 1984)
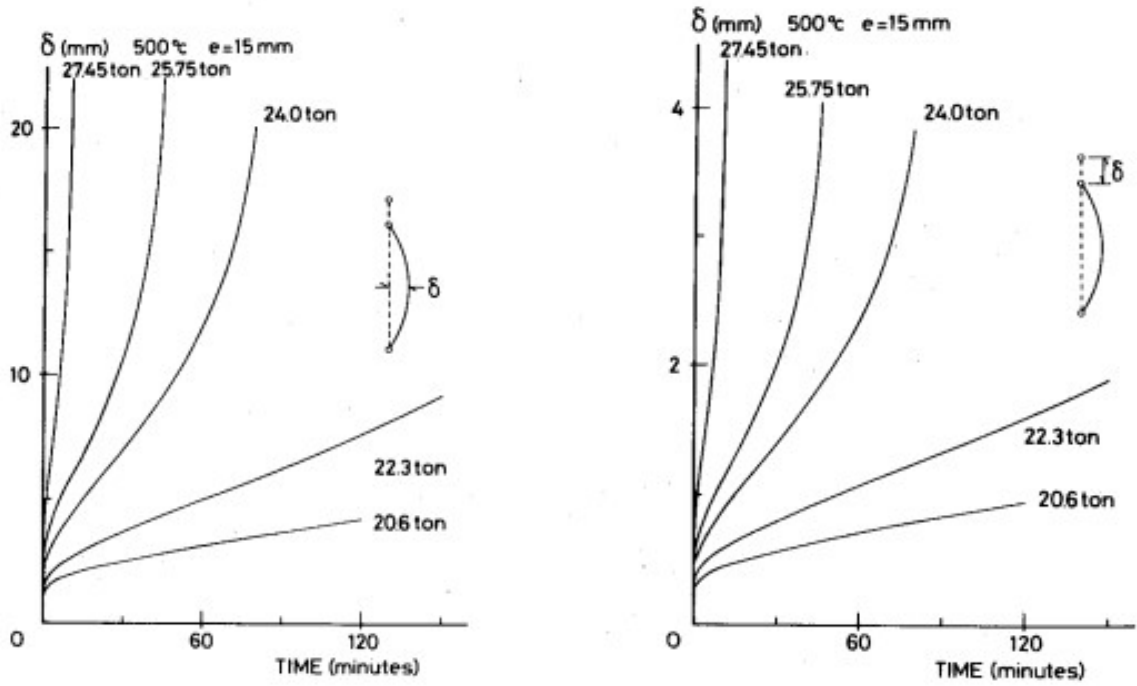
Figure 3-13 Lateral deflection and axial displacement versus time at 500 °C under various constant load (load eccentricity e=10mm) for H-85×75×8×12 columns in creep buckling tests (Furumura F., 1984)
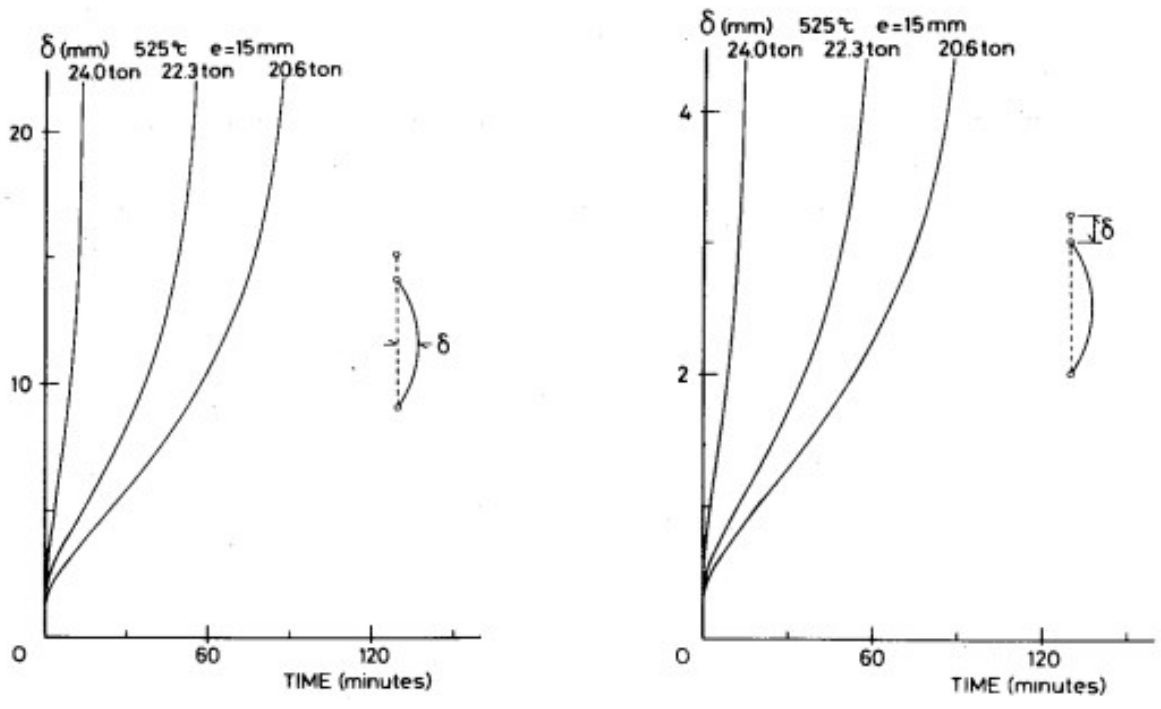
Figure 3-14 Lateral deflection and axial displacement versus time at 525 °C under various constant load (load eccentricity e=10mm) for H-85×75×8×12 columns in creep buckling tests (Furumura F., 1984)

Importantly, these figures demonstrate that the temperature, load amount, and load eccentricity all have a major effect on the buckling behavior of steel columns exposed to fire, as measured by the time to failure. Additionally, these figures demonstrate the critical role of primary creep in predicting the buckling behavior of steel columns in fire, as column displacements increase rapidly during the early stages of buckling tests. Following the initial stage, the rate of deflection and contraction becomes temporary constant. They then begin to accelerate again as a result of the increasing moment caused by the increased lateral defection, until the column specimen buckles. (Furumura F., 1984)

3.4. Other potential influencers on behavior of steel columns at elevated temperature

3.4.1. Effect of temperature on strength (Yang K.C., 2009)

The second set of specimens with a slenderness ratio of 34 exhibited ductile behavior with considerable inelastic deformation both at room temperature and in the fire state. Table 3-5 shows the strength decrease of columns as temperatures rise. Columns retain their nominal strength (P_n) at room temperature until temperatures reach 450 °C. The column strengths at 500 °C and 550 °C are 85 and 62% of the nominal strength at room temperature, respectively (P_n). When the temperature approaches 600 °C, the column strength drops to 42% of its nominal value.

Based on the findings of this set of column tests, it is demonstrated that steel columns with a slenderness ratio of 34 may maintain their stability at a design load of 0.85 P_n until 500 °C. As temperatures rise over 500 °C, the column strength can be calculated at a declining rate of 15% of the nominal strength for each 50 C temperature increment.

3.4.2. Effect of slenderness ratio (Yang K.C, 2006)

Researchers at the National Kaohsiung First University of Science and Technology conducted buckling tests on steel columns with varying cross sections resulting in different slenderness ratios to investigate the effect of slenderness ratio on the behavior of steel columns at elevated temperatures. Steel columns manufactured of ASTM A36 steel were tested at room temperature and 500 °C, whereas SN490 columns were tested at room temperature and at increased temperatures of 500 °C, 550 °C, and 600 °C.

Table 3-5 Experimental results of column specimens for SN490 steel with slenderness ratio of 34 (Yang K.C., 2009)

Specimen no.	Test temperature	P_{exp}/P_n
13	Room temperature	1.16
14	400 °C	1.23
15	450 °C	1.13
16	500 °C	0.85
17	550 °C	0.62
18	600 °C	0.42
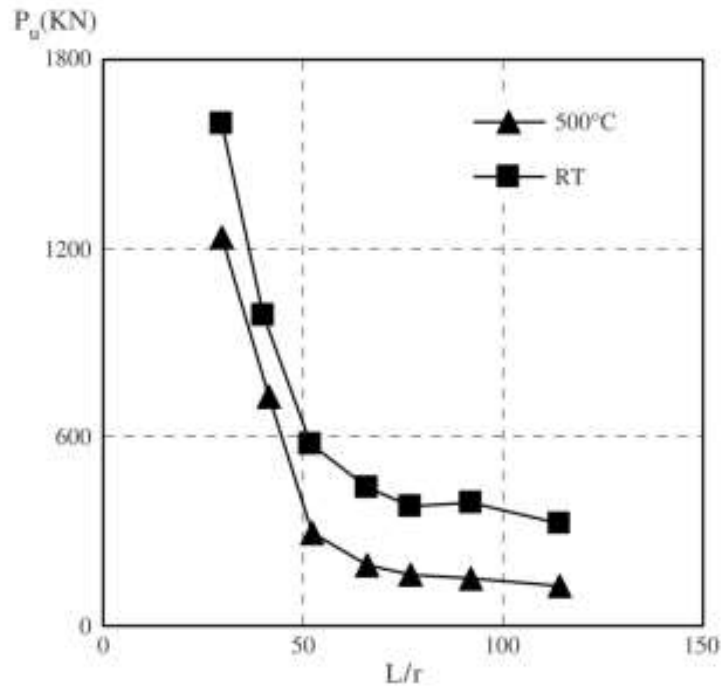
Figure 3-15 Buckling load-slenderness ratio plots for ASTM A36 steel columns meant to represent the effect of slenderness ratio on the behavior of steel columns at elevated temperature and obtained in the experimental program at the National Kaohsiung first university of Science and Technology (Yang K.C, 2006)

Figure 3-15 depicts the results of testing performed on column specimens of ASTM A36 steel. Maximum loads achieved in buckling tests at room temperature and at 500 °C are displayed against the respective slenderness ratios in this figure. Surprisingly, researchers at the National Kaohsiung First University of Science and Technology used this picture to describe how the slenderness ratio can affect the behavior of steel columns at high temperatures (Yang K.C, 2006). Based on the trend observed in the buckling load vs. slenderness ratio plot inFigure 3-15, it was established that the slenderness ratio had no effect on the elevated-temperature strength of steel columns with slenderness ratios greater than around 52. (Yang K.C, 2006). It should be emphasized once more that presenting results from column tests on columns with varying cross sections in the way given in Figure 3-15 does not provide any helpful information about the effect of slenderness ratio on the behavior of steel columns at elevated temperatures. A more appropriate approach to show these data is to depict buckling stresses as functions of slenderness ratio rather than loads.

Researchers at the National Kaohsiung First University of Science and Technology noticed this later in their paper (Yang K.C., 2009) and presented the data on SN490 steel columns in the form of buckling stress against slenderness ratio, as shown in Figure 3-16. It should be noted that, while this presentation of the buckling test results does not provide the entire picture, it does highlight a couple of interesting trends on how temperature and slenderness ratio combinations may alter the behavior of steel columns when subjected to fire. It is also worth noting that the presentations and discussions here are based on buckling tests on fixed-end column specimens.
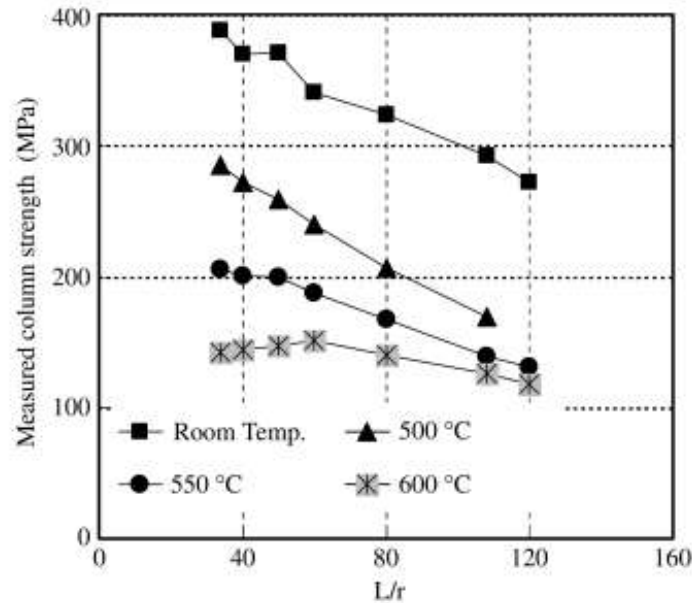
Figure 3-16 Buckling stress-slenderness ratio plots for SN490 steel columns meant to represent the effect of slenderness ratio on the behavior of steel columns at elevated temperature and obtained in the experimental program at the National Kaohsiung first university of Science and Technology (Yang K.C., 2009)

Figure 3-16 shows that, as expected, the strength of steel columns falls with increasing slenderness ratio, regardless of test temperatures. Furthermore, it can be seen that the behavior of steel columns with high slenderness ratios, particularly those regulated by elastic buckling, is not highly sensitive to temperature variations. In other words, temperature has a greater effect on the strength of shorter steel columns (controlled by inelastic buckling) than on the strength of longer steel columns (governed by elastic buckling). This second discovery, in the author's opinion, indicates the effect of thermal creep of steel on the buckling behavior of steel columns exposed to fire. This viewpoint is backed further by the sluggish displacement rate (0.07 in./min) used in the column testing at National Kaohsiung First University of Science and Technology, as well as the analysis provided later in this dissertation.

It should be underlined once more that the influence of slenderness ratio on the buckling behavior of steel columns at elevated temperatures can only be completely explored by comparing the behavior of columns with identical cross sections but varying lengths.

3.4.3. *Effect of residual stresses (Yang K.C., 2009)*

At room temperature, residual stress has a significant impact on column strength. The steel column yields before reaching the nominal yield strength when subjected to residual stress. As illustrated in Figure 3-17, the maximum residual stress in the column section can be calculated as the difference between the experimental findings of stub columns ($F_{y,exp}$) and the yield stress of steel ($F_{y,T}$). Table 3-6 shows the maximum residual stresses computed from the stub columns. These stresses have been normalized to 374 MPa, the yield stress of steel at room temperature.
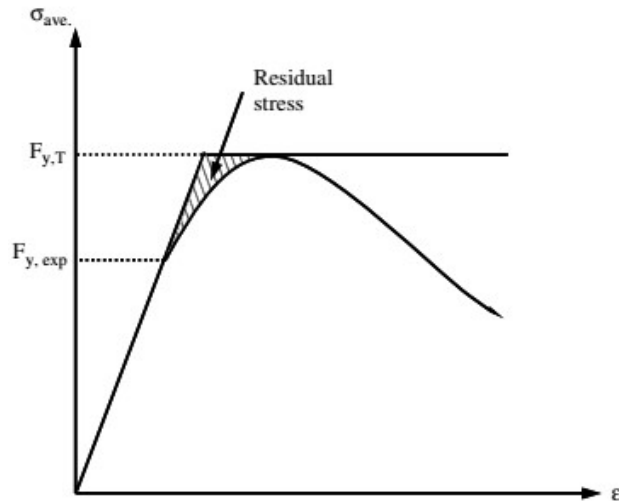
Figure 3-17 Maximum residual stress in stub column tests (Yang K.C., 2009)

Table 3-6 Experimental results of stub column specimens for SN490 steel (Yang K.C., 2009)

Specimen no.	b/t	Test temperature	$P_{exp.}/P_{yT}$	$P_{exp.}/P_n$	$F_{r,max}/F_y$
1		Room temperature	1.43	1.55	0.33
2	7	500 °C	1.66	1.13	0.01
3		550 °C	1.49	0.79	0.02
4		600 °C	1.28	0.52	0.02
5		Room temperature	1.30	1.40	0.22
6	8	500 °C	1.56	1.06	0.01
7		550 °C	1.40	0.74	0.06
8		600 °C	1.22	0.49	0.06
9		Room temperature	1.12	1.20	0.23
10	11	500 °C	1.21	0.80	0.11
11		550 °C	1.29	0.68	0.08
12		600 °C	1.18	0.48	0.05

As seen in Table 3-6, the fire state causes a significant release of residual stress. At room temperature, residual stress is greater than 20% of yield stress; but, at increased temperatures, residual stress diminishes to less than 10%. The failure behavior of stub columns also confirms the release of residual stress at increased temperatures. Stub columns failed after achieving the yield load at increased temperatures, with no premature failure. The ultimate strength of stub columns is greater than their yield load, as seen in Table 3-6. In the fire situation, no premature yielding due to residual stress of the column specimens is seen. The effect of residual stress on column strength can be ignored due to the discharge of residual stress in the fire situation.

Furthermore, the failure mode of inelastic column specimens revealed a limited effect of residual stress on column behavior in the fire state. Because of the release of residual stress in the fire condition, the failure mode of inelastic columns changed from global buckling at room temperature to inelastic local buckling at elevated temperature.

3.5. Summary

In this chapter, efforts have been made to describe the phenomenon of time-dependent or creep buckling and its significance in predicting the buckling strength of steel columns subjected to elevated temperatures due to fire. The chapter was started by introducing the concept of creep buckling and establishing it as a time-dependent inelastic buckling phenomenon. Furthermore, a review of past studies was conducted to acquire a better understanding of the column behavior at elevated temperatures. Nevertheless, several additional potential factors impacting the subject to fire column's behavior are explored.

Based on the background information provided on the phenomenon of time-dependent stability of steel columns subjected to fire, and based on the review of previous research, several key observations are made in the following. These observations tend to establish the motivation behind the research reported in this dissertation.

➢ As shown in the literature survey, several past analytical, computational and experimental studies have examined various aspects of column strength at elevated temperatures. However, compared to column tests at normal temperature, the experimental data on columns at elevated temperatures are rather limited. In fact, considering the many variables that can affect high temperature column buckling, the experimental database is quite meager.

➢ While there are a number of column tests at elevated temperatures reported in the literature, there are some significant shortcomings to these data. These shortcomings include lack of accompanying materials data, lack of information on loading rates, incomplete information on initial geometry, incomplete information on residual stresses, and inadequate care in boundary conditions. Considering the rate dependence of steel material properties at high temperatures, the lack of control and documentation of loading rates adds considerable uncertainty to the interpretation of the test data. Moreover, several investigators included measurements of initial geometry of column specimens, and measurement of residual stresses at room temperature. However, this important information is lacking from most reported experiments. Many experiments also appear to have questionable end fixtures for the column specimens. The end fixtures are generally intended to replicate "pinned" conditions. However, end fixtures were used that provided some rotational restraint. While small rotational restraint at room temperature may be acceptable, this restraint can introduce larger errors at high temperatures, due to the low stiffness of the column specimen.

➢ The time-dependent creep buckling phenomenon has seen only very limited study in structural-fire engineering research but is potentially of great importance. As already shown and discussed in Chapter 2, the displacement rate and time effects have large impacts on the steel strength at elevated temperatures, especially at temperatures higher than 400 °C. Further work is needed to fully characterize the effects of the time dependent stress-strain response of structural steel on the buckling behavior of steel columns at elevated temperatures due to fire.

- ➤ All in all, the apparent importance of creep together with the limited number of studies related to the influence of creep on column buckling suggest the need for more quality research on elevated-temperature creep phenomenon. Specifically, the understanding of how to quantify creep effects on column buckling is still very limited and adequate experimental data is lacking.

CHAPTER 4   STUDIES ON THE TIME-DEPENDENT BEHAVIOR OF HIGH STRENGTH STEEL BY COUPON TESTS AT ELEVATED TEMPERATURES

4.1. Overview

As addressed and emphasized in Chapter 2 and Chapter 3, understanding the mechanical properties and stress-strain behavior of structural steel at elevated temperatures is critical for analysing the behavior of steel columns exposed to fire. Additionally, it is highlighted that while substantial data on the elevated-temperature properties of structural steel have been published, significant gaps remain in the database on structural steel's elevated-temperature properties. Particularly, high strength steels, the most often utilized structural steel for high-rise buildings and massive bearing structures, have received less attention at elevated temperatures. As covered in greater detail in Chapter 2, of all the mechanical properties of structural steel at elevated temperatures, thermal creep plays a critical role in estimating the strength of steel columns exposed to fire. Again, it is demonstrated that experimental creep data on structural steels used in building construction are limited for the temperature and stress regimes relevant to structural-fire engineering applications, particularly for thermal creep of high strength steel at elevated temperatures due to fires.

To address the research needs summarized above and emphasized in Chapter 2 and Chapter 3, the author of this dissertation conducted a comprehensive analysis characterizing the rate- and time-dependent mechanical behavior of several high strength steels under the temperature and stress conditions encountered in structural-fire design applications. This chapter presents representative results from the comprehensive analysis applicable to the dissertation's subject.

As mentioned previously, the primary objective of this chapter is to present the results of an analytical study into the mechanical properties of high strength steels when exposed to elevated temperatures, with a particular emphasis on time-dependent or thermal creep effects. The chapter begins with the results of general tensile tests at elevated temperatures. Following that, the mechanical properties of high strength steel are explored, with a particular emphasis on the development and discussion of a trial-and-error technique for identifying the procedure for determining steel creep parameters. To account for the creep phenomenon during transient state heating, a user-defined subroutine was designed to simulate the behavior of high strength steel during transient state heating. Furthermore, the analysis results are compared to experimental results in order to determine the validity and limitations of those creep models. As part of the comprehensive material creep investigation of structural steel at elevated temperatures, constitutive equations in the form of a normalized power law have been developed to describe creep of high strength steels (YP400, YP500, and H-SA700) at elevated temperatures. These constitutive equations will be discussed in greater detail later in this chapter. Finally, the chapter concludes with some general observations on the

phenomenon of thermal creep in high strength steel and its effect on the strength estimation of steel columns exposed to fire.

4.2. Characterization of the mechanical properties of high strength steel at elevated temperatures

4.2.1. High-temperature properties of high strength steel

Numerous experimental studies have been performed to determine the structural steels' high-temperature properties (Bentz and Prasad (Bentz DP, 2007); Sakumoto et al. (Sakumoto Y, 1992); Anderberg (Y., 1988); Kirby and Preston (Kirby BR, 1988); Twilt (L., 1988); Outinen (J., 1999). However, the majority of these experiments were undertaken to determine the mechanical properties of mild steel with a yield strength of 250–350 MPa at elevated temperatures, and only a limited amount of test data is available on the thermal properties of structural steel. Recently, a few research have been published on the mechanical properties of high-strength structural steels at elevated temperatures. Chen et al. (Chen J, 2006) examined the yield strength, tensile strength, and elastic modulus of 5 mm thick steel sheet BISPLATE 80 (roughly similar to S690Q grade; nominal yield strength F_y = 690 MPa). Qiang et al. (Qiang X, Post-fire mechanical properties of high strength structural steels S460 and S690, 2012) (Qiang X, Dependence of mechanical properties of high strength steel S690 on elevated temperatures, 2012) (Qiang X, Deterioration of mechanical properties of high strength structural steel S460N under transient state fire condition, 2012) investigated the mechanical properties of S460 (European Standard; nominal yield strength F_y = 460 MPa) and S690 (European Standard; nominal yield strength F_y = 690 MPa) steel by heating and cooling 5 mm thick steel sheets. Wang et al. (Wang W, 2013) used 11 mm thick steel sheets to investigate the effect of temperature on the mechanical properties of Q460 (Chinese Standard; nominal yield strength F_y = 460 MPa) steel. However, the mechanical property tests for high-strength steel stated above are only applicable to thin steel sheets (5–11 mm) made using the quenching and tempered procedure. Choi et al. (Choi I-R, 2014) conduct experimental studies on the high-temperature thermal and mechanical properties of a newly developed high-strength steel, namely HSA800 (Korean Standard; nominal yield strength F_y = 650 MPa), in order to determine thermal conductivity, specific heat, and thermal elongation at temperatures ranging from 25 to 1000 °C. Additionally, high-temperature tensile tests were conducted to determine the yield strength, elastic modulus, and ultimate strength of HSA800 at predetermined temperatures ranging from 25 to 900 °C.

4.2.2. Definition of high strength steel

In recent years, high strength steels (HSS) have garnered considerable attention. Recent growth in the construction of high-rise buildings and long-span constructions has expanded the demand of high-strength steel. Large-sized members and ultrathick steel plates are employed in high-rise buildings to withstand the tremendous stresses imposed by lateral load resisting components such as outriggers and belt trusses, as well as vertical loads on the columns that support the lower level. HSS contribute to decreased cross sectional area, which

results in lighter structures (or a higher strength to weight ratio), greater clearance heights, and simplified fabrication and inspection.

Concerning the definition of HSS, The ASTM standard defines a nominal yield stress of 690 N/mm^2 for quenched and tempered steel which is the corresponding high strength steel used in plate form (Bjorhovde 2004). Additionally, the Hong Kong Standard defines high strength steel as having a nominal yield stress ranging from 460 to 690 N/mm^2 (Hong Kong Buildings Department 2005). The newly published European Standard has an assumed delineation point of 460 N/mm^2 to denote mild steel from high strength steel. In Australia, high strength structural steel is defined as steel that currently exceeds the yield stress of 450 N/mm^2 (AS 1998).

Following the tragedy at the World Trade Center, structural fire safety has become a significant concern when designing high-rise building structures. Until now, some study has been conducted on the mechanical properties of high-strength steel during and after fire. However, considering the significant discrepancies between experimental outcomes and design standards reported, investigations combining these findings are still scarce in the literature.

4.2.3. Modulus of elasticity (Young's modulus)

Young's modulus is a numerical constant named after the 18th-century English physician and physicist Thomas Young. It describes the elastic properties of a solid that is subjected to tension or compression in only one direction, such as a metal rod that returns to its original length after being stretched or compressed lengthwise. The Young's modulus is a property of a material that indicates its ability to withstand changes in length when subjected to lengthwise tension or compression. Young's modulus, also known as the modulus of elasticity, is the ratio of stress to strain in a material at its elastic stage, as shown in equation (4.1). It is frequently expressed as the tangent modulus to the stress-strain curve's initial linear elastic portion.

$$E = \frac{\sigma}{\varepsilon} \tag{4.1}$$

where E is Young's modulus, σ is the uniaxial stress and ε is the strain.

4.2.4. Yield strength

At room temperature, normal steel has a distinct and well-defined yield plateau in tension. However, high strength steels lack a clearly defined yield point at either room or elevated temperatures. Generally, the yield strength of mild steel is determined at strain levels of 0.2 % offset, or 0.5, 1.5, or 2.0 %. The yield strength offset by 0.2 % ($f_{0.2,T}$) is defined as the point at which the stress–strain curve intersects with the proportional line offset by 0.2 % strain (Figure 4-1). The yield strengths of $f_{0.5,T}$, $f_{1.5,T}$, and $f_{2.0,T}$ are those corresponding to the strain levels of 0.5, 1.5, and 2.0%, respectively. (Wang W, 2013)

Due to the lack of a clearly defined yield point, the yield strength of steel at elevated temperatures is defined differently in different design codes of practice (Wang W, 2013). The

European Convention on Steel Construction (ECCS 2001) specifies that yield strength at room temperature corresponds to a 0.2% offset strain level, while yield strength above 400 °C is assumed to be 0.5% nominal strain level. When temperatures are between 25 and 400 °C, yield strength is assumed to be the interpolation between 0.2% offset and 0.5% nominal strain. According to BS5950 (BSI 1990), yield strength at elevated temperatures can be determined at nominal strain levels of 0.5, 1.5, or 2% for various types of structural members. The yield strength at elevated temperature in EC3 (CEN 2005b) and Eurocode 4 (EC4) (CEN 2006) is calculated using a strain level of 0.2% offset. Kirby and Preston (1988) recommend the use of 1% nominal strain for evaluating the yield strength at elevated temperatures. AISC (2005) recommends that the properties for steel at elevated temperatures are adopted from the European Convention for Constructional Steelworks (ECCS) Model Code on Fire Engineering (2001).

4.2.5. Experimental Setup and material properties of high strength steel

4.2.5.1. YP400 and YP500

The high yield point steels YP400 and YP500 (Katsuo M, 2013) (Kohno M, 2017) (specified minimum yield strength of 400 N/mm2 and 500 N/mm2, respectively) are used for columns of seismic isolation structures and provide better performance in terms of strength, and weld ability. The general properties of YP400 and YP500 steel are described in the Table 4-1. The chemical components of YP400 and YP500 steels used in this paper are described in the Table 4-2.
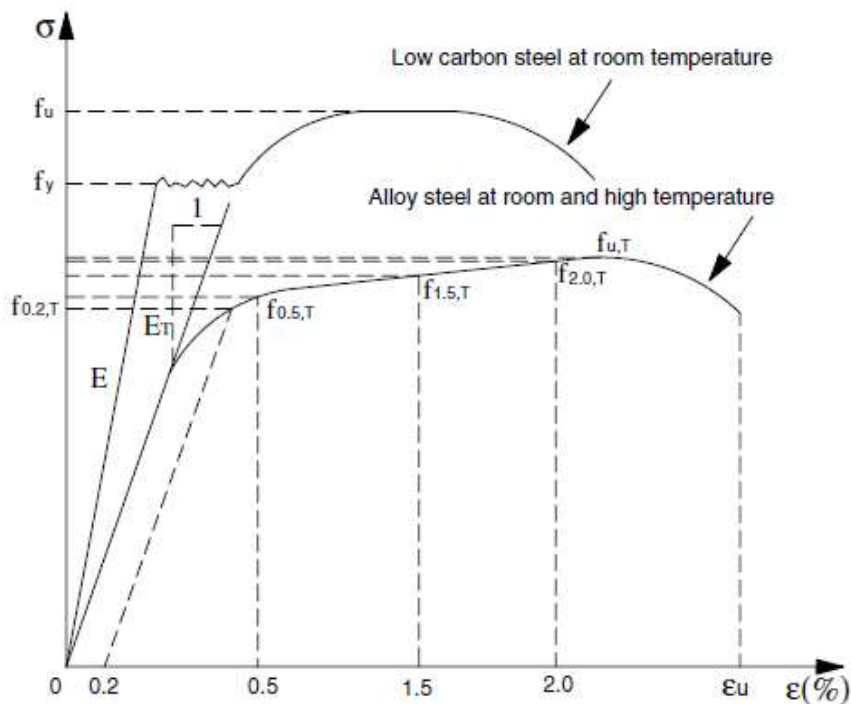
Figure 4-1 Typical representation (shapes) of stress–strain curves of steel at elevated temperature (Wang W, 2013)

Table 4-1 General properties of YP400 and YP500 steel

Type	C_{eq} (%)	P_{cm} (%)	Yield point (N/mm^2)	Tensile strength (N/mm^2)	Yield ratio (%)
YP400	$\leq$ 0.4	$\leq$ 0.26	$\geq$ 400 $\leq$ 550	$\geq$ 490 $\leq$ 640	$\leq$ 90
YP500	$\leq$ 0.44	$\leq$ 0.28	$\geq$ 500 $\leq$ 650	$\geq$ 590 $\leq$ 740	$\leq$ 90

Table 4-2 Chemical components of YP400 and YP500 steel (%)

Type	C	Si	Mn	P	S	Cu	C_{eq}	Ni	Cr	Mo	V	Nb	B	P_{cm}
YP400	0.14	0.27	1.27	0.013	0.002	0.01	0.37	0.20	0.01	0.00	0.00	0.00	0.00	0.21
YP500	0.10	0.22	1.54	0.010	0.002	0.01	0.40	0.20	0.13	0.00	0.06	0.02	0.00	0.20
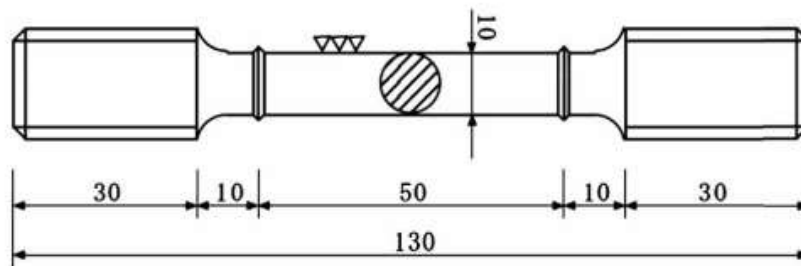
Figure 4-2 Dimensions of steel coupon for tensile tests

The tensile tests were carried out to evaluate the stress-strain behavior of YP400 and YP500 steels at various temperatures. The tension test is one of the most frequently used methods for material evaluation. The tension test is performed in its simplest form by holding the opposite ends of a test item within the load frame of a test machine. The methods for establishing tensile test conditions were based on Japanese Industrial standard JIS Z 2241 (JIS-Z2241, 2020) and JIS G 0567 (JIS-G-0567:2012, 2012). The thickness of the specimens prior to machining for YP400 and YP500 steel is 19 mm. The test coupon measured 130 mm in total length and the gauge length for tension measurement is 50 mm. The diameter of cross section of the tapered section is 10 mm. The configuration of a typical test coupon used in tensile test is as shown in Figure 4-2.

A total of 10 coupon tests for each type of steel YP400 and YP500 were carried out with the tension strain rate of 0.3%/ minutes before 10% of strain and increasing up to 7.5%/ minutes after 10 % of strain. There are five temperatures used in the range of 23-650 °C: 23, 350, 450,

550 and 650 °C. The displacements were recorded during the tensile tests and were used to generate the stress-strain curves of YP400 and YP500 steel (Katsuo M, 2013). These curves are plotted in Figure 4-3 and Figure 4-4. Jigs were attached to the top and bottom of the gauge length and elongation was measured. The relative movement of the jigs, or elongation, is measured by a displacement meter outside the furnace.
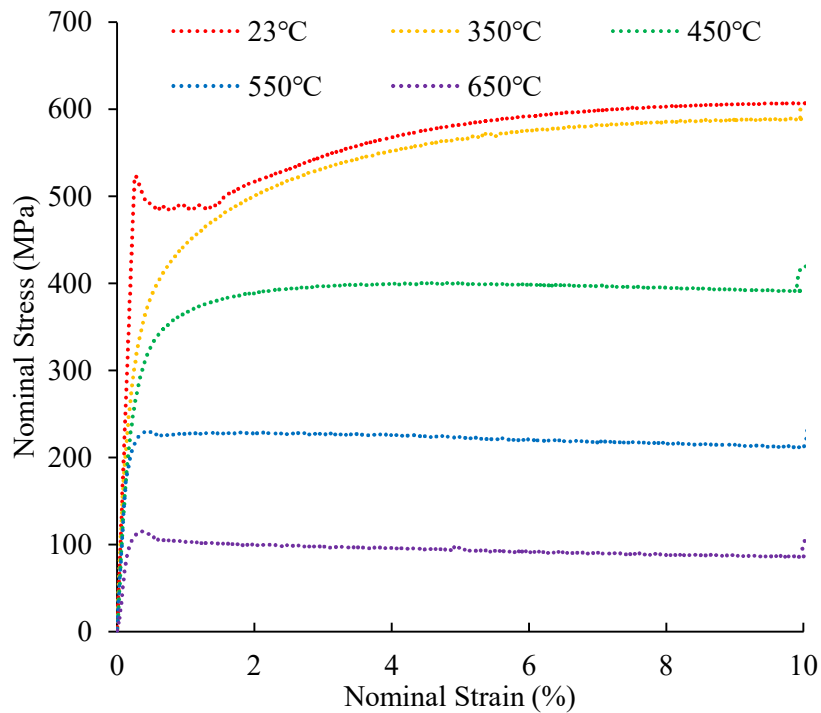
Figure 4-3 Stress-strain relationship curves of YP400 steel at different temperatures
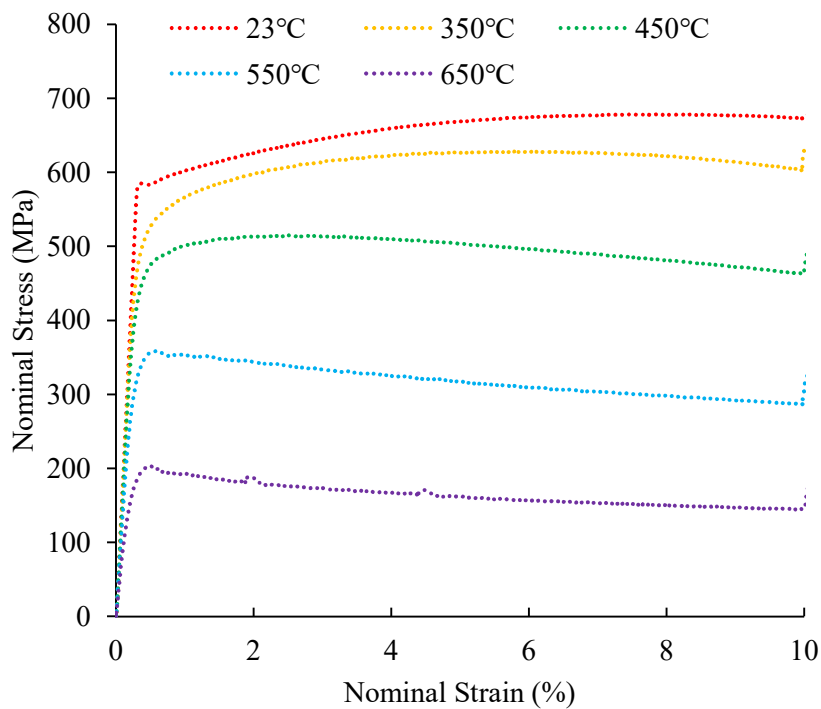
Figure 4-4 Stress-strain relationship curves of YP500 steel at different temperatures

Table 4-3 Mechanical properties of YP400 and YP500 steel at different temperatures.

Temperature (°C)	Elastic modulus (MPa)		0.2 % offset yield strength $f_{0.2}$ (MPa)		1%-strain strength $f_{1.0}$ (MPa)		Tensile strength f_u (MPa)	
	YP400	YP500	YP400	YP500	YP400	YP500	YP400	YP500
23	211,754	190,888	493	583	488	602	618	678
350	179,005	186,638	360	526	445	567	615	629
450	146,538	178,001	312	470	366	501	428	515
550	135,326	144,725	228	352	227	353	263	358
650	66,818	100,899	115	199	103	192	130	203

Mechanical properties of these steels at a specific temperature can be evaluated through steady state tests, in which the elastic modulus and the yield strength at high temperatures were determined in Table 4-3. The elastic modulus was computed from slope of the stress-strain curve in the initial approximate linear zone. To compare with other steels, the 0.2 % offset yield strength and strength at 1% strain levels were determined ($f_{0.2}$ and $f_{1.0}$ in Table 4-3).

4.2.5.2. H-SA700

The high strength steel H-SA700 (H-SA700, 2012) provide better performance in terms of strength and weld ability. The chemical compositions of high-strength steel H-SA700 used in this study are listed in the Table 4-4.

The tensile tests were carried out to evaluate the stress-strain behavior of H-SA700 steel at various range of temperatures. The tension test is one of the most used tests for evaluating materials. In its simplest form, the tension test is carried out by holding opposite ends of a test item within the load frame of a test machine. The shape and size of tensile test coupons were prepared in accordance with the JIS G 0567:2012 (JIS-G-0567:2012, 2012). The test coupon measured 130 mm in total length and the gauge length for tension measurement is 50 mm. The diameter of cross section of the tapered section is 10 mm. The type of coupon is II-10 with the configuration of a typical test coupon used in tensile test as shown in Figure 4-5.

A tensile force is applied by the machine with maximum load capacity of 100 kN, which results in the gradual elongation and eventual fracture of the test item. During this process, force-extension data is monitored and recorded. When properly conducted, the tensile test provides force-extension data that can quantitate several important mechanical properties of a material, such as elastic deformation properties, yield strength, and ultimate tensile strength as well as elastic and plastic strains. The heating system consisted of an electric furnace, the furnace temperature controller and the data acquisition system for recording and monitoring temperatures. The furnace could achieve temperatures up to 1100 °C. The displacement of the coupon specimens was probed using type DT-5S (Linear variable differential

transformer) with 0.5 μm of resolution. The data acquisition software (Trapezium2) was used to record the load–displacement data during the test.

A total of 6 coupon tests were carried out with the tension velocity of 0.3 %/minutes before 10 % of strain and increasing up to 7.5 %/minutes after 10 % of strain. There are six temperatures used in the range of 23-600 °C: 23, 350, 400, 500, 550 and 600 °C. The displacements were recorded during the tensile tests and were used to generate the stress-strain curves of H-SA700 steel. These curves are plotted in Figure 4-6.

Mechanical properties of steel at a specific temperature can be evaluated through steady-state tests, in which the elastic modulus and the yield strength at high temperatures were determined in Table 4-5. The elastic modulus was computed from slope of the stress-strain curve in the initial approximate linear zone. To compare with other steels, the 0.2 % offset yield strength and strength at 1 % strain levels were determined ($f_{0.2}$ and $f_{1.0}$ in Table 4-5).

Table 4-4 Chemical composition of H-SA700

	C	Si	Mn	P	S	Cu	Ceq
Chemical composition (%)	0.13	0.23	0.88	0.01	0.002	0.17	0.53
	Ni	Cr	Mo	V	Nb	B	Pcm
	0.04	0.80	0.32	0.02	-	-	-

Table 4-5 Mechanical properties of H-SA700 steel at different temperatures

Temperature (°C)	Elastic modulus (MPa)	0.2 % offset yield strength $f_{0.2}$ (MPa)	1%-strain strength $f_{1.0}$ (MPa)	Tensile strength f_u (MPa)
23	226,000	799	804	847
350	193,000	681	719	767
400	195,000	651	694	726
500	222,000	562	595	597
550	197,000	488	494	503
600	115,000	334	333	337
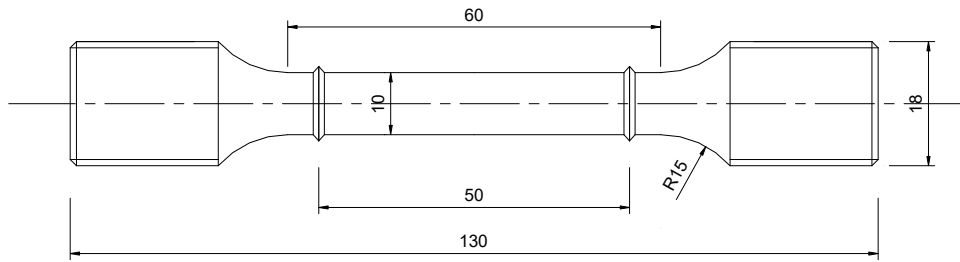
Figure 4-5 Dimensions of steel coupon for tensile tests
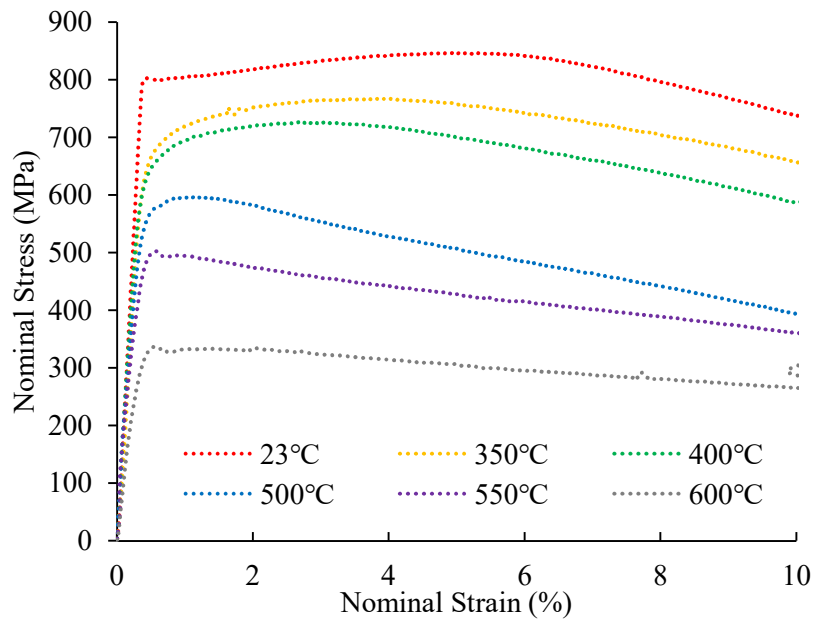
Figure 4-6 Stress-strain curves of H-SA700 steel at different temperatures

4.3. Characterization of the time- and temperature-dependent behavior of high strength steels

As described previously in Chapter 2, a deep understanding of the time-dependent mechanical properties of structural steel at elevated temperatures is crucial for forecasting the strength of steel members subjected to fire, particularly high strength steels such as YP400, YP500, and H-SA700.

As further demonstrated in Chapter 2, a comprehensive review of the literature on the mechanical behavior of structural steel at elevated temperatures reveals a problem of scarcity of experimental creep data on structural steels used in building construction for the temperature and stress regimes relevant to structural-fire engineering applications. Additionally, no data are available for high strength steels, the most often required kind of structural steel for usage in high-rise buildings and long span constructions.

This section presents the results of a comprehensive investigation of the high-temperature creep phenomena in high-strength steels. Throughout this section, the adverse consequences of high-temperature creep on steel constructions subjected to fire temperatures will be demonstrated and emphasized. By ignoring these impacts, as is presently done, erroneous and perhaps unsafe structural response predictions may be made.

4.3.1. Formulation of thermal creep of steel

A computational material creep model was developed for explicitly accounting for the creep of structural steel in the changing temperature environment of a building fire. The constitutive material law of Fields and Fields (Fields, 1989) in the form of power-law creep (Norton, 1929) (Bailey, 1930) was used in the formulation of the computational creep model in this study. The material creep model for H-SA700 steel was modified as part of the NIST investigation into the collapse of the WTC (NIST, 2005) as follows.

The creep material model by Fields and Fields (Fields, 1989) was used to develop deformation mechanism for the ASTM A36 steel over a temperature range of 350 to 650 °C, for periods of up to 4 hours and for the creep strain up to 6 %. To develop the procedure, it was further assumed that the total strain could be subdivided into three independent components under conditions of constant stress and temperature as the empirical equation as follows:

$$\varepsilon_T = \varepsilon_e + \varepsilon_p + \varepsilon_c \tag{4.2}$$

where ε_T is the total strain, ε_e is time independent elastic strain, ε_p is time independent plastic strain and ε_c is time dependent plastic strain or creep strain. Therefore, two components ε_e and ε_p are temperature and stress dependent, while the creep strain component ε_c is time, stress and temperature dependent.

Fields and Fields (Fields, 1989) represented the empirical equation in the form of power-law creep (Norton, 1929) (Bailey, 1930) in order to calculate the creep strain using a function that separates the time and stress dependent in the equation (4.3).

$$\varepsilon_c = A t^B \sigma^C \tag{4.3}$$

In this equation, t is time, σ is stress, and parameters A, B and C are temperature dependent material constants. These material constants are calculated by the formulas in equations (4.4)-(4.6).

$$B(T) = B_0 + B_1 T \tag{4.4}$$

where $B_0 = 1.1$ and $B_1 = 0.0035$

$$C(T) = C_0 + C_1 T \tag{4.5}$$

where $C_0 = 2.1$ and $C_1 = 0.0064$

$$A(T) = 10^{-(A_0 + A_1 T)} \tag{4.6}$$

where for $T < 500°C$, $A_0 = 6.10$, $A_1 = 0.573$ and for $T > 500°C$, $A_0 = 13.25$, $A_1 = -0.00851$.

In equation (4.3)-(4.6), T is in $°C$, t is in minutes, σ is in ksi, and ε_c is in percent (unitless).

During the WTC investigation (NIST, 2005), NIST also discovered that creep behavior is a critical input to finite element models of the WTC structures' response to fires. They

characterized the actual creep behavior of the important truss angle steel that made up the chords of the floor trusses in their studies. Furthermore, they developed a methodology for estimating the creep behavior of the other steels in the trusses, truss seat, perimeter columns, and core columns based on literature data. Their analysis retains the formalism of Fields and Fields (Fields, 1989), but they evaluated the temperature dependent parameters A, B, and C using different equations than Fields and Fields.

The constant C is evaluated as the stress exponent for creep rate $\frac{d\varepsilon}{dt}$ using extra strain rate data from the high-temperature tensile tests, and non-linear least squares fit to the $(\frac{d\varepsilon}{dt}, \sigma, T)$ data shown in equation (4.7)

$$C(T) = C_0 + C_1 T \tag{4.7}$$

where $C_0 = 3.233$ and $C_1 = 0.0117$

To ensure accurate representation of the creep behavior near and outside the boundaries of the experimental conditions, the parameter B was evaluated by the non-linear, least-squares fitting method in equation (4.8)

$$B(T) = B_0 + B_1 T^{B_2} \tag{4.8}$$

where $B_0 = 0.3982$, $B_1 = 3.5531 \times 10^{-11}$ and $B_2 = 3.6975$

Using the linear regression method, the parameter A could be represented by an exponential of a quadratic polynomial of temperature as shown in equation (4.9)

$$A(T) = \exp(A_0 + A_1 T + A_2 T^2) \tag{4.9}$$

where $A_0 = -55.4504$, $A_1 = 9.47600 \times 10^{-3}$ and $A_2 = -3.52064 \times 10^{-5}$; T is in °C, t is in seconds, σ is in MPa, and ε_c is in natural units (unitless).

In this study, the creep strain ε_c equation is followed by the form of Fields and Fields [3] as equation (4.3), but parameters A, B, C are retained in the form of NIST report [6] as equations (4.7)-(4.9).

In the WTC investigation (NIST, 2005), the NIST creep model is used for A242 steel, and NIST recommended using the ratio approach (NIST, 2005) to convert a creep model from one steel grade to another based on the ratio of tensile or yield strength (R_σ). This technique was initially employed to investigate the creep behavior of high yield point steels in this work, but it was found not suitable for YP400 and YP500 steels. As a result, the ratio technique is modified to obtain the values of creep parameters as follows.

This method was proposed by NIST (equation 6-19 of (NIST, 2005)), and the corrected stress can be calculated using the following equation:

$$\sigma_c = R_\sigma \sigma_a \tag{4.10}$$

where R_σ is the ratio of tensile or yield strength, σ_a is the applied stress.

The equation (4.3) will utilize the corrected stress and can be modified as shown in equation (4.11):

$$\varepsilon_c = At^B \sigma_c^C = (A \times R_\sigma^C)t^B \sigma_a^C \tag{4.11}$$

When this method is used to determine the values of the creep parameters A, B and C, the coefficient A is adjusted to convert the corrected stress return to the applied stress.

$$A_{\text{new}} = A \times R_\sigma^C \tag{4.12}$$

So that the parameter C were kept unchanged, and other parameters were changed to find more accurate results. Parameters in equations (4.7)-(4.9) were evaluated using a try and error approach for the stress-strain relationship between the experimental tensile test data and the analytical results by Abaqus. An equation of creep strain rate is required to formulate the computational material creep model and calculate time dependent strain. Creep strain rate can be expressed in two ways: strain-hardening format and time-hardening format. The creep strain rate in the strain-hardening formulation could be defined as a function of creep strain, as shown in equation (4.13), whereas in the time-hardening formulation, the creep strain rate is defined as a function of time as shown in equation (4.14) (Ottosen N, 2005). Previous studies (Harmathy, 1967) (Morovat M. L., 2011) (Hantouche E G, 2018) has demonstrated and confirmed that the strain-hardening formulation yields better and more accurate results when computing the creep strain. As a result, the Fields and Fields (Fields, 1989) equation is described in a strain-hardening formulation in this study.

$$\dot{\varepsilon}_c = F(\varepsilon_c; \sigma; T) = A^{\frac{1}{B}} B \varepsilon_c^{\frac{B-1}{B}} \sigma^{\frac{C}{B}} \tag{4.13}$$

$$\dot{\varepsilon}_c = F(t; \sigma; T) = ABt^{B-1}\sigma^C \tag{4.14}$$

In equations (4.13) and (4.14), $\dot{\varepsilon}_c$ is in per seconds. equation (4.13) can be further simplified through the change of parameters (A, B and C) as shown in equation (4.15):

$$\dot{\varepsilon}_c = \left[a\sigma^n \left(\varepsilon_c(m+1)\right)^m\right]^{\frac{1}{m+1}} \tag{4.15}$$

where $a = AB; m = B - 1$ and $n = C$.

The creep strain difference per iteration can be represented as follows:

$$\Delta\varepsilon_c = \left[\left(\frac{a\sigma^n}{1+m}\right)^{\frac{1}{1+m}} \times \Delta t + \varepsilon_c^{\frac{1}{1+m}}\right]^{1+m} - \varepsilon_c \tag{4.16}$$

In case of implicit creep integration in finite element program Abaqus, derivative of the strain difference with respect to stress needs to be included in the user subroutine CREEP as per Abaqus documentation (Dassault system simula corporation) and can be written as follows:

$$\frac{\partial \Delta \varepsilon_c}{\partial \sigma} = \frac{\Delta t n}{\sigma} \left(\frac{a\sigma^n}{m+1}\right)^{\frac{1}{m+1}} \left[\Delta t \left(\frac{a\sigma^n}{m+1}\right)^{\frac{1}{m+1}} + \varepsilon_c^{\frac{1}{1+m}}\right]^m \qquad (4.17)$$

When analyzing implicit integration in Abaqus, a tolerance is required to achieve accurate results by controlling the difference in creep strain change between iterative steps ($\Delta \varepsilon_{i+1} - \Delta \varepsilon_i < tolerance$). If a difference does not satisfy this condition, the iteration will be repeated with smaller Δt until the condition is satisfied. Based on equations (4.15)-(4.17), a user subroutine CREEP is developed to consider the changing of temperature conditions.

Previous research (Wang W., 2017) (NIST, 2005) (Hantouche E G, 2018) have shown that creep effects are insignificant at temperatures below 400 °C. To inhibit the formation of any creep strains below 400 °C, one condition is set to end the subroutine if temperature conditions are below this level. The transient-state creep analysis was performed in Abaqus to more accurately characterize the time dependent strain when both temperatures and stresses are considered variables. As mentioned before, the strain hardening formulation is used as a criterion to consider the change in stress. However, three temperature-dependent coefficients (a, m, n) vary over time as well. The equations of these temperature dependent coefficients were also included in the subroutine. It automatically calculates these coefficients based on the new temperature at the beginning of each increment step. The subroutine calculation process is summarized in Figure 4-7.
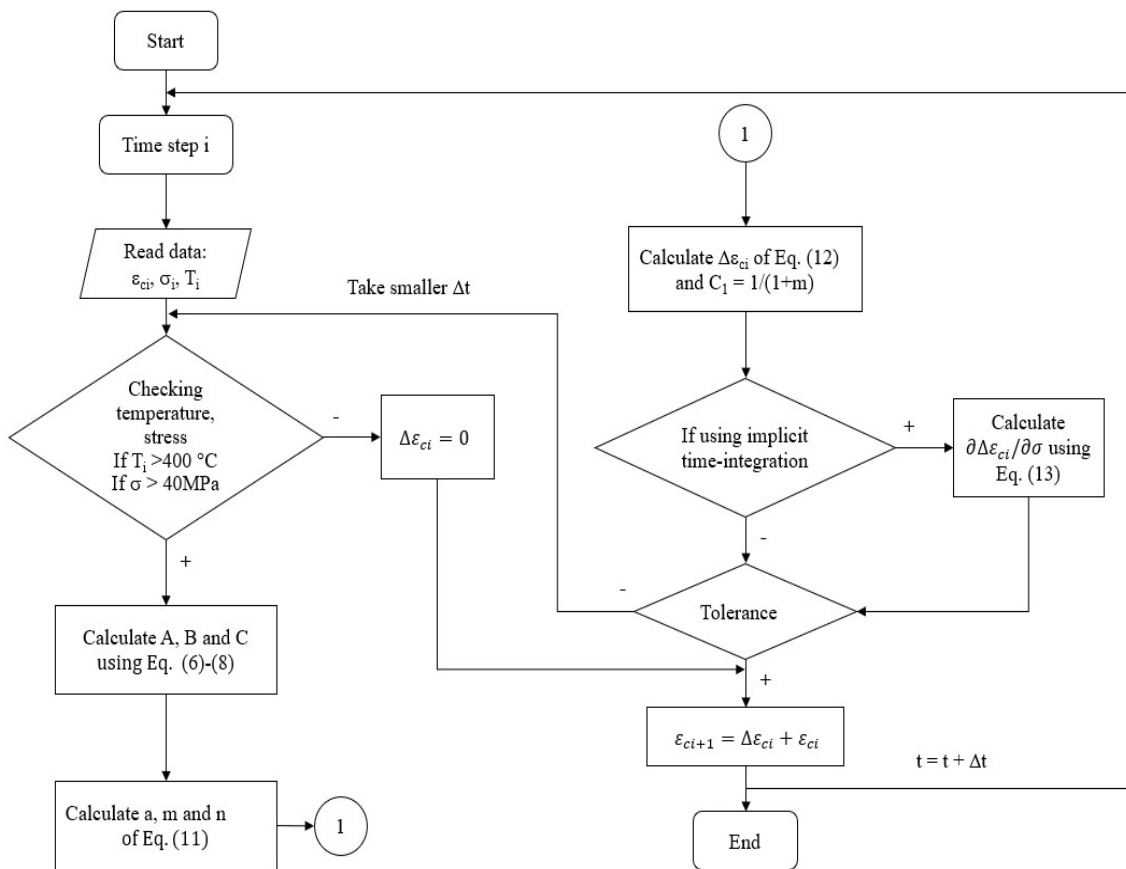
Figure 4-7 Flowchart representing the subroutine incremental solution

4.3.2. YP400 and YP500 steel

4.3.2.1. Determination of creep parameters

The creep parameters A, B, and C were established using the results of tensile tests. A trial-and-error technique was used to determine the most accurate stress-strain curves for the FE model that fit experimental data at various temperature conditions. A set of creep parameters are assumed to be analyzed, and the resulting analysis stress-strain curve is compared to the experimental target curve to determine its proximity. If the proximity is insufficient, one of the creep parameters is changed and the process is repeated. To apply the general minimum error method, this process must be repeated a very large number of times. Since this was not practically possible, the overall fitness of the stress-strain curves was determined visually.

To simulate the tensile tests on steel coupons, a three-dimensional numerical model was created using the finite element (FE) analysis software Abaqus. The coupon was modelled using an 8-node thermally coupled brick, trilinear displacement, and temperature element, C3D8T. The mesh size was controlled using an approximate global size of 2 mm. Figure 4-8 illustrates the finite element meshes used in the simulations. One side of the coupon model is assumed to be rigidly fixed (encastre) and limited to a reference point 1 (RP1). The other side of the coupon is constrained to a reference point 2 (RP2) and extracted at a tension rate of 0.3 %/minutes (0.0025 mm/minutes). The entire coupon model is set to a constant temperature value. The elastic modulus was determined using the tensile test results shown in Table 4-3.

When defining plasticity data in Abaqus, it is essential to use true stress and strain to properly analyze the data. Quite frequently, material test data are provided using nominal stress and strain values. In such cases, the following formulas are employed to transform the nominal stress-strain values of the plastic material to true stress-strain values.

The relationship between true strain and nominal strain is established by expressing the nominal strain as follows:

$$\varepsilon_{true} = \ln(1 + \varepsilon_{nominal}) \qquad (4.18)$$

The definition of true stress can be given by this equation:

$$\sigma_{true} = \sigma_{nominal}(1 + \varepsilon_{nominal}) \qquad (4.19)$$

Between room temperature and 400 °C, these total strain values can be divided into elastic and plastic strain components (when creep behavior can be neglected). The plastic strain is calculated by subtracting the elastic strain, defined as the true stress divided by the Young's modulus, from the total strain, as illustrated in the following equation:

$$\varepsilon_{plastic} = \varepsilon_{true} - \frac{\sigma_{true}}{E} \qquad (4.20)$$

The plastic material properties were described in a quite method described in Figure 4-9 that hypothetical curves representing instantaneous curves were created based on the true stress-plastic strain relationship observed during experimental tests at various temperatures. When

actual test curves tend to rise, these hypothetical curves closely resemble the test data for this strain range; however, when actual test curves tend to fall, the relationship between true stress and plastic strain is described as a logarithmic trendline as in format of an equation (4.21). The hypothetical curves with input data of plastic properties are depicted in Figure 4-10 and Figure 4-11. The yielding point is described in Section 4.2.5. as the beginning of the plastic zone.

$$\sigma_{\text{true}} = \alpha(T) \times \ln(\varepsilon_{\text{p}}) + \beta(T) \tag{4.21}$$

Where σ_{true} is true stress, ε_{p} is plastic strain, $\alpha(T)$ and $\beta(T)$ are coefficients at different temperatures.

The values of $\alpha(T)$ and $\beta(T)$ are shown in the Table 4-6.
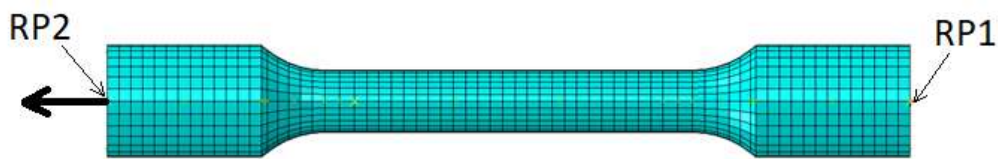
Figure 4-8 Tensile test modelling detail
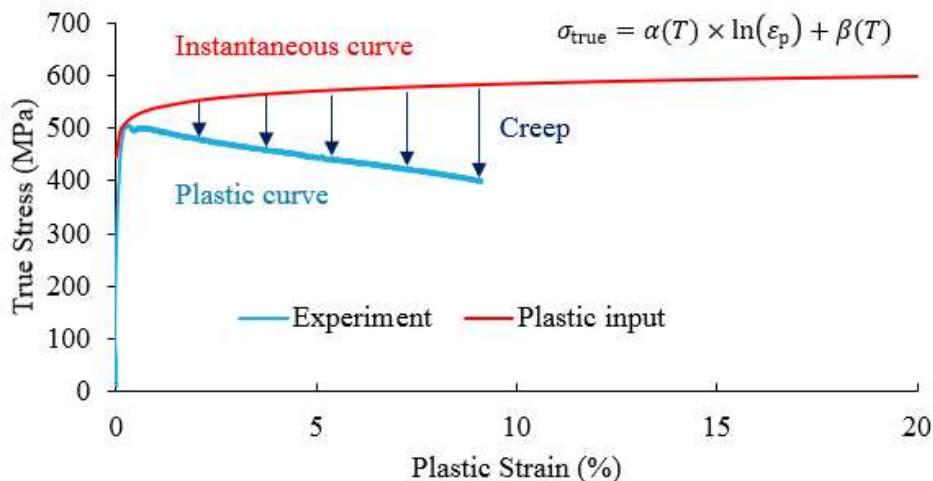
Figure 4-9 The description to define instantaneous curve.

Table 4-6 Values of $\alpha(T)$ and $\beta(T)$ for YP400 and YP500 steels

Temperature (°C)	$\alpha(T)$ (MPa)		$\beta(T)$ (MPa)	
	YP400	YP500	YP400	YP500
23	50	50	557	633
350	80	45	472	590
450	33	28	380	520
550	15	6.1445	260	369
650	5.56	5	128.11	217
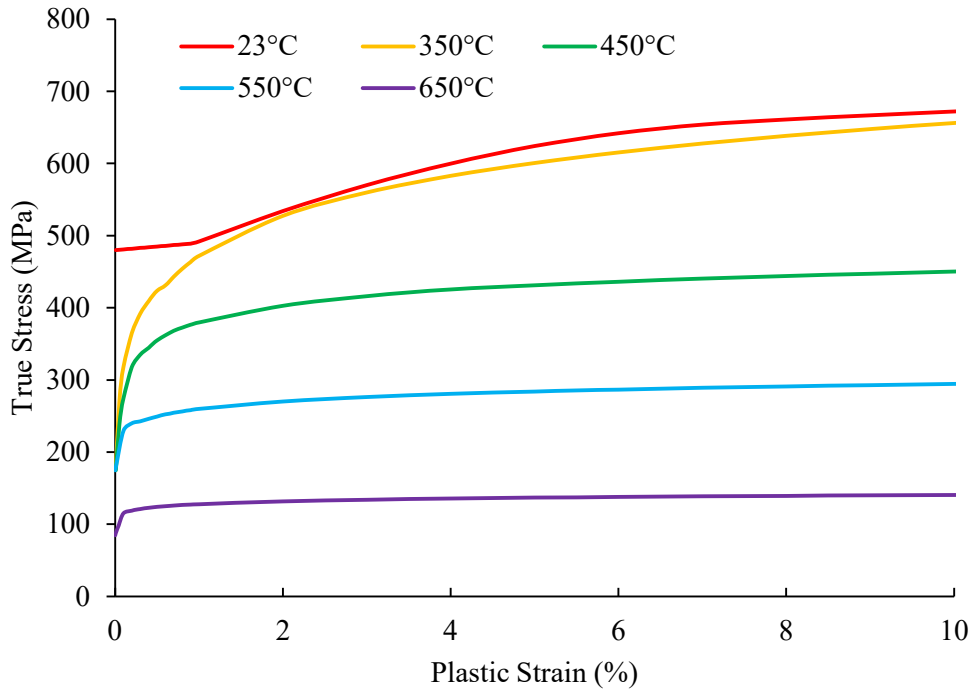
Figure 4-10 Plastic properties input data in Abaqus for YP400 steel
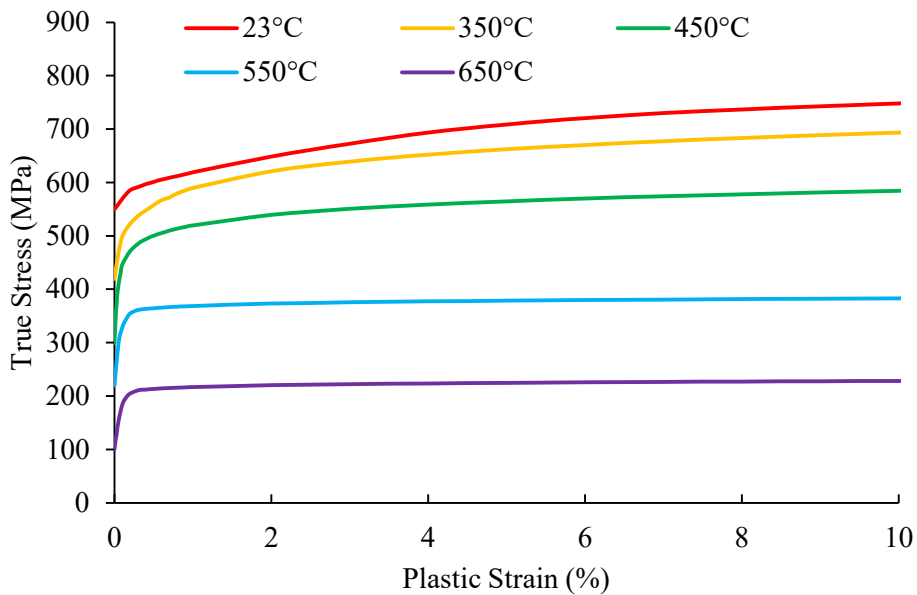
Figure 4-11 Plastic properties input data in Abaqus for YP500 steel

4.3.2.2. Verification of thermal creep models for steel

The FE analysis results are validated against the experimental data and are shown in Figure 4-12 and Figure 4-13. A trial-and-error approach is used to determine the most accurate stress-strain curves for the FE model that fit the experimental data at various temperatures. The user subroutine CREEP is used to characterize and change a set of parameters (A, B, and $C)$ at each temperature level (23, 350, 450, 550, and 650 °C). A smooth function is constructed that approximately fits a series of data points. If the parameters do not result in a

good fit to the tensile test curve, the estimates for *A* and *B* are increased or decreased, and this process is repeated until a good fit to the experimental data is obtained.

As shown in Figure 4-12 and Figure 4-13, tensile test results indicate that creep behavior does not exist at temperatures below 400 °C (at 23 and 350 °C), and the analysis results are completely consistent with the experimental results. At 450 °C, the creep effect of YP400 steel is quite small, in comparison to the quite noticeable creep effect of YP500 steel. Furthermore, YP400 steel has a clear yield plateau at 23°C, which complicates the simulation of steel behavior and impairs the analysis of steel behavior between 23 °C and 350 °C (this will be noticed when simulating columns in the Chapter 5). In comparison, because YP500 steel does not exhibit the yield phenomenon, the Abaqus program had no difficulty accurately simulating both the tensile test and the creep behavior of the steel.

Additionally, the stress degradation behavior of YP500 steel is clearly visible at elevated temperatures and might be explained by the creep behavior under consideration. If the stress is maintained at a steady level, the strain will increase over time, and vice versa, if the strain is maintained at a steady level, the stress will gradually decrease. It will result in the degrading of nominal stress behavior.

Given that the maximum strain of column, as determined by the column analyses described in 0, is less than 2%, these curves must fit within the strain range of 0% to 2% to characterize the values of parameters *A*, *B* and *C* in Table 4-7.

As illustrated in Figure 4-14, the creep impact is fairly minimal at 450 °C but becomes quite strong between 550 and 650 °C when there is a significant difference between the results of the analysis with and without creep behavior. Thus, the Creep subroutine accurately replicated the creep behavior of YP400 steel at elevated temperatures. In comparison, the difference between creep behavior analysis results for YP500 steel with and without creep is quite small between 450 and 550 °C when nominal strain does not exceed 2%, as illustrated in Figure 4-15. As is the case with YP400 steel, the creep effect is quite noticeable around 650 °C.

Table 4-7 The value of constant coefficients A, B and C at various temperature conditions

T (°C)	YP400		YP500		C
	lnA	B	lnA	B	
450	-61.976	0.9777	-67.237	1.458	8.498
550	-61.9071	0.8803	-71.038	1.580	9.668
650	-62.1897	1.2922	-70.645	1.592	10.838
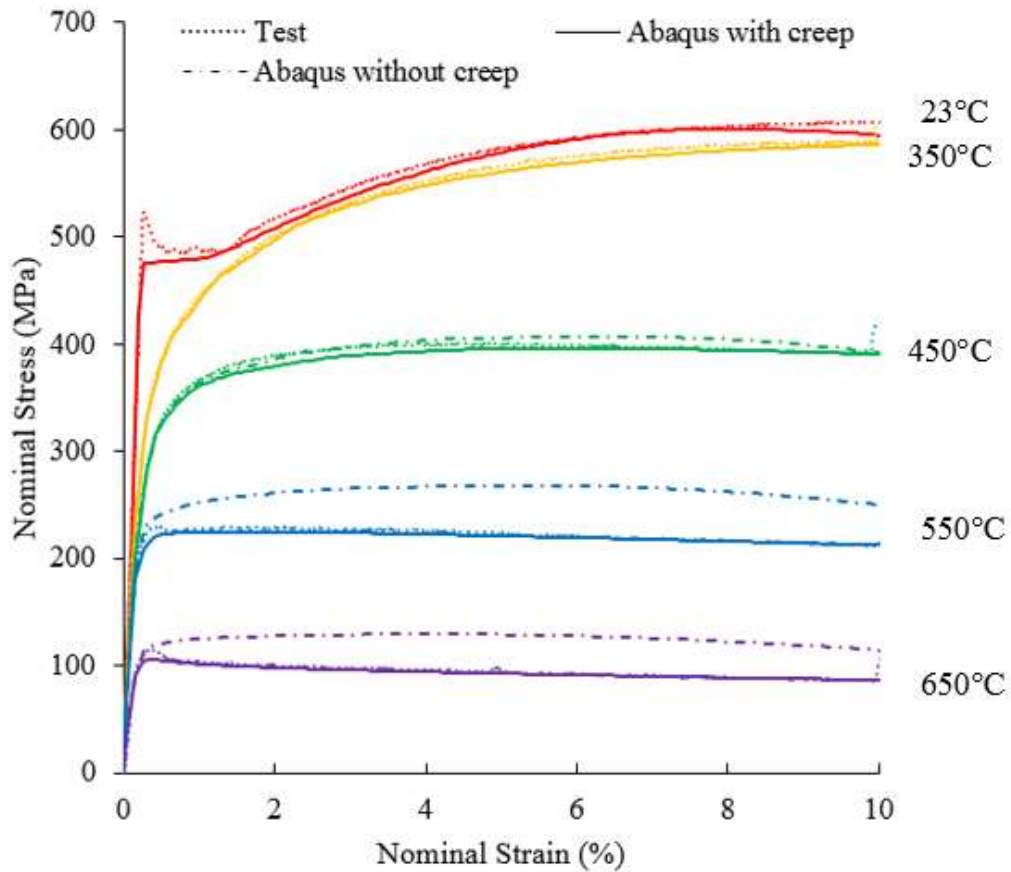
Figure 4-12 The stress-strain relationship between experimental and analytical results for YP400 steel (up to 10% of strain)
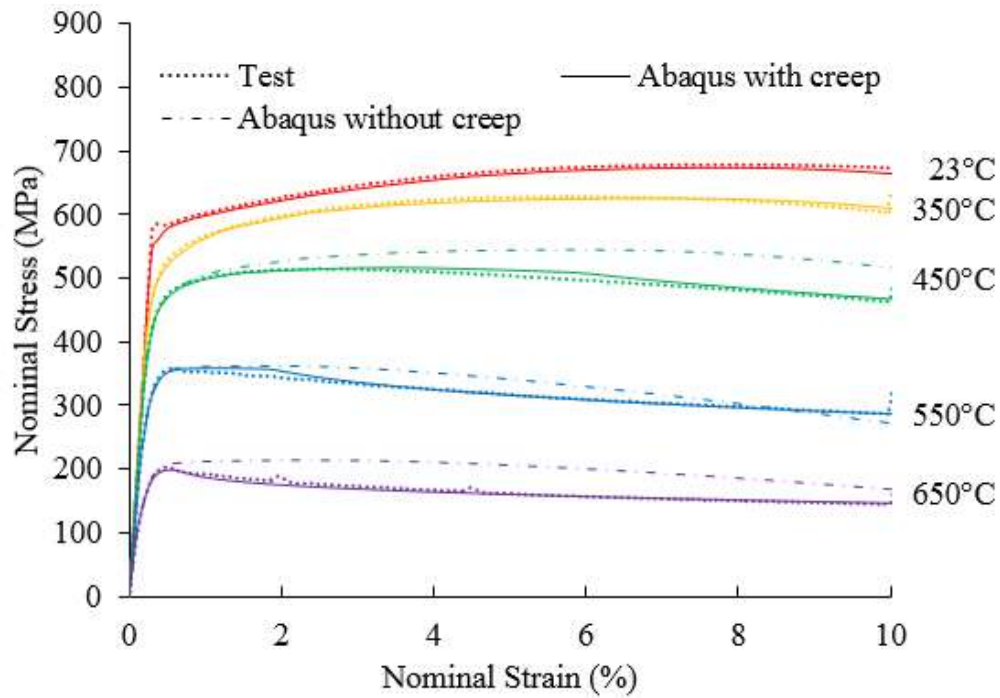
Figure 4-13 The stress-strain relationship between experimental and analytical results for YP500 steel (up to 10% of strain)

70
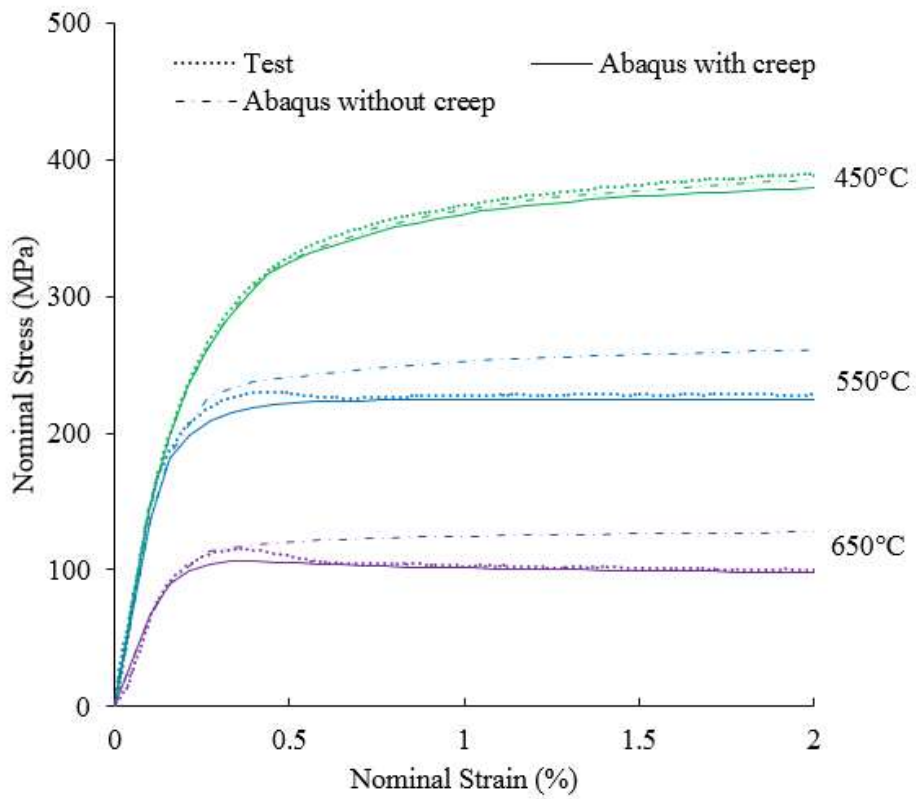
Figure 4-14 The stress-strain relationship between experimental and analytical results for YP400 steel (up to 2% of strain)
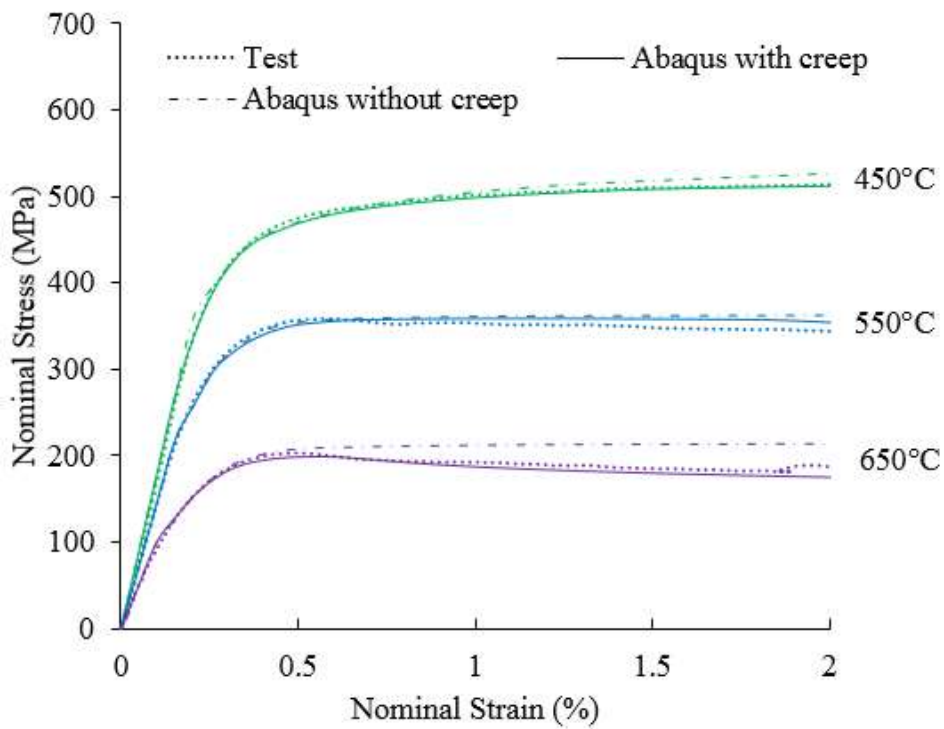
Figure 4-15 The stress-strain relationship between experimental and analytical results for YP500 steel (up to 2% of strain)

When comparing two analytical curves, it is assumed necessary to take creep into account in order to accurately reproduce the behavior of the YP400 and YP500 steel members analytically. The expressions of A, B and C in the temperature range from 400 to 650 °C are given in equations (4.22)-(4.24) for YP400 steel, in equations (4.25)-(4.27) for YP500 steel, where T is in °C. Between 400 and 450 °C, creep parameters will be calculated using these equations (4.22)-(4.27). The application of Fields and Fields' creep power law [4] has been demonstrated to be reasonable in numerous other studies, and the simulation results presented in this paper also demonstrate that it is reasonable for the temperature range 400 to 450 °C, despite the absence of test results at 400 °C.

YP400:

$$\ln A = -66.64 + 1.83 \times 10^{-2}T - 1.76 \times 10^{-5}T^2 \tag{4.22}$$

$$B = \begin{cases} 0.8759 + 5.9883 \times 10^{40} \times T^{-15.743} \\ \quad (450\,°C \leq T \leq 550\,°C) \\ 0.7544 + 1.8661 \times 10^{-25} \times T^{8.6955} \\ \quad (550\,°C \leq T \leq 650\,°C) \end{cases} \tag{4.23}$$

$$C = 3.233 + 0.0117 \times T \tag{4.24}$$

YP500:

$$\ln A = 1.775 - 0.2477 \times T + 2.097 \times 10^{-4} \times T^2 \tag{4.25}$$

$$B = 1.5944 - 1.3913 \times 10^{29} \times T^{-11.31} \tag{4.26}$$

$$C = 3.233 + 0.0117 \times T \tag{4.27}$$

4.3.3. H-SA700

4.3.3.1. Determination of creep parameters

A 3D numerical model, using finite element (FE) analysis Abaqus software, was created to simulate the tensile tests of steel coupon. An 8-node thermally coupled brick, trilinear displacement and temperature element, C3D8T, were utilized to model the coupon on Abaqus. The approximate global size of 2 mm was used to control the mesh size. The finite element meshes used in the simulations are shown in Figure 4-16. One side of the coupon model is considered rigidly fixed (encastre) and constrained to a reference point 1 (RP1). The other side of the coupon is constrained to a reference point 2 (RP2) and pulled out by axial force P with a tension velocity of 0.3 %/minutes (0.0025mm/minutes). A constant temperature value is set for the whole coupon model. The tensile test results shown in Table 4-5 were used for the elastic modulus and Poisson's ratio.

The plastic material properties were specified to depict instantaneous curves by hypothetical curves based on the true stress-plastic strain relationship of the experimental tests at various temperatures (similar with section 4.3.2.). When the actual test curves tend to rise, these hypothetical curves closely resemble the test data in this strain range; however, when the actual test result curves tend to fall, the relationship between true stress and plastic strain is

expressed as a logarithmic equation as in format of an equation (4.28). Figure 4-17 depicts these hypothetical curves with plastic properties input data.

$$\sigma_{\text{true}} = \alpha(T) \times \ln(\varepsilon_{\text{p}}) + \beta(T) \tag{4.28}$$

Where σ_{true} is true stress, ε_{p} is plastic strain, $\alpha(T)$ and $\beta(T)$ are coefficients at different temperatures.

The values of $\alpha(T)$ and $\beta(T)$ are shown in the Table 4-8.
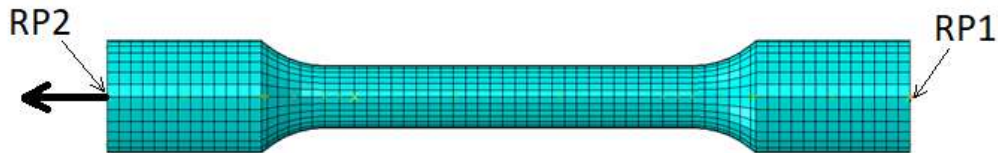
Figure 4-16 Tensile test modelling detail
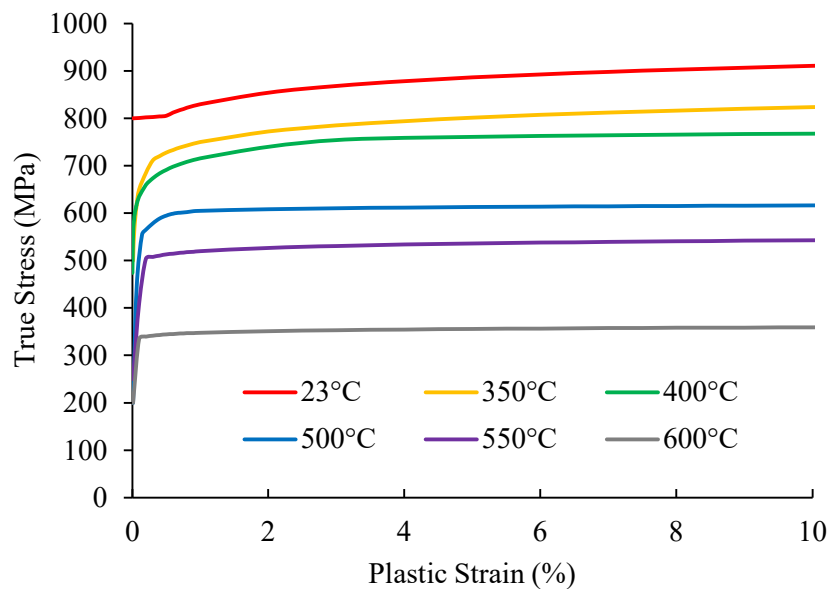
Figure 4-17 Plastic properties input data in Abaqus for H-SA700 steel

Table 4-8 Values of $\alpha(T)$ and $\beta(T)$ for H-SA700 steel

Temperature (°C)	$\alpha(T)$ (MPa)	$\beta(T)$ (MPa)
23	35	830
350	32	750
400	35 ($\varepsilon_{\text{p}} \leq 3\%$) 10 ($\varepsilon_{\text{p}} > 3\%$)	716 ($\varepsilon_{\text{p}} \leq 3\%$) 745 ($\varepsilon_{\text{p}} > 3\%$)
500	5	605
550	10	520
600	5	348
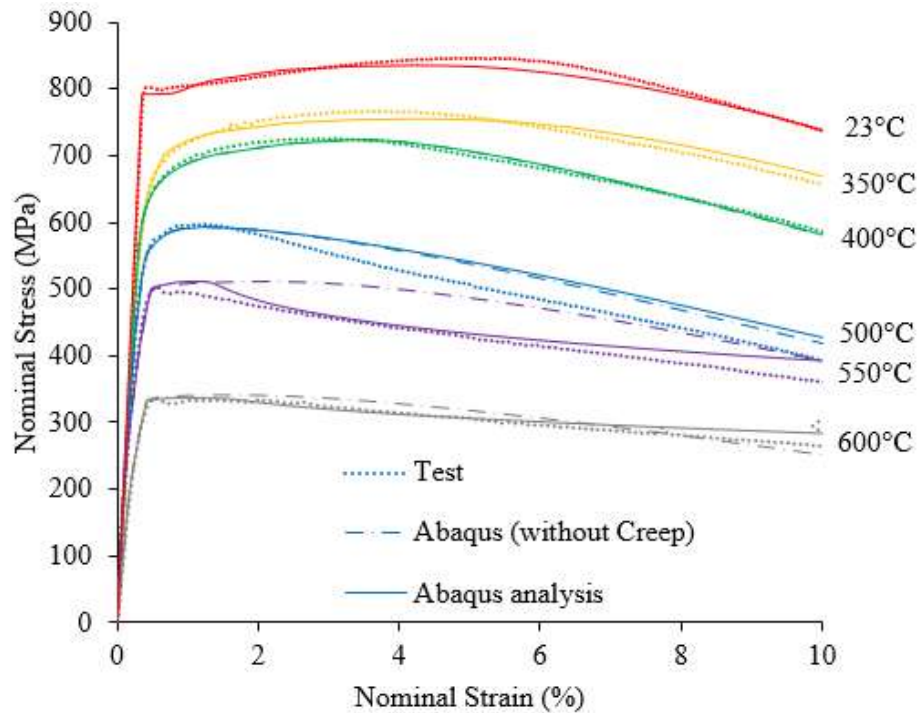
Figure 4-18 The stress-strain relationship between experimental and analytical results (Strain up to 10%) of H-SA700 steel

4.3.3.2. Verification of thermal creep models for steel

The results obtained from the FE analysis are first validated against the experimental data and shown in Figure 4-18. A try and error approach is used to find the most accurate stress-strain curves of FE model fit with experimental data at various temperature conditions. A set of parameters (*A*, *B* and *C*) is characterized at each level of temperature (23, 350, 400, 500, 550 and 600 °C) in the user subroutine CREEP and changed in which a smooth function is constructed that approximately fits to a series of data points. If the parameters did not lead to a suitable fit of the tensile test curve, the estimate for the parameters *A* and *B* is increased or decreased and then this process is repeated until a close fit with the experimental data is obtained.

The tensile test results presented in this study clarified that creep effects appeared when the temperature in steel exceeds 400 °C. Furthermore, the slope of the stress-strain curve is the most inclined, implying that the creep effect is strongest at 500 °C. From the observation of column analyses described in Chapter 5, it is found that the maximum strain of the column is not more than 2%, so these curves must fit in the strain range from 0% to 2%, as shown in Figure 4-19, to characterize the values of parameters *A*, *B* and *C* in Table 4-9. As illustrated in Figure 4-19, the difference between these two curves (with and without creep behavior) should have some influences on the behavior of the column. Although the difference was still small, it would reflect to the column behavior (especially to the maximum vertical displacement and collapse time as shown in Chapter 5).

Table 4-9 The value of constant coefficients A, B and C at various temperature conditions for H-SA700 steel

T (°C)	lnA	B	C
400	-65.60027	0.8467	7.913
500	-75.08951	1.6371	9.083
550	-74.29123	1.6303	9.668
600	-72.35974	1.3932	10.253
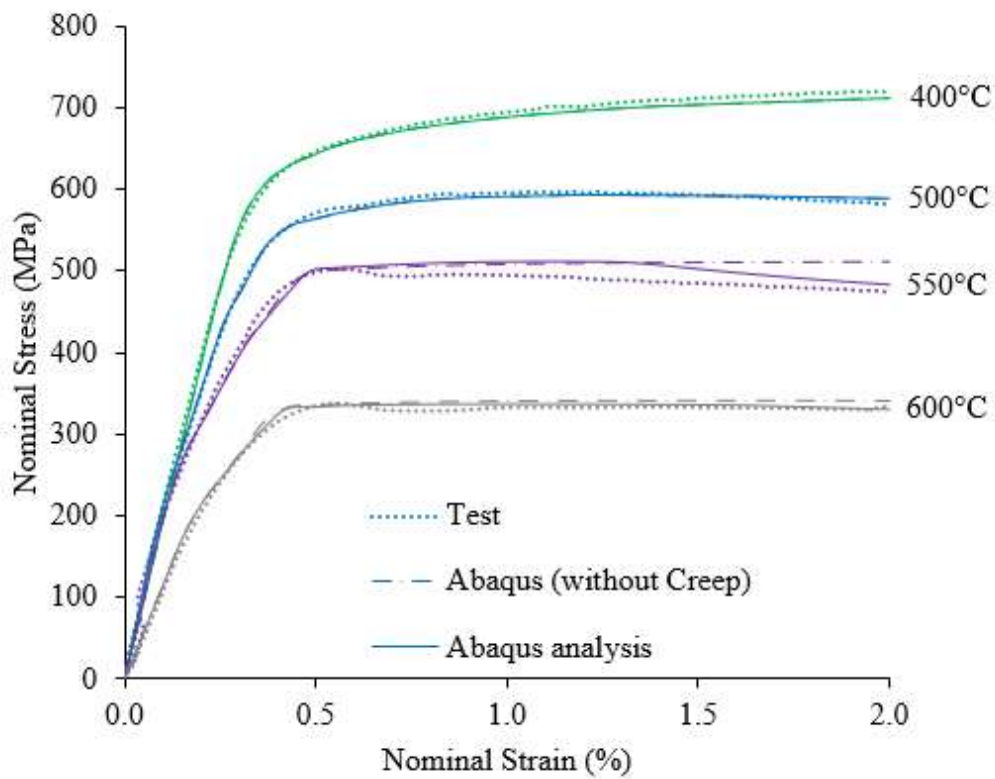
Figure 4-19 The stress-strain relationship between experimental and analytical results (Strain up to 2%) of H-SA700 steel

The proper consideration of creep is required when comparing two analytical curves to analytically reproduce the behavior of the H-SA700 column. The deformed shape is shown in Figure 4-20 by comparing the real tests and the analytical results in Abaqus. Tensile test analysis results in deformation shapes that are generally comparable to those observed during the real test. However, because to the emphasis on creep behavior analysis, the destructive tensile test simulation is omitted.

After obtaining the value of A, B and C, the expressions of these parameters are given in two temperature range: from 400 °C to 500 °C and from 500 °C to 600 °C. In the temperatures range 400-500 °C, a hypothetical stress-strain curve at 450 °C as shown in Figure 4-21 is defined to describe more accurately the expression of these parameters. The expressions of A, B and C for H-SA700 steel are given in equations (4.29)-(4.31).

$$\ln A = \begin{cases} -47.5365 - 5.3731 \times 10^{-3} \times T - 9.9466 \times 10^{-5} \times T^2 & 400\ °C \le T \le 500\ °C \\ -20.7462 - 0.22201 \times T + 2.2664 \times 10^{-4} \times T^2 & 500\ °C \le T \le 600\ °C \end{cases} \quad (4.29)$$

$$B = \begin{cases} 0.78868 + 3.0307 \times 10^{-33} \times T^{12.02201} & 400\ °C \le T \le 500\ °C \\ -10.96 + 4.8212 \times 10^{-2} \times T - 4.6046 \times 10^{-5} \times T^2 & 500\ °C \le T \le 600\ °C \end{cases} \quad (4.30)$$

$$C = 3.233 + 0.0117 \times T \quad (4.31)$$

where T is in °C.

(a) (b)

Figure 4-20 The tensile specimen after test (a) and tensile simulation result (b) of H-SA700 steel
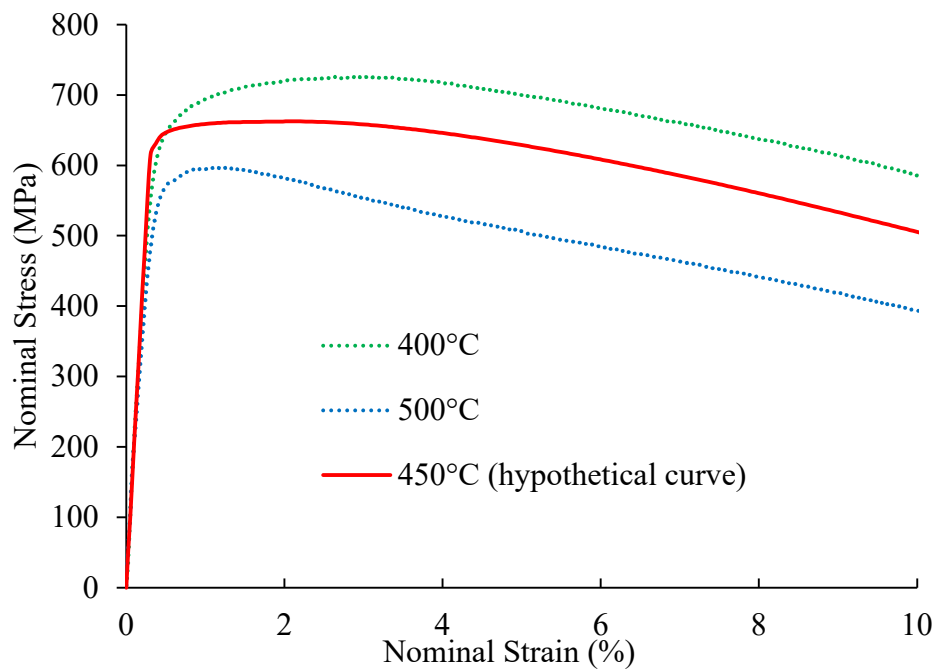
Figure 4-21 The hypothetical stress-strain curve at 450 °C for H-SA700 steel

4.4. Summary and observations

This chapter began with an introduction to high strength steel and its mechanical properties. The results of tensile tests conducted at elevated temperatures on high yield point steels YP400 and YP500, as well as high strength steel H-SA700, were given, together with testing methodology and general properties. The process for developing the thermal creep model was also established based on Fields and Fields' creep material model and the actual creep behavior of the critical truss angle steel used in the WTC investigation.

To identify the most correct creep parameters for the high strength steel utilized in this work, a trial-and-error approach was conducted to determine the most accurate stress-strain curves for the FE model that fit experimental data at various temperatures. The plastic material properties were then defined using hypothetical curves based on the observed stress-plastic strain relationship during experimental tests at various temperatures. Then, these thermal creep models were validated by comparing the stress-strain curves generated by Abaqus analytical results to those generated by experimental data.

Several major observations are made in the following based on the results of tensile tests done at various temperature settings to define the mechanical behavior of high yield point steels YP400 and YP500, and high strength steel H-SA700 at elevated temperatures.

The experimental program and results described in this chapter generated essential experimental data on the influence of thermal creep on the elevated-temperature response of high strength steels, thereby filling significant gaps in the database of high strength steel mechanical properties at elevated temperatures.

The test results provided in this chapter demonstrate that creep strains can be fairly severe in fire-prone building structures. This shows that disregarding creep may result in very erroneous structural response estimates for some types of structure-fire problems, such as steel columns exposed to fire.

Additionally, when compared to experimental data, existing creep models for structural steel subjected to fire may provide inaccurate predictions. It is difficult to interpret creep models, and it is unknown how far they may be evolved once the model parameters have been fitted to experimental data. Given the potential importance of creep in structural-fire engineering study, significant work is required to develop more robust and accurate steel creep models.

CHAPTER 5   STUDIES ON THE TIME-DEPENDENT BEHAVIOR OF HIGH STRENGTH STEEL COLUMNS AT ELEVATED TEMPERATURES

5.1. Overview

As described in Chapter 3, the ability of steel columns to support their design loads is highly reliant on the time- and temperature-dependent mechanical properties of steel at elevated temperatures caused by fire. When discussed in Chapter 2, structural steel degrades in strength and stiffness as a function of temperature, most notably at or above around 400 °C. Furthermore, steel's strength reduction is similarly proportional to the time of exposure to elevated temperatures. Indeed, the time-dependent reaction of structural steel, or thermal creep, is significant in estimating the time of collapse, the critical temperature, and also the deformation shape of steel columns exposed to fire temperatures. To be more precise, creep of steel results in the creep buckling phenomena, in which the behavior of a steel column is determined not only by its slenderness and temperature, but also by the duration of the applied force.

This chapter summarizes the research that was conducted on various types of high strength steel in order to characterize the time-dependent or creep behavior of steel columns at increasing temperatures. To define creep behavior of steel columns at elevated temperatures, analytical solutions based on Fields and Fields' constitutive material law (Fields, 1989) and modified as part of the NIST investigation into the collapse of the World Trade Center (NIST, 2005) are produced. The user CREEP subroutine's material creep models for high strength steels (YP400, YP500, and H-SA700) were also utilized to characterize the creep behavior of a steel column subjected to fire in the finite element program ABAQUS. The results of computational creep behavior studies conducted with Abaqus are also compared to experimental data in order to validate the analytical and computational processes mentioned previously. Additionally, thermal expansion coefficient values for these steels were identified and proposed, as the Eurocode 3 values are incompatible with high-performance steels. The plastic properties, thermal properties, and initial imperfection of high strength steels have all been explored as potential influencers of their time-dependent behavior.

Finally, the chapter concludes with some general observations about the results of the analytical, computational, and experimental experiments presented throughout the chapter on the phenomena of creep behavior.

5.2. Potential influencers of behavior analysis of high strength steel columns at elevated temperature

5.2.1. Thermal expansion coefficients

Figure 5-1 illustrates a comparison of thermal strain between HSA800 test data (Choi I-R, 2014) and design models. All design models predict a linearly rising pattern of thermal strain. However, the Eurocode 3 model includes a transition range of thermal strain between 750

and 860 °C to account for the phase change of steel at these temperatures. Correlations between test findings for high-strength steel and mild steel are excellent, particularly up to 700 °C. After a temperature increase of more than 750 °C, the Eurocode 3 model accounting for phase change produces a more realistic prediction than the ASCE and AISC models.

In the studies of high strength steel BISPLATE 80, the thermal elongation of the specimens was determined at a tensile stress of 1 MPa (0.15 ksi), which is near to free thermal expansion, and compared to the thermal elongation computed according to ASCE Manual (1992), British Standard 5950-8 (1998), and European Code 3 Part 1.2 (2001) in Figure 5-2.
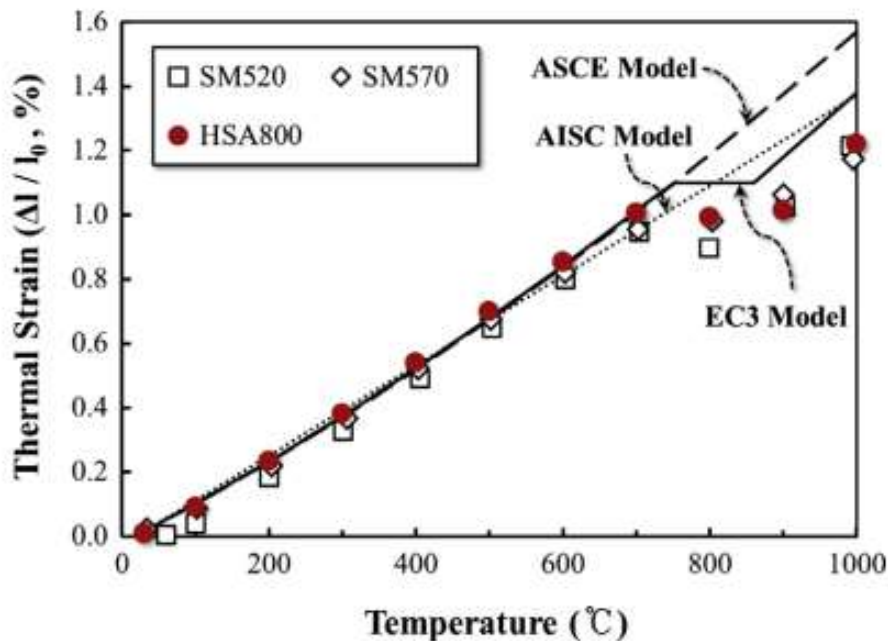
Figure 5-1 Comparison of thermal strain predicted by design models with test results of HSA800 steel (Choi I-R, 2014)
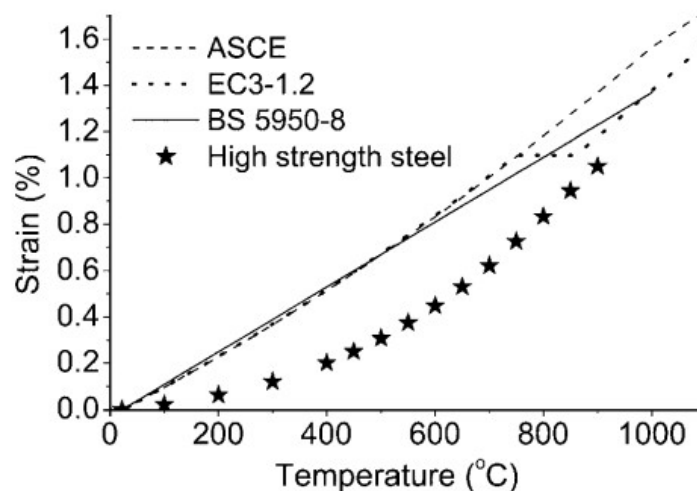
Figure 5-2 Comparison of thermal elongation predicted by ASCE, BS 5950-8, and EC3-1-2 with test results of high strength steel BISPLATE 80 (Chen J, 2006)

The vertical axis of the graph indicates the strain's thermal elongation in percentage percent values, while the horizontal axis reflects various temperatures. The comparison demonstrates that the thermal elongation test values for high strength steel are smaller than those predicted by ASCE (1992), BS 5950-8 (1998), and EC3-1-2 (2001). Although the 1 MPa (0.15 ksi) tensile stress had a minor effect on thermal elongation at ambient temperature, it had a modest effect as the temperature increased.

Through studies on high-strength steel (Chen J, 2006) (Choi I-R, 2014), thermal elongation values for HSS have been found to be much less than those estimated by the standards.

5.2.2. *Effect of initial geometric imperfections on creep behavior predictions*

Similar with previous simulation models of creep behavior (Morovat M. L., 2011), (Morovat M. E., April 2016), (Wang, 2019), (Morovat M-A, 2011), this paper incorporates imperfection into the simulation model in order to improve simulation accuracy. Generally, the experimental test and the simulation experiment are slightly different. Typically, the simulated components are rigid or perfectly straight, with no axis deviation. However, during the manufacturing process, the column will never be perfectly vertical, and there will always be imperfections, even if they are minor. Although the deviation is small, it results in different stress magnitudes on the compression and tension sides of the column when loads are applied at high temperatures. The column will collapse even sooner than normal calculations due to the imperfection, force effect, and creep behavior. As a result, a possible deviation has been added to the column parameter to simulate the column's curvature under load as the temperature rises.

5.3. Experimental studies of creep behavior of high strength steel columns

5.3.1. *YP400 and YP500 steel*

5.3.1.1. *Experimental data set*

For steel YP400 and YP500, a four-sided box column with a section of 450x19 mm and 400x19 mm and a length of 4,300 mm was welded and assembled. The column is loaded to its long-term design axial load of 8,158 kN for YP400 and 8,653 kN for YP500 and heated in the column test furnace at the Building Research Institute of Japan for three hours using the ISO 834 standard fire temperature curve (ISO 834-1, 1999) as illustrated in Figure 5-3. The observational measurement system records displacement and temperature data. The bearing connection of the column is a pin-pin connection in this experiment. The column is completely encased in a 25 mm thick blanket of alumina silicate fiber.

The steel temperatures were defined at 24 points using thermocouples. At the top plate, the vertical displacement of the column was determined. Column experiments were generally considered collapsed when the amount of co-axial contraction and the rate of axial contraction exceeded the values specified in the following equation:

- Maximum axial contraction (mm): h/100 = 43 mm.
- Maximum axial contraction rate (mm/min): 3h/1000 = 12.9 mm/min.

where *h* is the initial height of specimen (mm) h = 4,300 mm.
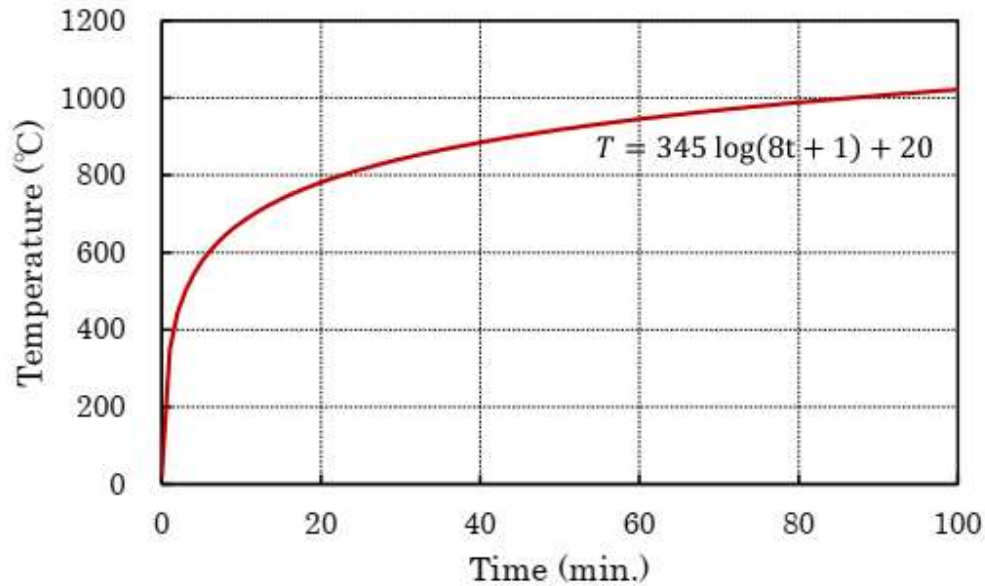
Figure 5-3 ISO 834-1 Standard fire temperature curve

5.3.1.2. Finite element model discretization

A finite element model has been developed that accurately describes the actual experiment for YP400 and YP500 steels using the finite element program Abaqus. Additionally, the specifications are precisely simulated in comparison to the test specimen used in the experiment. In order to make the columns behave in the same way in the simulation as in the experiment, the boundary conditions were set as much as possible as in the experiment. The column was modelled using an 8-node thermally coupled brick, trilinear displacement and temperature element, C3D8T. The mesh size was controlled using an approximate global size of 50 mm. Figure 5-4 illustrates the mesh detailing. The column was designed to perform the test under pin-pin conditions, with a long-term design axial load. The upper and lower ends boundary conditions are constrained by two corresponding reference points (RP-1 and RP-2). RP-1 is considered 300 mm above the equivalent base position due to the structure of the furnace used. As a result, the column's effective length is assumed to be 4,600 mm. The average temperature of steel measured by 24 thermocouples during the experiments are assigned directly to the column section inside the furnace. The upper section of the 300 mm long column is not intended to be in contact with the furnace heating, and the steel temperature in this section is considered to be one-third of that in the lower section, based on the temperature measurements of several similar column tests using this furnace. Steel temperatures can reach over 550 °C in less than three hours, as illustrated in Figure 5-5.

Furthermore, an Eigen buckling mode analysis was used to model initial geometric imperfections. Figure 5-6 illustrates four common Eigen buckling modes. For global buckling deformation, the starting shape of the column was used as the shape of the first buckling mode, while for local buckling deformation, a combination of the first and fourth buckling modes was used. The magnitude of the imperfection was calculated as a fraction of the column length, resulting in an initial out-of-straightness of *h*/1000.
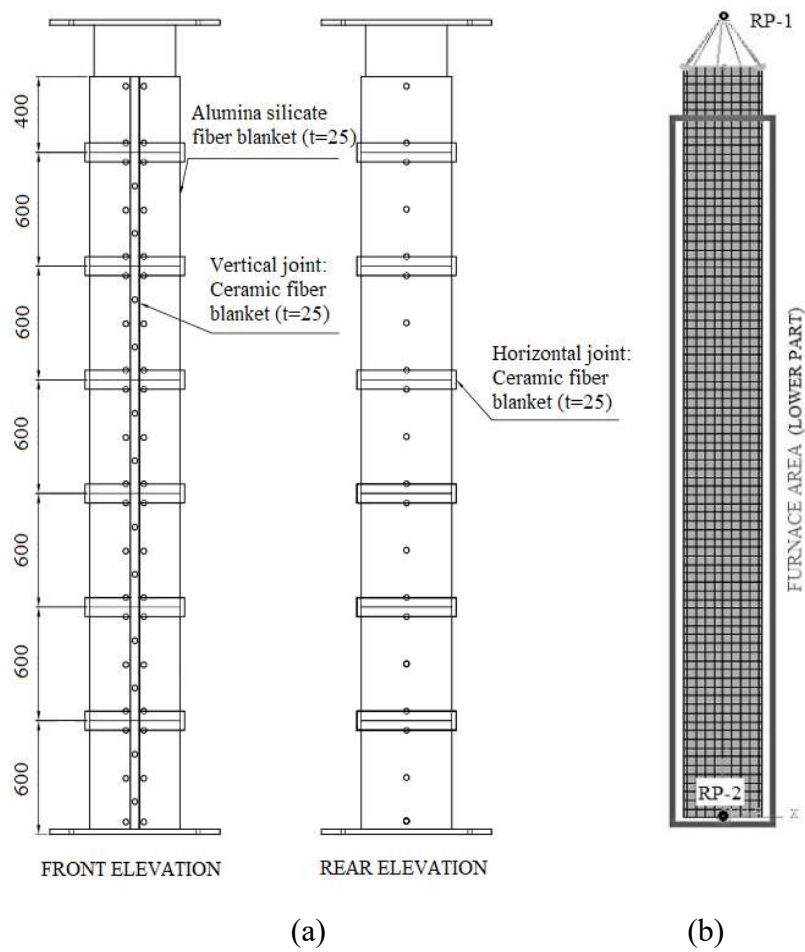
Figure 5-4 Column experimental (a) and modelling details (b)
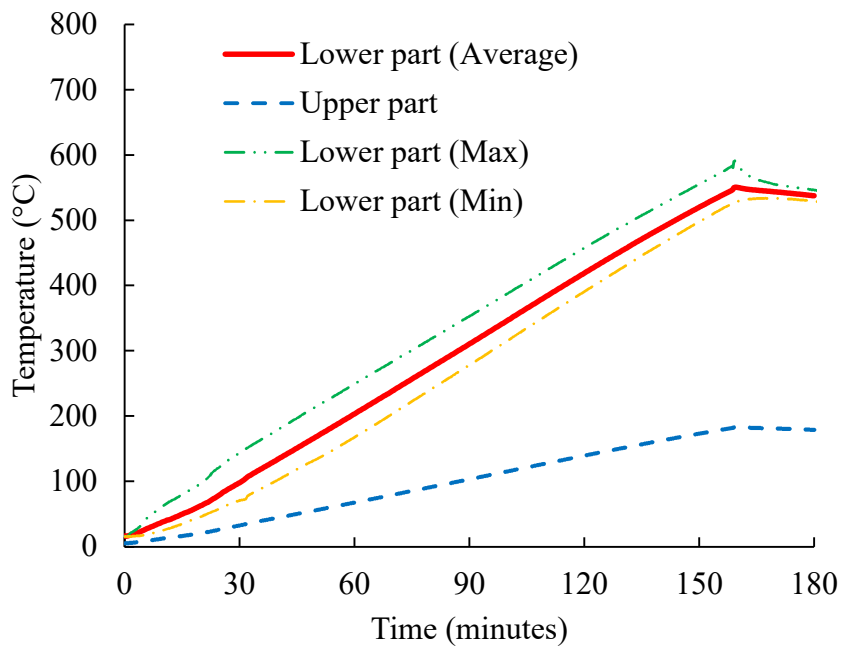
Figure 5-5 Temperature input data in Abaqus for YP400 and YP500

Mode 1   Mode 2   Mode 3   Mode 4
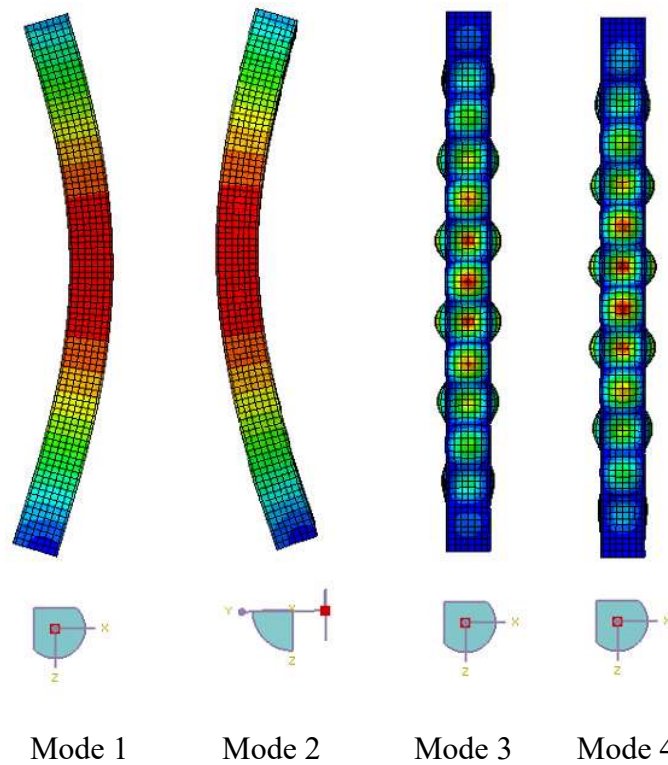
Figure 5-6 Four Eigen modes in Abaqus

5.3.1.3. Analytical column model results

The test was conducted under conditions of transient heating. The validated models (with or without the creep subroutine and an imperfection model) are used to demonstrate that the FE model accurately predicts experimental results in terms of maximum vertical displacement and time required to reach it.

One of the most critical factors affecting the accuracy of column simulations is the thermal expansion coefficient values. However, because the thermal expansion coefficient was not determined in the experiment with YP400 and YP500 steels, the coefficient of thermal expansion is identified from the column test results.

At low increasing temperatures, the column expands, resulting in an increase in column length. Due to the fact that the column displacement caused by axial force has been eliminated from the data and the creep effect is negligible at temperatures less than 400 °C, the vertical displacement of the column as the steel temperature increases from room temperature to 400 °C can be attributed mostly to thermal expansion. As a result, as illustrated in Figure 5-7, averaging can be used to approximate the coefficient of thermal expansion. Above 400 °C, it is estimated that the coefficient of thermal expansion follows the same pattern. This figure indicates that the thermal expansion coefficients of high strength steels estimated in the experiment are less than those predicted by Eurocode 3 (Eurocode3, 2005). Choi et al. (Choi I-R, 2014) and Chen et al. (Chen J, 2006) also demonstrated that the ASCE and Eurocode 3 predictions for thermal elongation of high strength steel are greater than the measured values. The test results indicate that the vertical displacement of the

columns is significantly less than that calculated by using the thermal expansion coefficient specified by Eurocode 3, as illustrated in Figure 5-8. The values of thermal expansion coefficient proposed in this study are more reasonable for high strength steels YP400 and YP500.

The vertical displacement of columns versus time and temperature for these models is depicted in Figure 5-9 and Figure 5-10. These charts demonstrate that the creep models consistently outperform the non-creep models. In comparison to the measured data, values for the maximum positive (elongated) vertical displacement, the time at the peak displacement point, and the steel temperature at that point were reliably predicted. On the other hand, the non-creep model produces larger vertical displacement values, or the column maintains bearing capacity even after the critical temperature is exceeded. At 475 °C, the column with YP400 steel will have the maximum displacement of 16.36 mm, which corresponds to the point at which the column has reached its bearing capacity in the experiment. Similarly, the column of YP500 steel also has the greatest displacement of 20.6 mm at 480 °C.
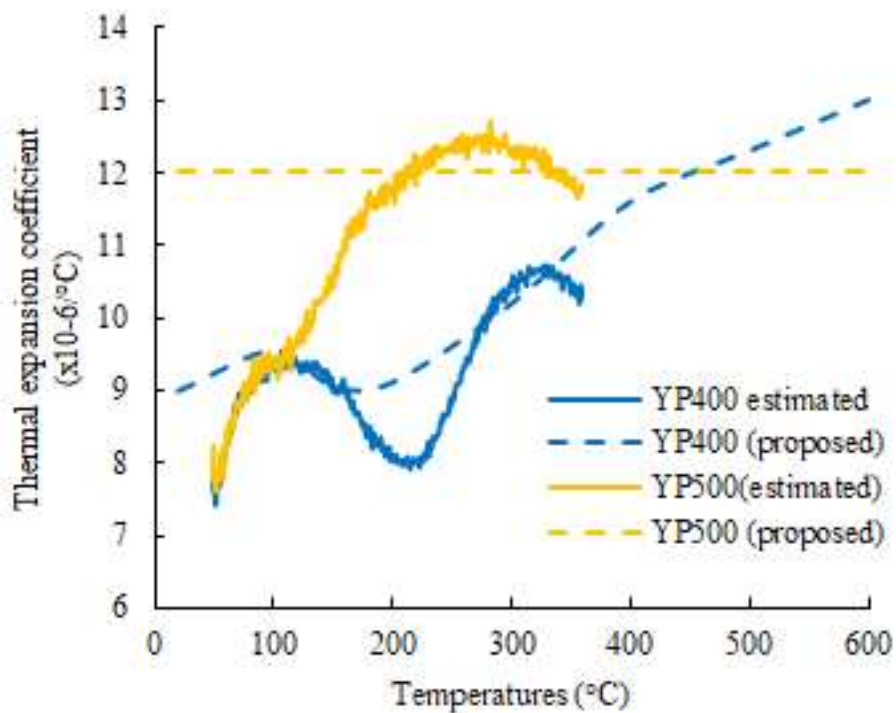
Figure 5-7 Thermal expansion coefficient values
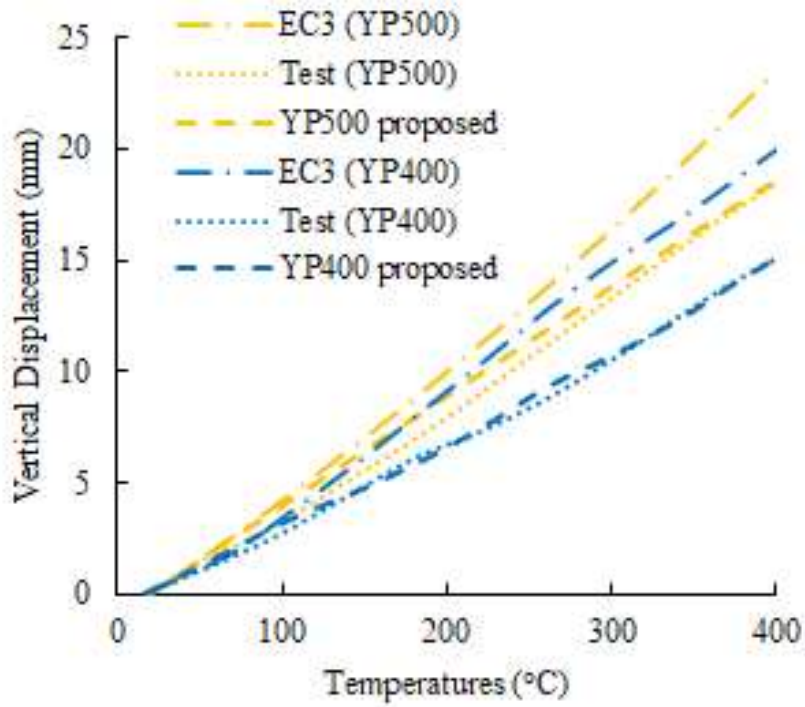
Figure 5-8 Comparison on vertical displacement of simulation model using thermal expansion coefficient in EC3 and proposed values
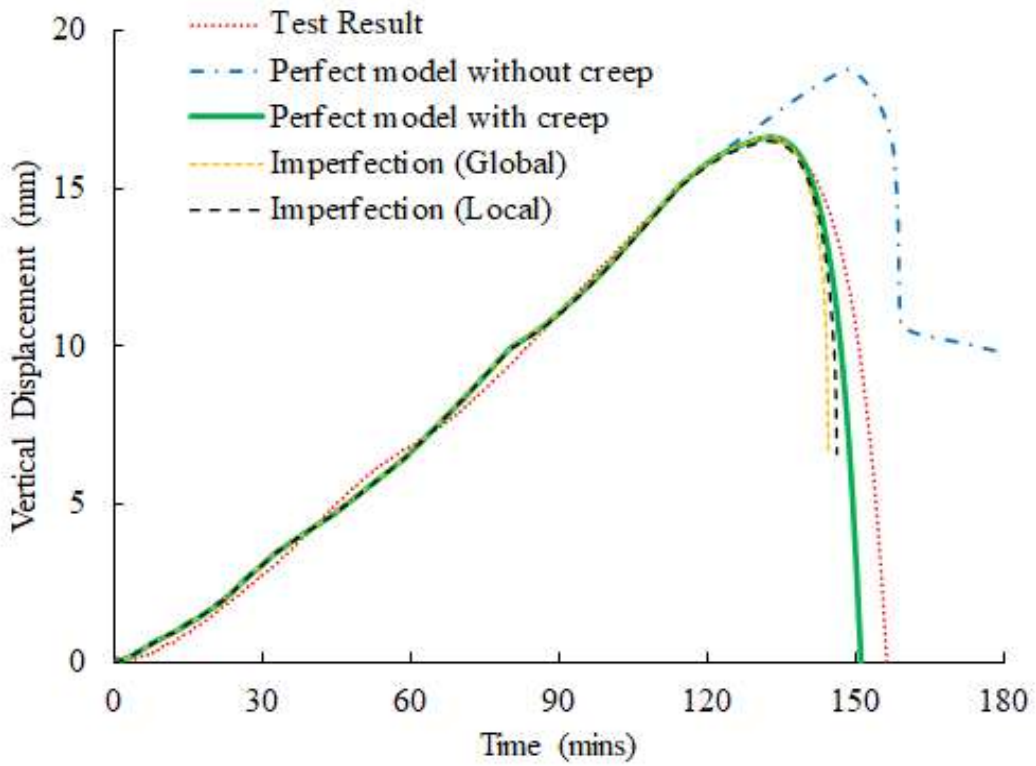
Figure 5-9 (a) Vertical displacement versus time curves of YP400 column model
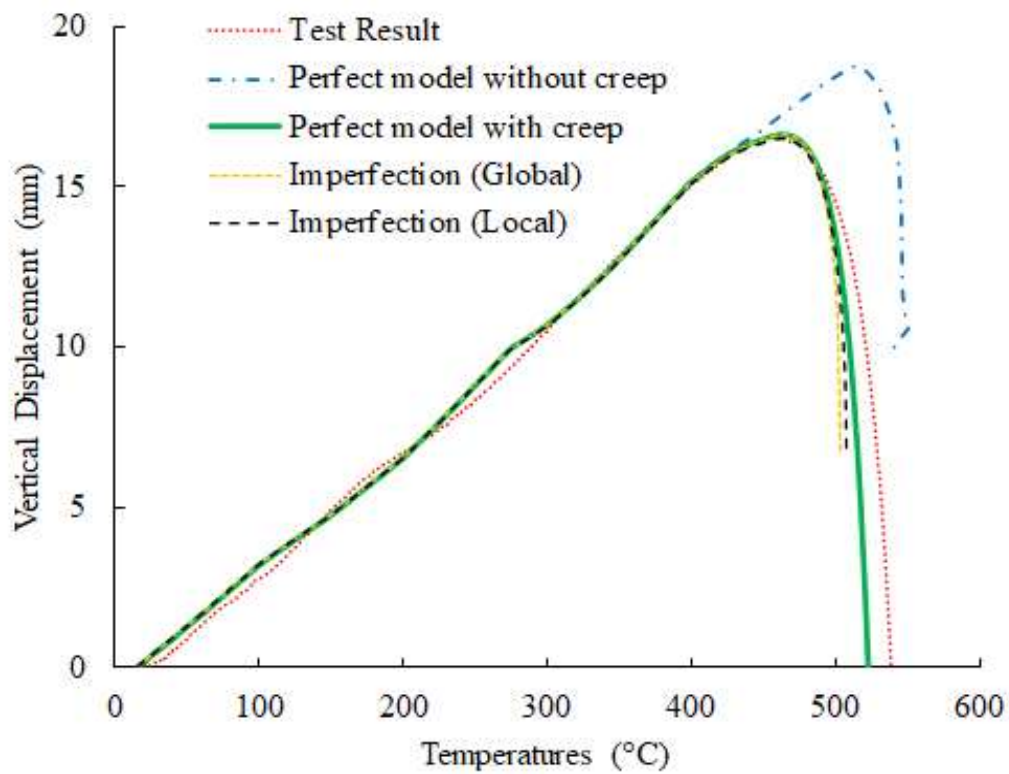
Figure 5-9 (b) Vertical displacement versus temperature curves of YP400 column model
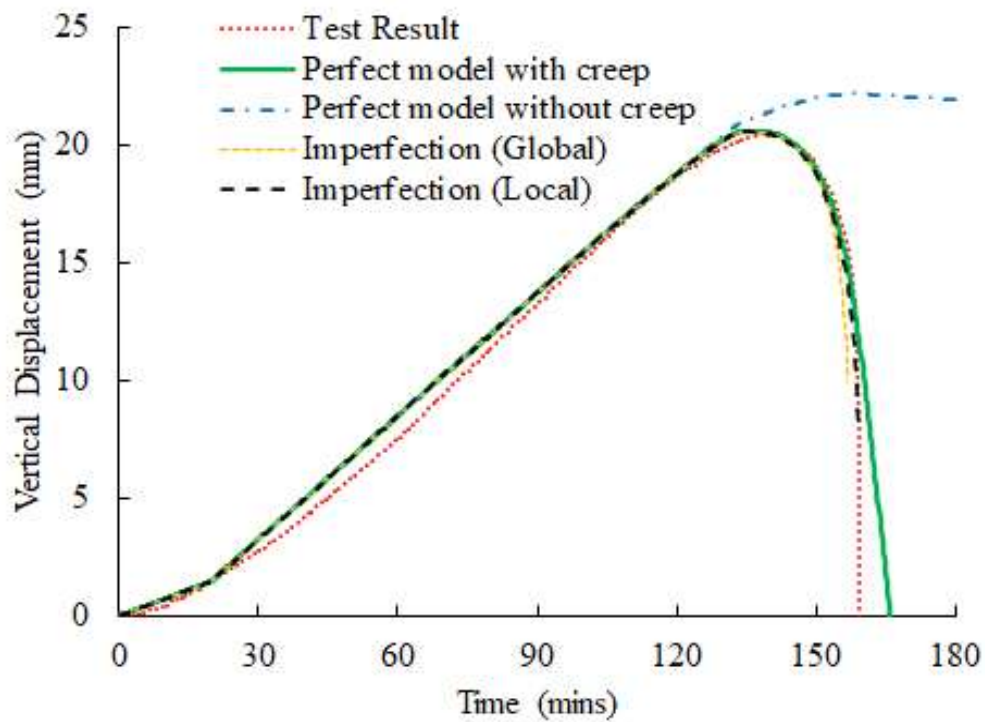
Figure 5-10 (a) Vertical displacement versus time curves of YP500 column model
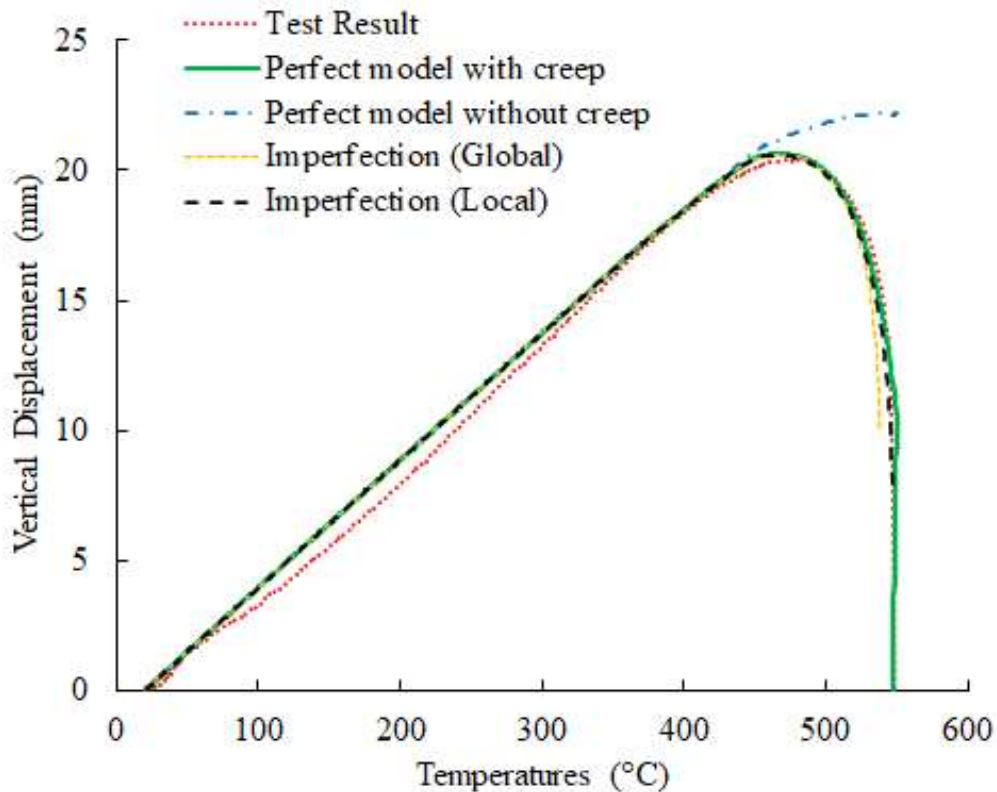
Figure 5-10 (b) Vertical displacement versus temperature curves of YP500 column model

The simulated results for YP400 steel deviate from the test results in the temperature range of 200 to 350 °C. One of the reasons for this discrepancy may be the yielding occurrence at 23 °C, which results in inaccurate analysis in this temperature range. Between 23 and 350 °C is a quite huge temperature range, and the Abaqus software requires additional data to perform more accurate simulations. Furthermore, predicting the thermal expansion coefficient to be linear in this temperature range may not be realistic.

As illustrated in Figure 5-9 and Figure 5-10, the simulations without the creep effect resulted in erroneous forecasts of the maximum vertical displacement and the critical temperature. Although the peak point of time and vertical displacement in this study were not corresponding to the collapse criteria described in ISO 834, they were found to be quite significant in monitoring column behavior under high temperatures. Along with the addition of initial imperfection to aid not only in the prediction of deformation shape, but also the analysis will offer more accurate results (YP500 steel). However, the addition of the imperfection mode rendered the analysis impossible until the column model collapsed, which explains why the curves of the imperfection models abruptly ceased to exist. The failure modes and deformation shapes of the FE models reflect those of the experiment, as illustrated in Figure 5-11 and Figure 5-12. These imperfect FE models were capable of predicting more evident global and local buckling deformations.

(a)   (b)   (c)
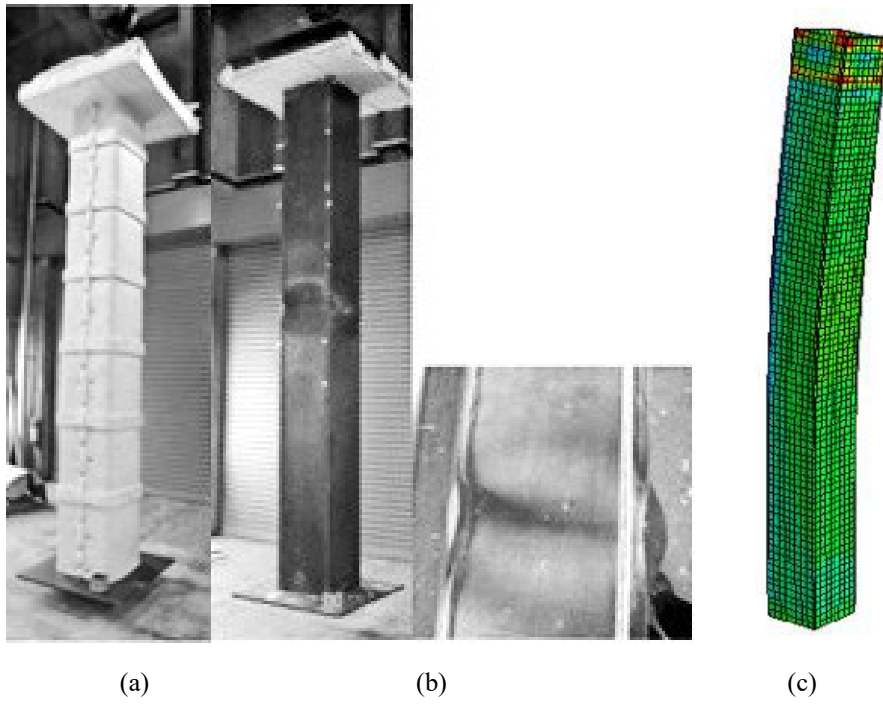
Figure 5-11 YP400 column before (a), after (b) the test and analytical deformation shape (c)

(a)   (b)   (c)
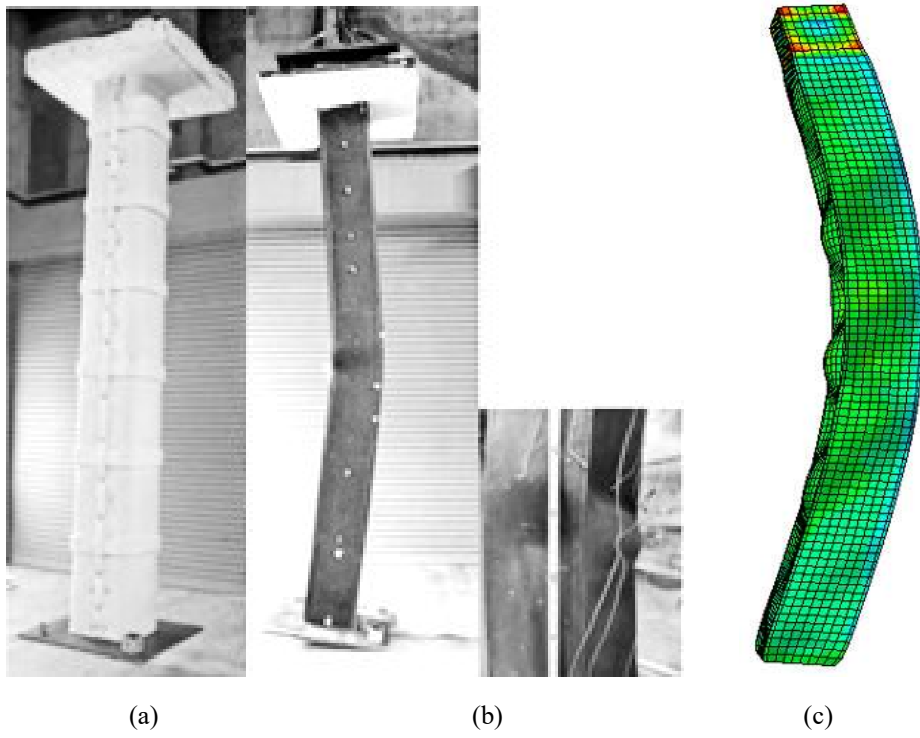
Figure 5-12 YP500 column before (a), after (b) the test and analytical deformation shape (c)

5.3.2. H-SA700 steel

5.3.2.1. Experimental data set

A four-sided box column with a section of 350x19 mm and a length of 4,300 mm was welded and assembled. The column is loaded to its long-term design axial load of 9,592 kN and heated for 3 hours by ISO 834 standard fire temperature curve as illustrated in Figure 5-3 in column test furnace in the Building Research Institute of Japan. The observational measurement system collects data such as displacement and temperature. The bearing connection of the column in the experiment is a pin-pin connection. The column is encased in a 25 mm thick alumina silicate fiber blanket.

The steel temperatures were measured with K-type thermocouples at 24 points as illustrated in Figure 5-13. The vertical displacement of the column was measured at the base plate. Column experiments were generally considered collapsed when the amount of co-axial contraction and the rate of axial contraction exceeded the following equation:

- Maximum axial contraction (mm): $h/100 = 43$ mm.
- Maximum axial contraction rate (mm/min): $3h/1000 = 12.9$ mm/min.

where h is initial height of specimen (mm) $h = 4,300$ mm.

5.3.2.2. Finite element model discretization

A FE model has been developed that uses simulation software Abaqus to accurately describe the actual experiment. The specifications are also precisely simulated in comparison to the actual experiment. Boundary conditions were used to make the column behave similarly to the experiment, with the more accurate the simulation, the more reasonable the results. A solid element was used in Abaqus. An 8-node thermally coupled brick, trilinear displacement and temperature element, C3D8T, were utilized to model the column on Abaqus. The approximate global size of 50 mm was used to control the mesh size. The mesh detailing is shown in Figure 5-13. The column was designed to perform the test under pin-pin conditions, with a long-term design axial load of 9,592 kN applied. The two boundary conditions of the upper and lower ends of the columns are constrained with two corresponding reference points (RP). Due to the structure of the furnace used, RP1 is considered 300 mm below the equivalent base position. Therefore, the effective length of the column is considered as 4,600 mm. Furthermore, steel temperature profiles are directly assigned to the column section, which is divided into two parts based on average temperature measured by 24 thermocouples in the real test. The upper part of the 300 mm long column is not intended to interact with the furnace and the steel temperature here is considered to be one-third that of the lower part of the column. Steel temperatures can rise to more than 600 °C in three hours, as illustrated in Figure 5-14.

(a)   (b)
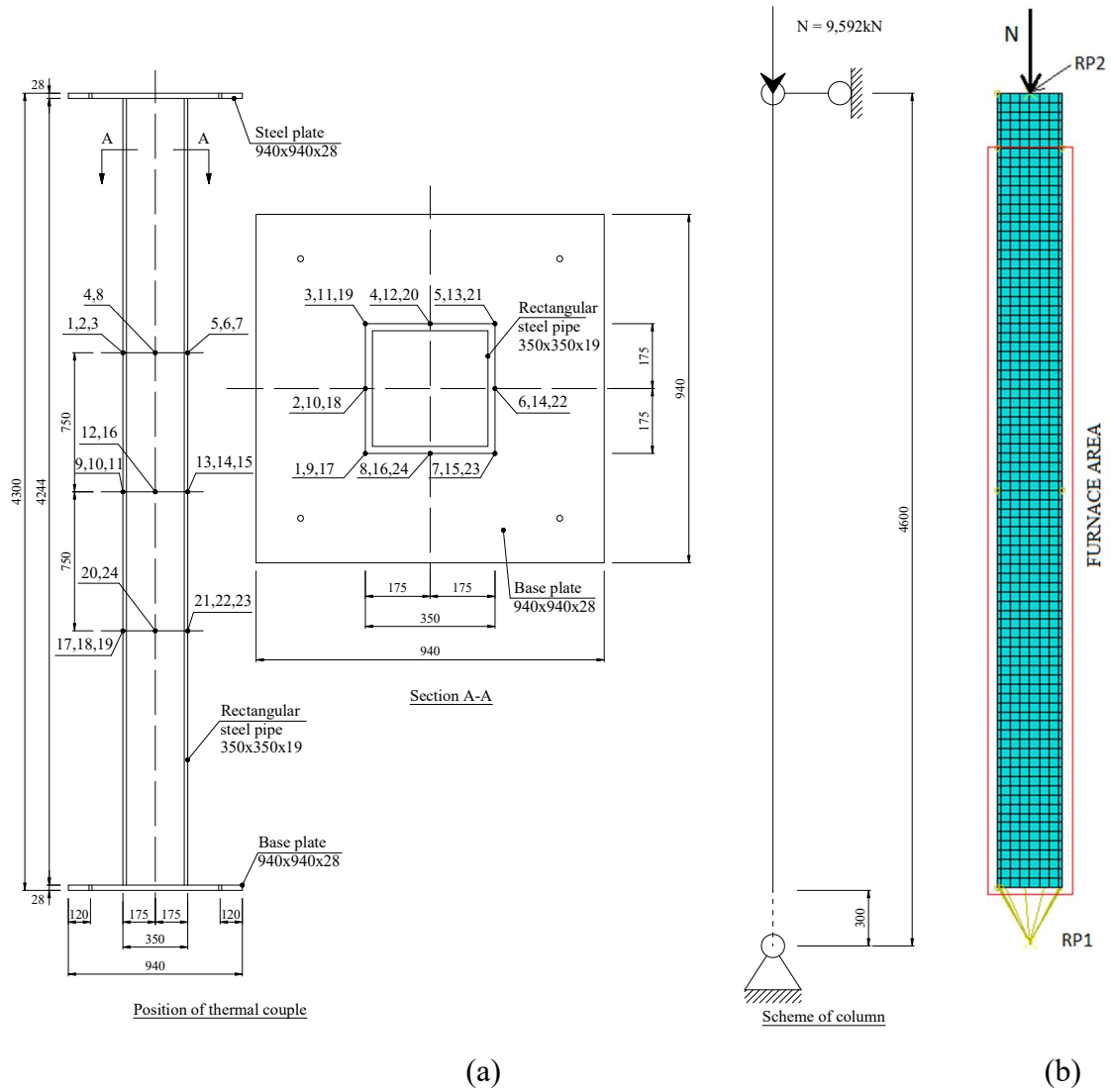
Figure 5-13 Column specimen (a) and modeling details (b)
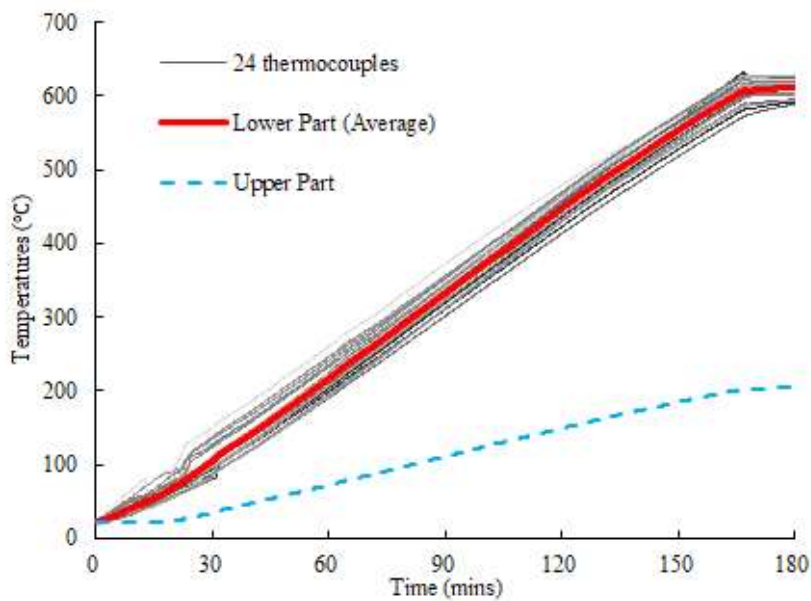
Figure 5-14 Recorded and average temperatures in column test

| Mode 1 | Mode 2 | Mode 3 | Mode 4 |
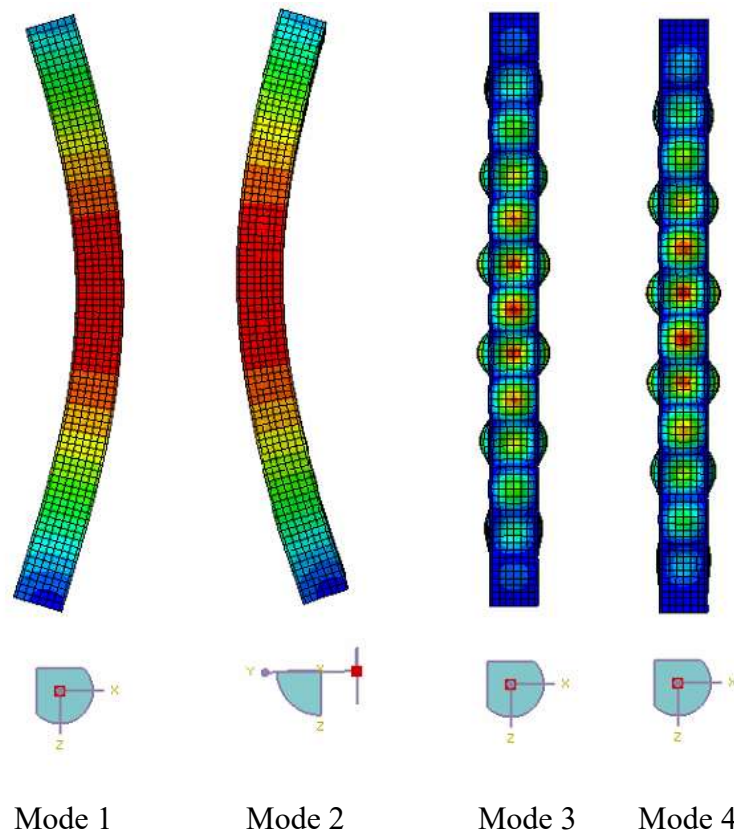
Figure 5-15 Four Eigen modes in Abaqus

To model initial geometric imperfections, an Eigen buckling mode analysis was performed. Figure 5-15 illustrates four common Eigen buckling modes. The first and second modes, respectively, indicate global buckling deformation along the X and Y axes. These third and fourth modes, respectively, reflect local buckling deformation along the X and Y axes. For global buckling deformation, the starting shape of the column was used as the shape of the first buckling mode, and the combination of the first and fourth buckling modes was used for local buckling deformation. The magnitude of the imperfection was determined as a fraction of the column length, resulting in an initial out-of-straightness of $h/1000$.

5.3.2.3. Analytical column model results

The test was conducted under transient heating conditions. The validated models (with or without creep subroutine and imperfection model) are used to demonstrate that the FE model predicts the experimental results with reasonable accuracy in terms of the maximum vertical displacement and the time to reach it.

The column undergoes thermal expansion at low increasing temperatures, resulting in an increase in column length. Because the column displacement caused by axial force has been eliminated from the data, and the creep effect is very small when the temperature is less than 400 °C, the vertical displacement of the column when the temperature of the steel increases from room temperature to 400 °C can be attributed to thermal expansion. As a result, as shown in Figure 5-16, the coefficient of thermal expansion can be approximated by averaging. After 400 °C, the coefficient of thermal expansion is estimated to follow the same pattern.

This figure indicates that the test values of high strength steel thermal expansion coefficients are less than the values predicted by EC3 (Eurocode3, 2005). Choi et al. (Choi I-R, 2014) and Chen et al. (Chen J, 2006) also clarified in their studies that the ASCE and Eurocode 3 predictions of thermal elongation of high strength steel are larger than tested data. The test results show that the vertical displacement of column is noticeably less than that predicted using the thermal expansion coefficient in Eurocode 3 as illustrated in Figure 5-17. Those values proposed by this study is more reasonable for high strength steel H-SA700. The Figure 5-18 and Figure 5-19 show the relationship between the vertical displacement versus time and temperature for these models.
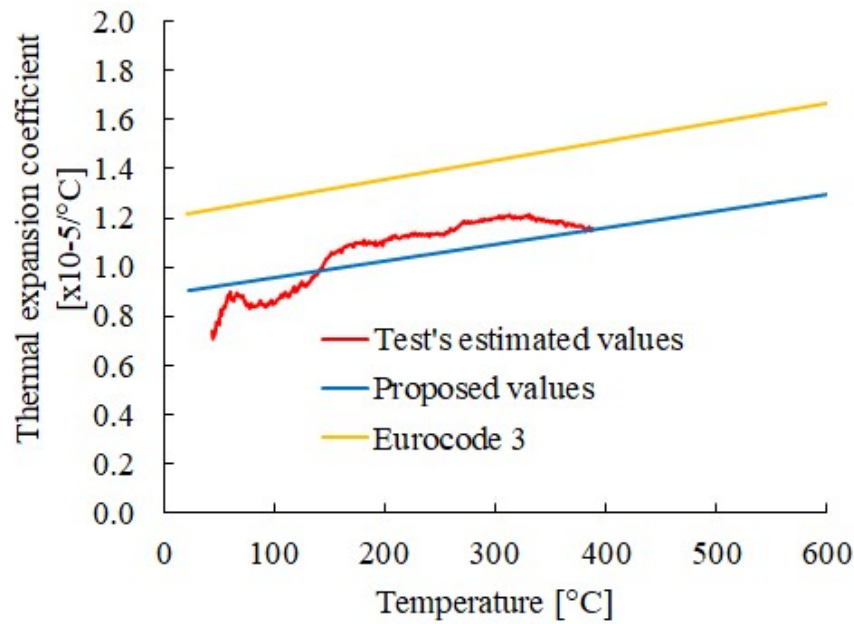
Figure 5-16 Thermal expansion coefficients of column
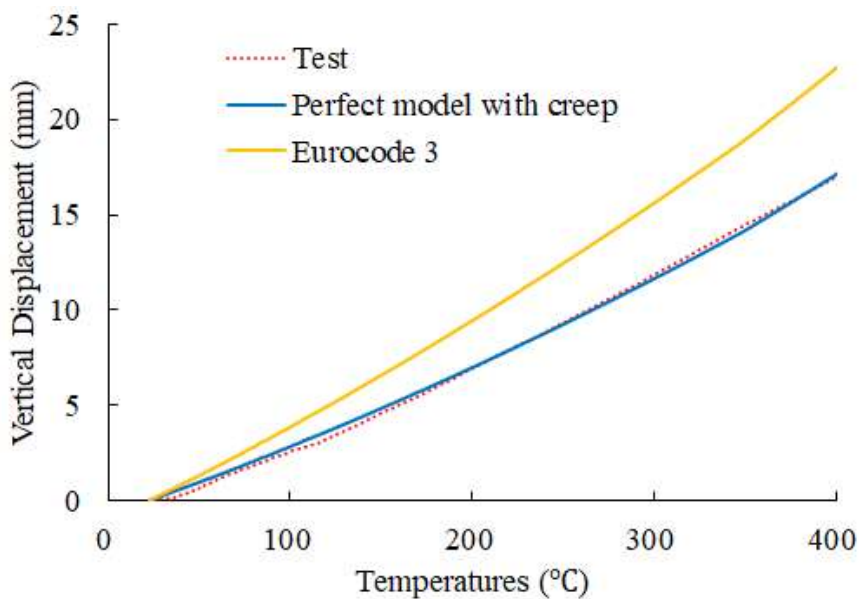
Figure 5-17 Comparison on vertical displacement of simulation model using thermal expansion coefficient in EC3 and predicted values
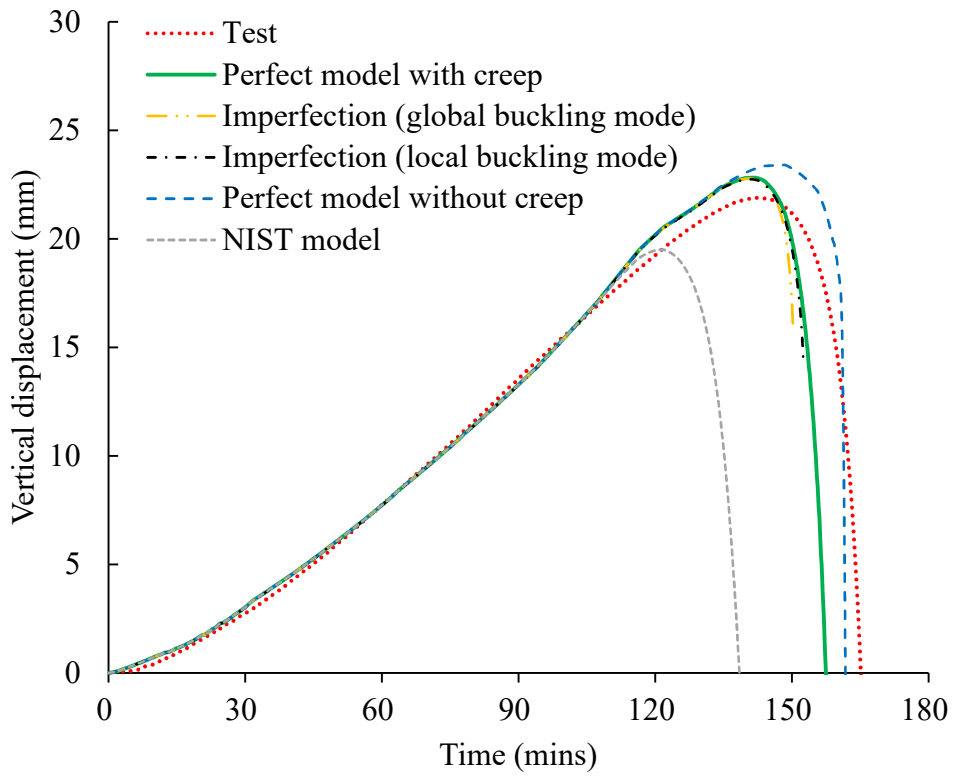
Figure 5-18 The vertical displacement versus time curve of column model
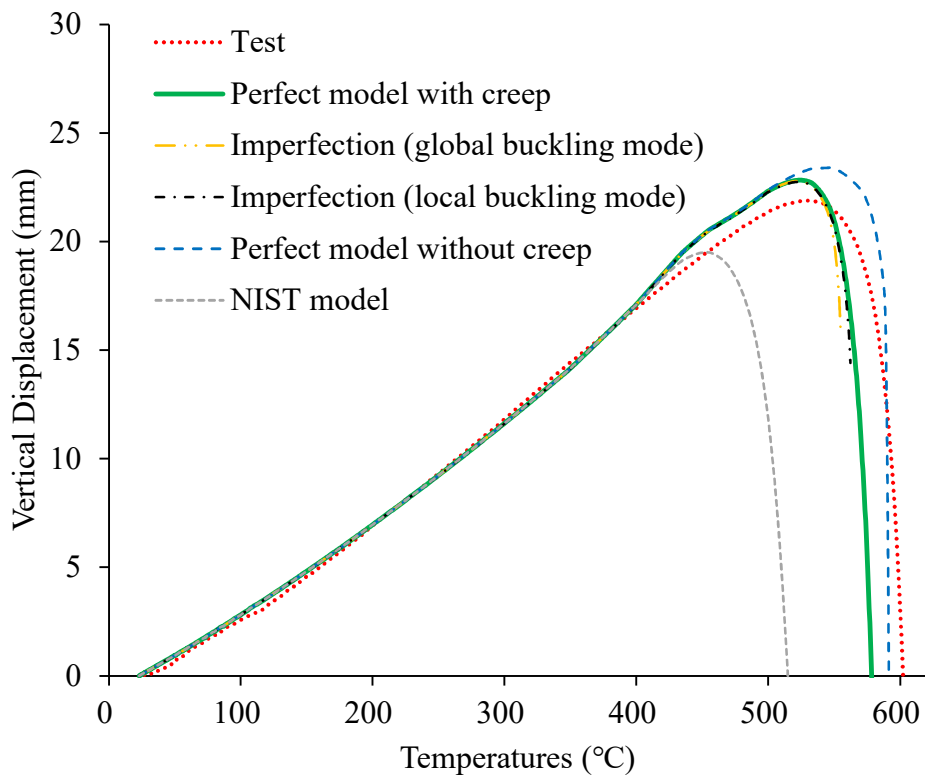
Figure 5-19 The vertical displacement versus temperature curve of column model

Thermal creep is explicitly modeled as a user subroutine CREEP that is characterized by tensile tests. The maximum heating temperature in the column test is up to 610 °C, and the duration of fire exposure is greater than 3 hours. At 530 °C, the column displacement begins to decrease indicating the development of the column failure stage. When the maximum elongation time and temperature are compared, the FE model cannot accurately perform the behavior of the column after high deformation. In fact, when conducting experiments on large components such as columns, the furnace is turned off after the peak point, so the temperature curve of the steel usually does not increase anymore but goes horizontally, and the vertical displacement of the column increases rapidly. However, in the simulations presented here, the temperature in the steel continues to rise after the peak point, resulting in a difference between the actual and simulated data after the peak point, even though the displacement and time of the peak point are very close. Thus, it can be said that the difference in the collapse phase of the column between the real test and its analytical model is reasonable.

As shown in Figure 5-18 and Figure 5-19, the simulation results without creep effect led to erroneous forecasts of maximum vertical displacement and collapse temperature. Likewise, this study also used an approach in NIST report (NIST, 2005) to use the A242 steel to predict the creep behavior of H-SA700. After converting to corrected stress by scaling the tensile strength of A242 to that of the H-SA700 (equation 6-19), the NIST model was unable to effectively replicate the behavior of this steel column.

Figure 5-20 and Figure 5-21 compare the column model analysis results when creep behavior is used with two magnitudes of imperfection, h/1000 and h/500, to those obtained when creep behavior is not used. It is straightforward to see that altering the magnitude of imperfection has a small effect on the maximum vertical displacement, as well as in comparison to the result of the perfect model. When creep behavior is omitted, the results are considerably different, particularly when estimating critical temperature or collapse time. As a result, selecting an appropriate creep model is critical during the analytical phase. The analysis with creep effect will produce more accurate results, along with the addition of initial imperfection to aid in the prediction of deformation shape. The failure modes and deformation shapes of finite element models resemble those of the experiment as shown in Figure 5-22. The local buckling is appeared as shown in the dash-dot circle of close view between experimental column test Figure 5-22(b) and analysis model Figure 5-22(e). These FE models with imperfection were capable of predicting the global and local buckling deformations more obvious.
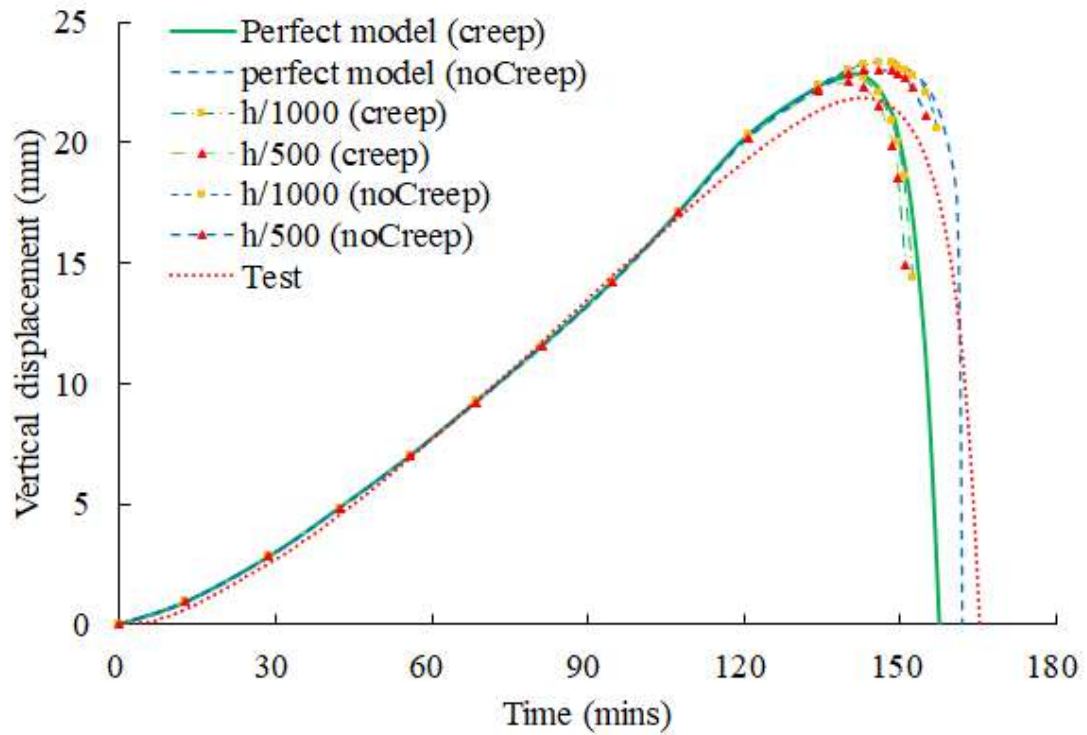
Figure 5-20 The vertical displacement versus time curve of column model (for different magnitude of imperfection)
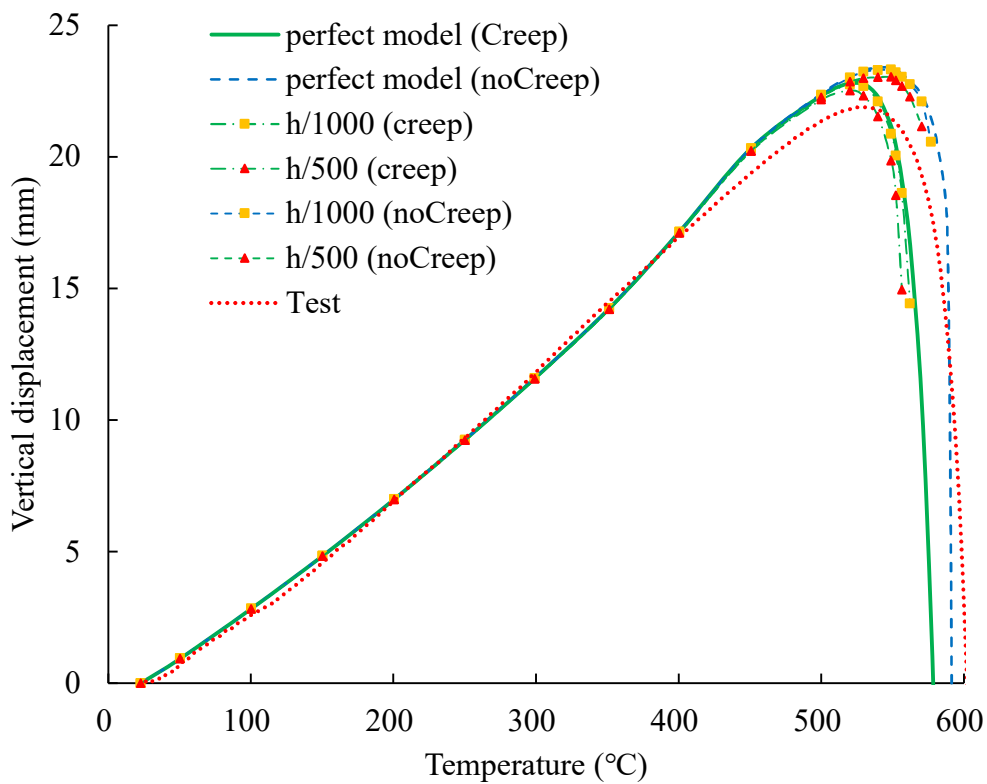
Figure 5-21 The vertical displacement versus temperature curve of column model (for different magnitude of imperfection)
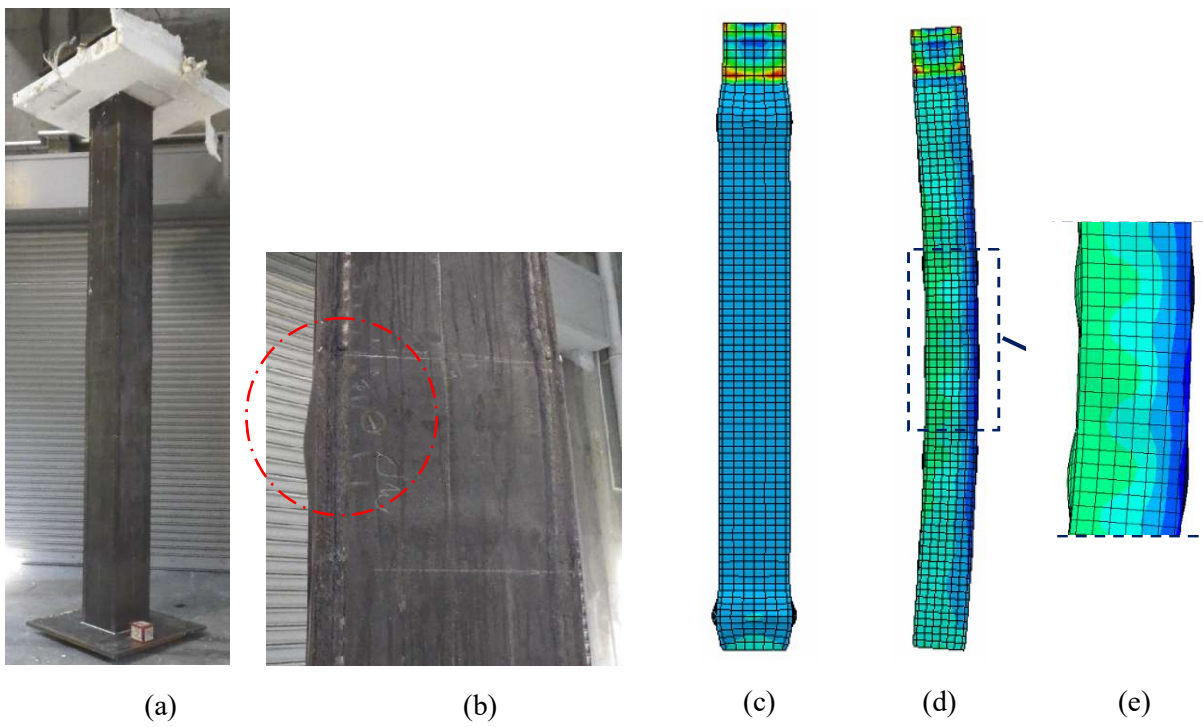
Figure 5-22 Deformation shape of experimental column test: (a) overview and (b) close view; and FE models: (c) perfect model and local buckling imperfection model: (d) overview and (e) close view (Deformation scale factor: 5)

5.4. Summary and conclusions

Chapter 5 discussed various experimental results on high-strength steel columns, as well as some other research findings about potential influences on steel column behavior. The results of the computational method for column test based on material creep models provided in Chapter 4 are also analyzed using the Abaqus finite element software and compared to experimental results. Additionally, a thermal expansion coefficient is suggested for each steel grade YP400, YP500, and H-SA700, based on the vertical displacement of the column at temperatures less than 400 °C and on previously performed experiments. Additionally, two types of imperfection models (local and global buckling modes) are addressed in the study, including a different magnitude of imperfection. The outcomes of analyses with and without creep behavior were also compared.

Several fundamental observations regarding the creep behavior of steel columns subjected to fire are made based on the results of analytical, computational, and experimental experiments presented in this chapter as following:

➢ Thermal expansion coefficient values for these steels were identified and proposed because the values specified by Eurocode 3 are unreasonable. Plastic properties, thermal properties, and initial imperfection have all been investigated as potential influencers of time-dependent behaviors of high strength steels.

➢ The proposed method could be used with the same grade of steel without requiring full-scale structural or creep tests. In this study, the simulation analysis was used to determine the peak point of time and temperature versus displacement, deformation shape, and creep properties of the high yield point steel columns. The results were quite accurate when compared to the experimental results.

➢ The yield phenomenon may have an adverse effect on the analytical results. The experiment to determine the coefficient of thermal expansion is implied to be critical for simulating the behavior of steel structures, especially at temperatures below 400 °C. Furthermore, when conducting experiments over a wide temperature range, the absence of data should be avoided.

➢ Ignoring the creep effect may result in inaccurate and unconservative forecasts of structural response to fires. This research should be expanded in the future to develop more simplified and practical models that incorporate the creep effect in additional structural components without the need for creep tests.

CHAPTER 6   CONCLUSIONS AND FUTURE WORK

6.1. Summary

This dissertation has reported results of the studies on the behavior of high strength steel columns when subjected to elevated temperatures due to fire. Analytical, computational, and experimental means were incorporated to conduct the research reported in this dissertation. The purpose of this research is to develop a methodology for explicitly incorporating creep behavior of high strength steel into finite element models using general tensile test data at elevated temperatures.

The concept of thermal creep of structural steel and different approaches in quantifying the effect of thermal creep on the stress-strain behavior of structural steel were discussed. Constitutive models for the thermal creep of structural steel at elevated temperatures were further reviewed. A try and error approach was used to determine the most accurate stress-strain curves for the FE model that fit experimental data at various temperature conditions. A set of creep parameters are assumed to be analyzed, and the resulting analysis stress-strain curve is compared to the experimental target curve to determine its proximity. The constitutive creep equations were developed to account for the material creep effect of high-strength steels. Additionally, thermal expansion coefficient values for these steels were identified and proposed because the values specified by Eurocode 3 are unreasonable. Plastic properties, thermal properties, and initial imperfection have all been investigated as potential influencers of time-dependent behaviors of high yield point steels. The effect of yield phenomenon was also investigated.

The proposed method could be used with the same grade of steel without requiring full-scale structural or creep tests. In this dissertation, the simulation analysis was used to determine the peak point of time and temperature versus displacement, deformation shape, and creep properties of the high strength steel columns. The results from computational creep behavior studies of steel column were also presented and compared with the experimental results to verify analytical and computational procedure. The requirement and significance of creep behavior analysis in understanding the behavior of steel columns in general, and structures made of high-strength steel in particular, have been established.

6.2. Observations and conclusions

Several conclusions and observations from this research are as follow:

➤ As shown in the literature survey, there is a scarcity of experimental data on thermal creep of structural steels, especially for high strength steels. Additionally, the experimental data on columns at elevated temperatures are also rather limited. The experimental program and results described in this chapter generated essential experimental data on the influence of thermal creep on the elevated-temperature response of high strength steels, thereby filling significant gaps in the database of high strength steel mechanical properties at elevated temperatures.

➤ The test data presented in this dissertation show that creep strains can be quite significant for temperatures, stress levels, and time durations representative of building structures exposed to fire. This suggests that ignoring creep may lead to highly inaccurate predictions of structural response for some classes of structure-fire problems such as steel columns subjected to fire.

➤ By comparing experimental and analytical results, the values of thermal expansion coefficient for high strength steel are identified and smaller than those indicated in standards. Additionally, the thermal expansion coefficient test is critical for precisely replicating the behavior of columns at elevated temperatures.

➤ The approach of representing plastic properties as a logarithmic equation is well suitable for simulating thermal creep behavior using a finite element program. The approach for developing the creep model through general tensile tests was also demonstrated to be practical, owing to the high similarity between analytical and experimental data.

➤ The yield phenomenon may have an adverse effect on the analytical results. Furthermore, when conducting experiments over a wide temperature range, the absence of data should be avoided.

6.3. Future research directions

Several issues have been identified as requiring additional study or research as a result of the presented in this research study. These issues are as follows:

➤ The accuracy of the analytical solutions developed in this study needs to be improved due to discrepancies between analytical and experimental results at a variety of temperatures (H-SA700 steel).

➤ Additional research is necessary to obtain exhaustive experimental creep data and material models for structural steel at elevated temperatures. Particular attention should be paid to determining the time-dependent impacts on the compressive stress-strain response of structural steel at elevated temperatures. In other words, it is necessary to evaluate the thermal creep of structural steel in compression.

➤ The creep models given in this study should be validated against various types of steel structures to ascertain their validity for high strength steels (for example: beam, joint connection or whole frame).

➤ If a steel column is not allowed to expand freely, the thermal expansion associated with heating can generate considerable internal axial stresses. When analyzing column safety under fire loading, it is essential to include the forces generated in steel columns as a result of constrained thermal expansion. Significant work is required to examine the internal forces that can have a dominating effect on column response. The time effects in the form of stress relaxation are of particular relevance because they may have an effect on the forces generated in steel columns due to restricted thermal expansion.

➤ The procedure for determining the creep parameters and creating the creep model needs to be simplified and made more precise.

REFERENCES

Bailey, R. (1930). Creep of Steel under Simple and Compound Stress. *121*(2), 129-265.

Bentz DP, P. K. (2007). Thermal performance of fire resistive materials I. Characterization with respect to thermal performance models.

Chen J, Y. B. (2006). Behavior of high strength structural steel at elevated temperatures. *132*.

Choi I-R, C. K.-S.-H. (2014). Thermal and mechanical properties of high-strength structural steel HSA800 at elevated temperatures. *63*.

Dassault system simula corporation. (n.d.). Abaqus ver 6.14 Documentation.

Eurocode3. (2005). *Design of steel structures, Part 1. 2: Structural fire design.* Brussels: European Committee for Standardization (CEN).

Fields, B. F. (1989). Elevated Temperature Deformation of Structural Steel.

Fujimoto, M. F. (1980). Primary Creep of Structural Steel (SS 41) at High Temperatures. *Transactions of Architectural Institute of Japan, 296*, 145-157.

Furumura F., a. T. (1984). Creep Buckling of Steel Columns at High Temperatures: Part I - Development of Creep Buckling Test Apparatus. *Transactions of Architectural Institute of Japan, 59*(10), 164-173.

Furumura, F. A.-J. (March 1986). Creep buckling of steel columns at high temperatures. *No.361*.

GB/T 228.1-2010. (2010). *Metallic materials-tensile testing-Part 1: method of test at room temperature.* Beijing: Standardization Administration of the People's Republic of China, China Standard Press.

Hantouche E G, K. K. (2018). Modeling creep of steel under transient temperature conditions of fire. *Fire Safety Journal, 100*, 67–75.

Harmathy, T. (1967). A comprehensive creep model. *89*(3).

H-SA700. (2012). *High strength 780 N/mm2 steel for building construction (H-SA700), Product Specifications MDCR 0015-2012.* the Iron and Steel Federation of Japan.

ISO 834-1. (1999). *Fire Resistance Tests – Elements of Buildings Construction – Part-1 General Requirement.* Switzerland: International Organization for Standardization.

J., O. (1999). Mechanical properties of structural steels at elevated temperatures.

JIS-G-0567:2012. (2012). *Method of elevated temperature tensile test for steels and heat-resisting alloys.* Japan Industrial Standards, Japanese Standards Association.

JIS-Z2241. (2020). *Metallic materials - Tensile testing - Method of test at room temperature.* Japanese Standards Association.

Katsuo M, S. T. (2013). Fire Resistance of High Yield Point Steel Column. *Summaries of Technical Papers of Annual Meeting, Fire prevention* (pp. 47-48). Architectural Institute of Japan.

Kirby BR, P. P. (1988). High temperature properties of hot-rolled structural steels for use in fire engineering design studies. *13*(1).

Knight, D. D. (1971). *Prediction of Isothermal Creep.* BHP.

Kohno M, M. Y. (2017). FEM Analysis of YP500 Steel Columns considering Creep at Elevated Temperatures. *Summaries of Technical Papers of Annual Meeting, Fire prevention* (pp. 177-178). Architectural Institute of Japan.

L., T. (1988). Strength and deformation properties of steel at elevated temperatures. *13*(1).

Li, G.-Q. Z. (2012). Creep effect on buckling of axially restrained steel columns in real fires. *71*.

Morovat M-A, E. M.-D.-M. (2011). Importance of time-dependent material behavior in predicting strength of steel columns exposed to fire. *Appl. Mech. Mater., 82*, 350–355.

Morovat, M. E. (April 2016). Experimental examination of creep buckling of steel columns in fire.

Morovat, M. L. (2011). Analysis of creep buckling of steel columns subjected to Fire. *Structures Congress, ASCE.*

NIST. (2005). *Federal building and Fire safety investigation of the World Trade Center Disaster, Mechanical properties of Structural steels, Report NIST NCSTAR 1-3D .* National Institute of Standards and Technology.

Norton, F. (1929). The Creep of Steel at High Temperatures.

Okabe, T. a. (2007.1). Numerical analysis of fire resistant tests of press-formed steel column (BCP325) . *No. 611*.

Ottosen N, R. M. (2005). The mechanics of constitutive modeling. *Elsevier*.

Qiang X, B. F. (2012). Dependence of mechanical properties of high strength steel S690 on elevated temperatures. *30*.

Qiang X, B. F. (2012). Deterioration of mechanical properties of high strength structural steel S460N under transient state fire condition. *40*.

Qiang X, B. F. (2012). Post-fire mechanical properties of high strength structural steels S460 and S690. *35*.

Rabotnov, G. a. (1957). Creep Stability of Columns and Plates. *Journal of the Mechanics and*, 27-34.

Sakumoto Y, Y. T. (1992). High-temperature properties of fire-resistant steel for buildings. *118*(2).

Van den Broek, J. (1947). Euler's Classic Paper "On the Strength of Columns". *American Journal of Physics, 15*(4), 309-314.

Wang W, L. B. (2013). Effect of temperature on strength and elastic modulus of high-strength steel. *25*.

Wang W., Y. S. (2017). Studies on temperature induced creep in high strength Q460 steel. *Materials and Structures*, 50-68.

Wang, W. Z. (2019). Creep buckling of high strength Q460 steel columns at elevated temperatures. *157*.

Williams-Leir, G. (1983). Creep of Structural Steel in Fire: Analytical Expressions. *7*(2), 73-78.

Y., A. (1988). Modeling steel behavior. *13*(1).

Yang K.C, H. L. (2006). Performance of Steel H Columns Loaded under Uniform Temperature. *Journal of Constructional Steel Research, 62*(3), 262-270.

Yang K.C., a. R. (2009). Structural Behavior of Centrally Loaded Steel Columns at Elevated Temperature. *Journal of Constructional Steel Research, 65*(11), 2062-2068.

ACKNOWLEDGMENTS

APPENDIX A

SUBROUTINE USED IN FINITE ELEMENT PROGRAM ABAQUS

A.1 YP400

```
C                     FOR YP400  F-F model (NIST)
      SUBROUTINE CREEP(DECRA,DESWA,STATEV,SERD,EC0,ESW0,P,QTILD,
     1 TEMP,DTEMP,PREDEF,DPRED,TIME,DTIME,CMNAME,LEXIMP,LEND,
     2 COORDS,NSTATV,NOEL,NPT,LAYER,KSPT,KSTEP,KINC)
C
C   remark  TIME DTIME ( in ABAQUS second is used)
C
      INCLUDE 'ABA_PARAM.INC'
C
      CHARACTER*80 CMNAME
C
      DIMENSION DECRA(5),DESWA(5),STATEV(*),PREDEF(*),DPRED(*),TIME(2),
     1 COORDS(*)
C
      DO 3 KK=1,5
    3 DECRA(KK)=0.D0
C
C   IF(QTILD.LT.40.) GO TO 10
C
      IF(TEMP.LT.400.0) GO TO 10
      IF(QTILD.LT.40.0) GO TO 10
C                           creep F-F model NIST
      TZ=TEMP
      IF(TZ.LT.550.0) THEN
         ADA=exp(-66.6393+1.8275E-2*TZ-1.7584E-5*TZ**2)
         BDA=0.8637+3.6618E24*TZ**-9.6135
         CDA=3.233+0.0117*TZ
      ELSE
         ADA=exp(-66.6393+1.8275E-2*TZ-1.7584E-5*TZ**2)
         BDA=0.7544+1.8661E-25*TZ**8.6955
         CDA=3.233+0.0117*TZ
      END IF
C
         A =ADA*BDA
         XN=CDA
         XM=BDA-1.0
C
      C1=1./(1.+XM)
C                                 STRAIN HARDENING
      TERM1=(A*QTILD**XN*C1)**C1
CCC      TERM2=TERM1*DTIME+EC0**C1  ( DTIME is second )
C                                                  ( remain second )
      TERM2=TERM1*DTIME+EC0**C1
C
CCC      STATEV(1)=TERM2/TERM1     ( TERM2/TERM1 is second )
C                                                  ( remain second )
      STATEV(1)=TERM2/TERM1
      DECRA(1)=(TERM2**(1.+XM)-EC0)
C
CCC      DECRA(5)=XN*DTIME*TERM2**XM*TERM1/RQTILD  ( DTIME is second )
C                                                  ( remain second )
      DECRA(5)=XN*DTIME*TERM2**XM*TERM1/QTILD
   10 CONTINUE
C
      RETURN
      END
```

A.2 YP500

```fortran
C                      FOR YP500  F-F model (NIST)
      SUBROUTINE CREEP(DECRA,DESWA,STATEV,SERD,EC0,ESW0,P,QTILD,
     1 TEMP,DTEMP,PREDEF,DPRED,TIME,DTIME,CMNAME,LEXIMP,LEND,
     2 COORDS,NSTATV,NOEL,NPT,LAYER,KSPT,KSTEP,KINC)
C
C   remark  TIME DTIME ( in ABAQUS second is used)
C
      INCLUDE 'ABA_PARAM.INC'
C
      CHARACTER*80 CMNAME
C
      DIMENSION DECRA(5),DESWA(5),STATEV(*),PREDEF(*),DPRED(*),TIME(2),
     1 COORDS(*)
C
      DO 3 KK=1,5
    3 DECRA(KK)=0.D0
C
C   IF(QTILD.LT.40.) GO TO 10
C
      IF(TEMP.LT.400.0) GO TO 10
      IF(QTILD.LT.40.0) GO TO 10
C                         creep F-F model NIST
      TZ=TEMP
        ADA=exp(1.77588-0.24774*TZ+2.09724E-4*TZ**2)
        BDA=1.5944-1.3913E29*TZ**-11.31
        CDA=3.233+0.0117*TZ
C
CCC       A =ADA*BDA*60.0
        A =ADA*BDA
        XN=CDA
        XM=BDA-1.0
C
C            A=2.5E-27
C            XN=5.
C            XM=-.2
C
      C1=1./(1.+XM)
C                              STRAIN HARDENING
      TERM1=(A*QTILD**XN*C1)**C1
C
CCC     TERM2=TERM1*DTIME+EC0**C1  ( DTIME is second )
C                                            ( remain second )
      TERM2=TERM1*DTIME+EC0**C1
C
CCC     STATEV(1)=TERM2/TERM1     ( TERM2/TERM1 is second )
C                                            ( remain second )
      STATEV(1)=TERM2/TERM1
      DECRA(1)=(TERM2**(1.+XM)-EC0)
C
CCC     DECRA(5)=XN*DTIME*TERM2**XM*TERM1/RQTILD  ( DTIME is second )
C                                            ( remain second )
      DECRA(5)=XN*DTIME*TERM2**XM*TERM1/QTILD
   10 CONTINUE
C
      RETURN
      END
```

A.3 H-SA700

```fortran
C                        FOR SA700  F-F model (NIST)
      SUBROUTINE CREEP(DECRA,DESWA,STATEV,SERD,EC0,ESW0,P,QTILD,
     1 TEMP,DTEMP,PREDEF,DPRED,TIME,DTIME,CMNAME,LEXIMP,LEND,
     2 COORDS,NSTATV,NOEL,NPT,LAYER,KSPT,KSTEP,KINC)
C
C   remark  TIME DTIME ( in ABAQUS second is used)
C
      INCLUDE 'ABA_PARAM.INC'
C
      CHARACTER*80 CMNAME
C
      DIMENSION DECRA(5),DESWA(5),STATEV(*),PREDEF(*),DPRED(*),TIME(2),
     1 COORDS(*)
C
      DO 3 KK=1,5
    3 DECRA(KK)=0.D0
C
C   IF(QTILD.LT.40.) GO TO 10
C
      IF(TEMP.LT.400.0) GO TO 10
      IF(QTILD.LT.40.0) GO TO 10
C                        creep F-F model NIST
      TZ=TEMP
      IF(TZ.LT.500.0) THEN
         ADA=exp(-47.5365-5.3731E-3*TZ-9.9466E-5*TZ**2)
         BDA=7.8868E-1+3.0307E-33*TZ**12.022013
         CDA=3.233+0.0117*TZ
      ELSE
         ADA=exp(-20.7462-2.2201E-1*TZ+2.2664E-4*TZ**2)
         BDA=-4.6E-5*TZ**2+4.8212E-2*TZ-1.1E1
         CDA=3.233+0.0117*TZ
      END IF
C
         A =ADA*BDA
         XN=CDA
         XM=BDA-1.0
      C1=1./(1.+XM)
C                                    STRAIN HARDENING
      TERM1=(A*QTILD**XN*C1)**C1
C
CCC      TERM2=TERM1*DTIME+EC0**C1  ( DTIME is second )
C                                                  ( remain second )
      TERM2=TERM1*DTIME+EC0**C1
C
CCC      STATEV(1)=TERM2/TERM1     ( TERM2/TERM1 is second )
C                                                  ( remain second )
      STATEV(1)=TERM2/TERM1
      DECRA(1)=(TERM2**(1.+XM)-EC0)
C
CCC      DECRA(5)=XN*DTIME*TERM2**XM*TERM1/RQTILD  ( DTIME is second )
C                                                  ( remain second )
      DECRA(5)=XN*DTIME*TERM2**XM*TERM1/QTILD
   10 CONTINUE
C
      RETURN
      END
```